課程博士

学位授与年月：2022 年 3 月

関西大学審査学位論文

# Development of transition-metal nanoparticles catalysts for sustainable organic transformations

（遷移金属ナノ粒子触媒を用いた環境調和型有機分子変換反応の開発）

理工学研究科　総合理工学専攻

化学・物質工学分野

有機化学領域

19D6010　　永田　達己

博士論文要旨

理工学研究科総合理工学専攻
有機化学
19D6010
永田達己

博士論文論題
Development of transition-metal nanoparticles catalysts for sustainable organic transformations (遷移金属ナノ粒子触媒を用いた環境調和型有機分子変換反応の開発)

**Abstract(概要)**

触媒を活用した有機分子変換反応は，ワッカー反応やクロスカップリング反応など有機合成において多くの革新をもたらしており，触媒に用いられる金属資源の低減化や代替のための技術開発は重要な課題である．金属ナノ粒子は高い比表面積を有しており， 表面に露出している配位不飽和原子割合が多く触媒材料として注目されている．従来，触媒活性の高いシングルナノサイズ粒子を溶液中で合成し安定化させるには金属に強く配位して凝集を制御する高分子やチオールなどの有機物の利用が必須と考えられていた．

*N, N*-ジメチルホルムアミド(DMF)を溶媒，保護剤，還元剤として用いて担体や保護剤を用いることなく合成されるパラジウムナノクラスターが鈴木－宮浦反応クロスカップリング反応に高い触媒活性を示すことを見出した．保護剤フリーで合成された金属ナノ粒子は高い触媒回転数を示し再利用な可能である特徴を有しており，従来にない環境調和型分子変換プロセスが構築可能となる．

以上の経緯により本研究は環境負荷の低い有機分子変換反応の開発を指向し，高活性シングルナノサイズ金属微粒子の触媒作用に注目した．DMF 保護金属ナノ粒子の高度利用及び新規ナノ粒子を作成し，環境調和型反応へ応用した．本博士論文では第 1 章では環境調和型分子変換反応を指向した触媒開発の背景を述べる．第 2 章ではサイズ制御チオール保護金ナノクラスターを用いた含窒素化合物合成反応について述べる．第 3，4 章では DMF 保護金属ナノ粒子触媒を用いた有機ケイ素化合物の合成と反応の詳細について述べる．第 5 章では DMF 保護ルテニウムナノ粒子触媒を用いたアルコールの反応について詳細を述べる．第 6 章では本研究で得られた成果について総括する．

【各章の要旨】

**第 1 章 General introduction(背景)**

触媒を用いた分子変換プロセスは，我々の身近に存在する工業化成品の製造において役割が極めて大きい．年々深刻となる環境問題への対応，ならびに持続可能な合成プロセス開発には高活性な触媒が重要な役割を果たす．このため触媒として大量に使用される白金，パラジウム，イリジウムなどの希少金属の代替・効率的利用は重要課題として活発に研究されている．加えて近年ではグリーンケミストリーの 12 箇条に従い，有機分子変換においても物質を最大限活用する合成手法，反応促進剤をできる限り使用せず環境負荷を抑えたプロセス開発が強く必要とされている．

例えば耐熱性，透明性に優れる機能性環状オレフィン高分子は Schrock らが開発したモリブデン触媒, Grubbs-Hoveyda らによって開発されたルテニウム触媒を用いて開環重合メタセシス重合(ROMP Ring-opening metathesis polymerization)により得られる．前周期遷移金属の中でも特異な金属-多重結合錯体の反応性が知られているニオブを用いた ROMP の触媒作用について研究成果をまとめた.

またアルキン，アルケン，ニトリルのような入手容易な化合物群を出発分子とし，遷移金属錯体を用いて行う[2+2+2]環化付加反応は原理上廃棄物を生じない原子効率の高い反応である．合成されるピリジン，ピリミジン，トリアジンは医薬品や農薬に用いられる有用な化合物群であり遷移金属触媒へのアルキンの酸化的付加，メタラサイクルの形成を鍵として原子効率よく環化生成物を得る手法の最近の研究成果をまとめた.

***N, N*-Dimethylformamide-protected single-sized metal nanoparticles and their use as catalysts for organic transformations** (*N, N*-ジメチルホルムアミド保護金属ナノ粒子の有機分子変換反応への応用) 環境負荷の低い分子変換を達成する触媒におけるナノ粒子の役割は大きい. 微小粒子の活性表面を最大限活用することは, 従来にない環境調和型分子変換が可能となると考えられる. *N, N*-ジメチルホルムアミド(DMF)は高沸点極性溶媒として様々な分野で使用されている．DMF は沸点近くで加熱すると自己分解し金属還元能を有する様々な化合物に分解することが知られている．この性質を利用し DMF を溶媒，保護剤，還元剤として利用すると保護剤を別途加えず高い触媒活性を有する微粒子が合成できる．DMF 保護金属ナノ粒子を触媒として用いた種々の有機分子変換について最近の研究成果をまとめた.

**第 2 章 Thiolate-protected $Au_{25}$ $(SC_2H_4Ph)_{18}$ nanoclusters as a catalyst for intermolecular hydroamination of terminal alkynes(チオール保護金ナノクラスターを用いた末端アルキンのヒドロアミノ化反応)**

イミンは含窒素化合物の合成における重要なビルディングブロックでありヒドロアミノ化反応は原子効率よくイミン化合物を合成する重要な手法である．金触媒を用いたヒドロアミノ化反応は従来酸性反応促進剤が用いられてきた．環境負荷軽減の観点から反応促進剤を用いないヒドロアミノ化反応の開発は材料，創薬化学において重要な課題である.

本章では金ナノクラスター$Au_{25}(SCH_2CH_2Ph)_{18}$ を酸素雰囲気において用いると反応促進剤を必要とせず末端アルキンとアミンのヒドロアミノ化反応に高い触媒活性を示すことを見出した．触媒が配位性溶媒に良分散する性質を利用して再沈殿操作を行い基質及び目的生成物と触媒の分離・回収に成功した．最大 5 回のヒドロアミノ化触媒として再利用が可能であり基質適用範囲の検討結果と合わせて詳細を述べる.

**第 3 章 Dimethylformamide-stabilised palladium nanoclusters catalysed coupling reactions of aryl halides with hydrosilanes/disilanes(DMF 保護パラジウムナノクラスター触媒によるハロゲン化アリールとヒドロシラン/ジシランのカップリング反応)**

芳香族有機ケイ素化合物群は蛍光材料, 医薬品などに用いられる化合物であり，これまで

に Pd 錯体とかさ高いリン系配位子によって副反応の進行を抑制し選択的に目的生成物を合成している．DMF 保護パラジウムナノ粒子触媒を用いると従来必須であったリン系配位子を必要とせずケイ素-炭素結合の形成に高い触媒活性を示すことを見出した．本章ではパラジウムナノ粒子触媒の前処理操作によって生じる粒子表面状態の XPS(エックス線光電子分光法)による解析，反応基質の適用範囲の検討，パラジウムナノ粒子触媒の回収再利用操作の詳細について述べる．

**第 4 章 *N*, *N* -Dimethylformamide-protected $Fe_2O_3$ combined with Pt nanoparticles : Characterization and catalysis in alkene hydrosilylation (酸化鉄-白金混合ナノ粒子触媒によるアルケンのヒドロシリル化反応)**

シランカップリング剤は分子内に有機部材と無機材料と結合する官能基を有し材料に機能を付与できる有用な化合物である．そのため，半導体封止剤や自動車タイヤ等を高機能化するための材料に使用される．従来，工業的ヒドロシリル化反応は白金触媒を用いて行われているが，使用される白金は回収不能であった．さらに，従来法では触媒が生成物に残存し製品機能が劣化するなどの課題があり，これらを解決するヒドロシリル化触媒の開発が求められている．

本章では DMF 保護酸化鉄ナノ粒子と白金ナノ粒子を触媒として混合し用いることでアルケンとアルコキシシランを用いたヒドロシリル化反応が高収率で進行することを見出した．本研究では，触媒反応前後の金属ナノ粒子のキャラクタリゼーションに関する解析，効率的な触媒リサイクル法および大スケール (キログラムスケール) 合成において本触媒プロセスが効率的に機能することに関してもその結果をあわせて述べる．

**第 5 章 Dimethylformamide-stabilized ruthenium nanoparticles catalysed Guerbet reaction of primary alcohol(DMF 保護ルテニウムナノ粒子を用いた直鎖アルコールのゲルベ反応)**

$\beta$ 位分岐アルコール(ゲルベアルコール)は高分子量でありながら同炭素数の直鎖アルコールと比べて融点が低くなるため，直接もしくは中間体として化粧品，潤滑剤，可塑剤に用いられる化合物である．ゲルベアルコールの合成においては不均一系触媒では 200 °C 以上の高温を必要とするため副生成物の抑制が困難であり，均一系錯体触媒を用いた反応においても反応制御のため添加剤が必要であった．

本章では，DMF 法による還元法によりルテニウムナノ粒子を調製し STEM, XPS, XAFS 分析によるキャラクタリゼーションを行った結果ならびに．調製したルテニウムナノ粒子を触媒として用いた高選択的ゲルベアルコールの合成を指向した反応条件の最適化，及び経時変化観察の結果の詳細について述べる．

**第 6 章 General Conclusion**

本研究によって得られた，遷移金属ナノ粒子触媒を用いて行った有機分子変換反応の結果を総括する．

以上

# Development of transition-metal nanoparticles catalysts for sustainable organic transformations

2022

Tatsuki Nagata

Kansai University

# Contents

Chapter 1. General introduction ..... 3
Chapter 2. Thiolate-protected $Au_{25}$ $(SC_2H_4Ph)_{18}$ nanoclusters as a catalyst for intermolecular hydroamination of terminal alkynes ..... 49
Chapter 3. Dimethylformamide-stabilized palladium nanoclusters catalysed coupling reactions of aryl halides with hydrosilanes/disilanes ..... 62
Chapter 4. *N,N*-Dimethylformamide-protected $Fe_2O_3$ combined with Pt nanoparticles : Characterization and catalysis in alkene hydrosilylation ..... 81
Chapter 5. Dimethylformamide-stabilized Ru nanoparticles catalyzed Guerbet reactions. ..... 108
Chapter 6. General Conclusion ..... 121
List of Publications ..... 122
Acknowledgements ..... 123

# Chapter 1. General introduction

Catalyst-based molecular transformation processes play an important role not only used on laboratory scale, but also in the production of chemical industry. Especially, in the production of the pharmaceutical industry and fine chemicals, a vital matter of waste is mainly caused by stoichiometric reagents in traditional organic transformations.[1] Highly active catalysts propose solutions for environmental issues that are becoming more serious every year. The development of an atom-economical, green, practical transformation is strongly desired.[2] Transition-metal catalyzed transformation from readily available starting materials would be a powerful methodology.

For example, A3 (Alkyne, Aldehyde and Amine) coupling reaction, could be used to allow for propargyl amines with higher atomic efficiency than the traditional Grignard reaction. The addition reactions such as [2+2+2] cycloaddition, hydroamination, and hydrosilylation belongs the greenest reactions category, where all atoms from the reactants are included in the final products. [3] Chapter1 part A summarize development of [2+2+2] cycloaddition since 2010-2020. In addition, Olefin metathesis is widely used in the fields of organic chemistry, polymer chemistry, and materials science as an efficient methodology of C-C bonds formation under mild conditions.[4] Ring-opening metathesis polymerization (ROMP) of olefin metathesis reaction can produce polymers with excellent heat resistance and transparency by hydrogenation the multiple bonds in the polymer chain after polymerization.[5]

## Metal nanoparticles

Metal nanoparticles (>100 nm) and nanoclusters (<2 nm) (M NPs and NCs) have attracted significant interest because of their high surface to volume ratios, nano-catalysts have high catalytic activities. These exceptional features of metal nanoparticles make the for application, as catalysts, sensing, biology, electronics.[6] Metal nano-catalysis conform with the twelve principles of green chemistry. The development of metal nano-catalysis eliminates the need for Ligands, external additives for conventional transformation.[7] The pioneering work conducted by Haruta, which enabled low-temperature Au NP-catalyzed CO oxidations, has had a considerable impact on nano-catalysis.[8]

In general, M NPs and M NCs are synthesized from metal precursors by reduction in the presence of stabilizers in the liquid phase, i.e., the bottom-up method (Scheme 1). The bottom-up approach has been used to access a variety of M NPs with a size-controlled NP core in the presence of surface stabilizers.[9] However, stabilizers such as phosphine and thiolate surfactants, and polymers are needed to avoid excess aggregation, which hampers access to catalytically active unsaturated surface sites.

**Scheme 1 Schematic diagram of metal nanoparticle preparation pathways**

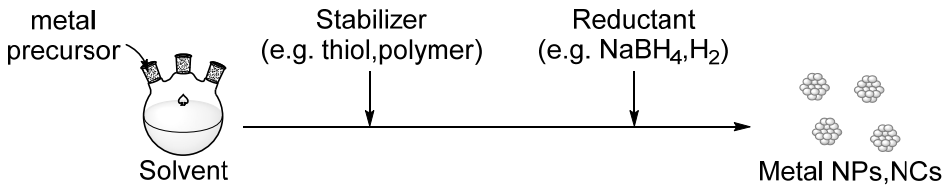


Surfactant-free synthesis provides a simple way to provide maximum access to catalytically active sites. Surfactant-free means preparation in the absence of added external stabilizing agents. Such metal NPs are stabilized by solvents or the ions of reducing agents or salts. In catalytic applications of NPs, capping molecules act as stabilizers and also affect the catalytic performance because of charge transfer between the metal and stabilizer.[10] The relationship between surface properties and catalytic behavior is attracting considerable research interest because of its potential importance in enabling new organic transformations to be achieved. Chapter 1 part B summarize a development of DMF-protected metal nanoparticles for catalytic application.

In this thesis, research achievement has been devoted to design and applications of a novel practical, green, and atom-economical catalyst system using metal nanoparticles.

In chapter 2, $Au_{25}(SC_2H_4Ph)_{18}$ nanocluster were found to have high catalytic activity for hydroamination of terminal alkynes. The reaction proceeds under air or $O_2$. The presence of molecular oxygen has a positive effect on the catalyst activity. The catalyst can be separated from the reaction mixture and reused.

In chapter 3, *N,N*-dimethylformamide Pd nanoparticles have been achieved cross-coupling reactions of aryl halides with hydrosilylation/disilanes. The cross-coupling reactions proceeded without ligands with low catalyst loadings. The Pd nanoparticles can be recycled five times under both hydrosilane and disilane reaction conditions.

In chapter 4, the combination of DMF protected $Fe_2O_3$ NPs and Pt NPs for the hydrosilylation of various industrially relevant alkenes and tertiary silanes. The DMF-protected $Fe_2O_3$ and Pt NPs catalysts were characterized by TEM, XAFS, and XPS. The catalyst of DMF-protected $Fe_2O_3$ NPs combined with Pt NPs can be recycled for five cycles by a simple extraction using hexane/DMF. The developed combination $Fe_2O_3$ /Pt NPs catalyst is effective up to the 1-kilogram scale.

Chapter 5 demonstrates the synthesis DMF-protected Ru NPs and their catalytic performance in Guerbet reaction of primary alcohols. The Ru NPs were prepared in one-step and thoroughly characterized by TEM, XPS, XAFS, FT-IR, TG-TOF-MS. The

Ru NPs catalyzed Guerbet reaction affords branched alcohols in up to 92 % yield in the absence of any external ligand and solvent.

In chapter 6, the results and conclusions of the various developments covered in this thesis have been summarized.

## Part A
## Transition-Metal-Mediated/Catalyzed Synthesis of Pyridines, Pyrimidines, and Triazines by [2+ 2+ 2] Cycloaddition Reactions

Six-membered N-heterocycles are widely found scaffolds in compounds in a variety of fields such as pharmaceuticals, polymers, agrochemicals, and organic dyes.[1] The [2+2+2] cycloaddition reaction is an atomically efficient reaction using transition metal complexes with readily available compounds such as alkynes, alkenes, and nitriles. Nitrogen-containing six-membered heterocycles such as pyridines, pyrimidines, and triazines are useful in pharmaceuticals and agrochemicals. Pyridines and pyrimidines are significant structural components of pharmaceuticals (Scheme 1).[2]

1,3,5-Triazines (*s*-triazines) are also used as bioactive compounds. Atrazine and simetryn are used as agrochemicals (Scheme 2).[3] These versatile applications of six-membered N-heterocycles have motivated synthetic chemists to explore efficient and environmentally benign access to these compound classes.

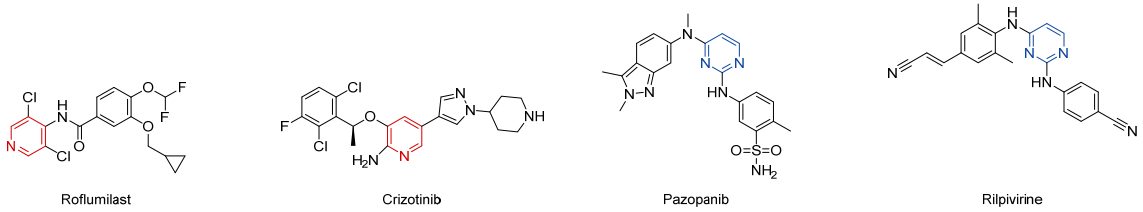


Scheme 1. Examples of pharmaceuticals with pyridine and pyrimidine units.

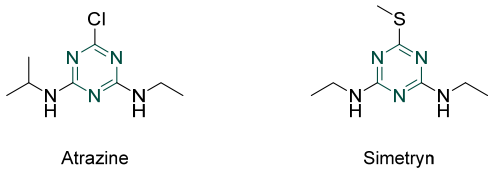


Scheme 2. Example of s-triazine-containing agrochemicals.

The first successful [2+2+2] cycloaddition was reported by Reppe et al. in 1948.[4] This led to the development of transition- metal-mediated/catalyzed transformations for synthesizing substituted carbo- and hetero-cyclic rings.[5] The synthetic utility of this reaction type arises from the ease of attaching substituents to aromatic rings. Compared to the traditional synthetic methods listed in Scheme 3,[6] [2+2+2] cycloaddition is an efficient alternative for the direct synthesis of N-containing six-membered heterocycles such as pyridines, pyrimidines, and triazines.

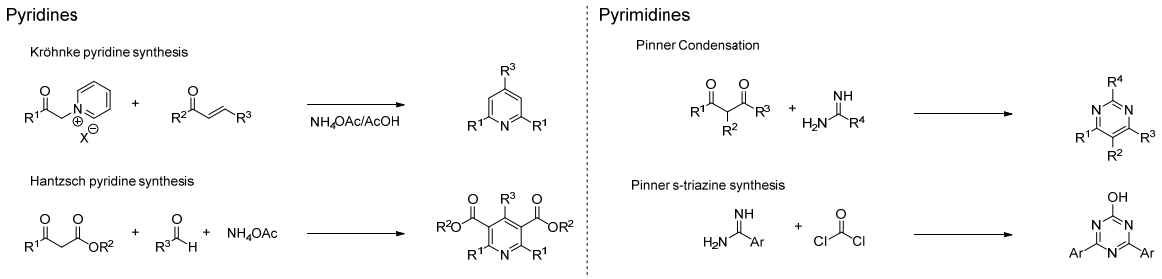


Scheme 3. Representative named reactions for heterocycle synthesis.

In addition, alkynes and nitriles are readily available and easy to handle starting materials. The development of synthetic methods for pyridines, pyrimidines, and triazines by metal-mediated/catalyzed [2+2+2] cycloadditions of alkynes/diynes and nitriles has therefore attracted considerable attention.

## 2. Synthesis of pyridines

### 2.1 General pyridine synthesis strategies via [2+2+2] cycloadditions

The proposed reaction mechanism for transition-metal- mediated/catalyzed pyridine synthesis is based on the common mechanism for cyclotrimerization of three alkyne units. The proposed overall reaction cycle is shown in Scheme 4. As previously reported,[7] there are two possible reaction pathways. First, pathway (A), which is the most general mechanism for pyridine construction. The catalytic cycle starts with oxidative addition of two alkynes or a diyne **1** to form metal cyclopentadiene **2.** Reaction with a nitrile via [2+2] or [4+2] addition, or insertion gives pyridine **3**. In the final step, reductive elimination from the metal center gives a pyridine derivative. In contrast, in pathway (B), the heterocoupling alkyne and nitrile generates the aza-metallacycle. Subsequent alkyne insertion or [4+2] addition gives **5**, and reductive elimination affords the desired pyridine derivative.

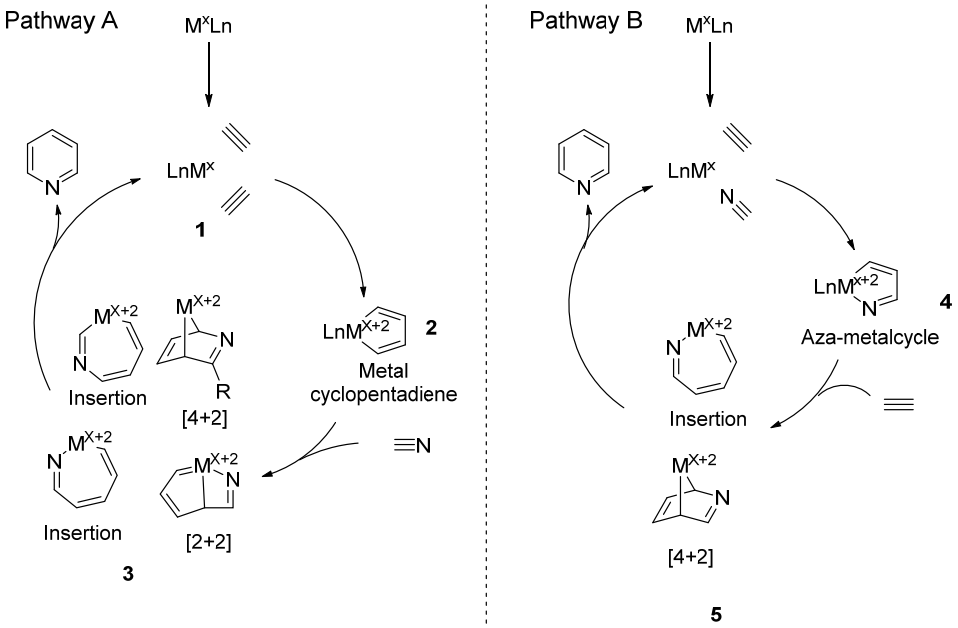


Scheme 4. Schematic [2+2+2] cycloaddition of alkynes and nitriles process via (A) metallacyclopentadiene or (B) azametallacycle as key intermediate.

## Group 4 metals (Ti, Zr) and Nb -mediated / catalyzed pyridine synthesis

### 2.2 Titanium-meditated pyridine synthesis

The early work on the use of Ti(II) alkoxide, derived from Ti(O$^i$Pr)$_4$/2$^i$PrMgCl, to mediate pyridine synthesis was discussed by Urabe et al. (Scheme 5).[8] The authors classified the reactions into four type. A divalent Ti(II) alkoxide reagent enabled completely regioselective coupling of two different, unsymmetrical acetylenes and a nitrile to form a single-isomer pyridine.

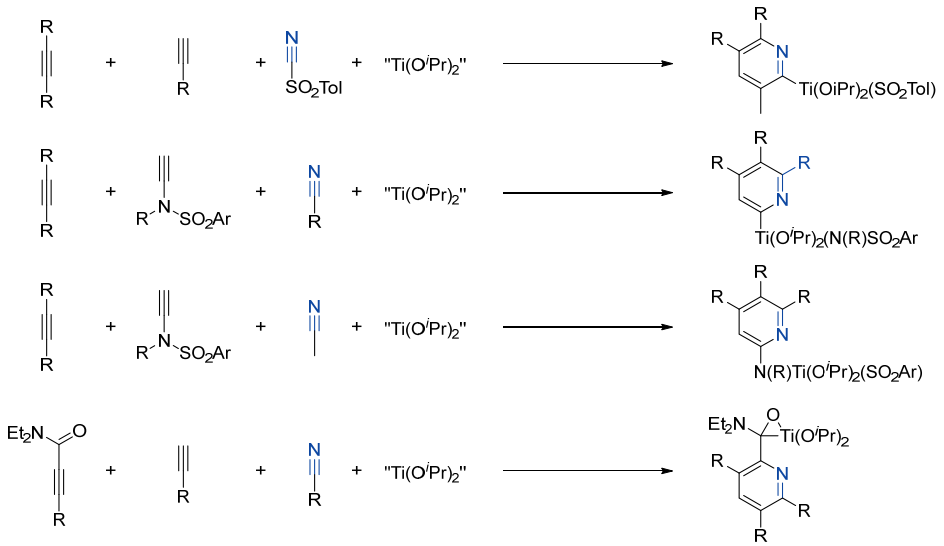


Scheme 5. Reaction of Ti(O$^i$Pr)$_2$ with alkynes and nitriles.

Later, Six and co-workers developed pyridine synthesis by using Ti(O$^i$Pr)$_4$/$^n$BuLi and an alkynenitrile. The in situ-generated Ti mediates alkyne trimerization and pyridine synthesis.[9] For example, addition of $^n$BuLi (3.3 mmol) to a mixture of diphenylacetylene (1.0 mmol) and Ti(O*i*Pr)$_4$ (2.2 mmol) in THF (10 mL) resulted in formation of titanacyclopropene species. After stirring for 2 h at 0 °C, a solution of hex-5-ynenitrile (1.25 mmol) in THF (1.0 mL) was added dropwise. The substituted pyridine was obtained in 59% yield (Scheme 6).

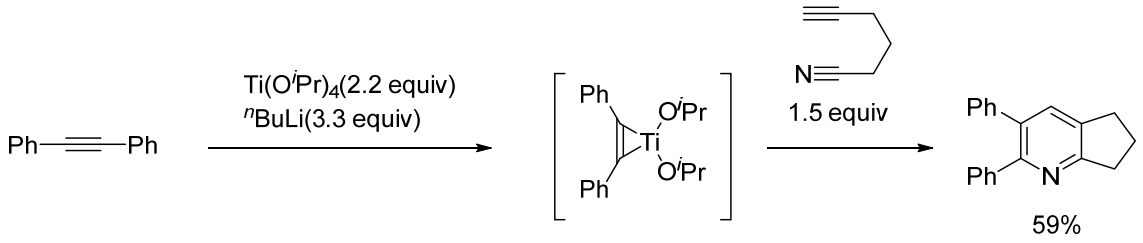


Scheme 6. Synthesis of fused bicyclic pyridine by Ti(O*i*Pr)$_4$/*n*BuLi-mediated cycloaddition.

2.3 Zirconium- mediated pyridine synthesis

Early work for Zirconium mediated [2+2+2] cycloaddition of alkyne with nitrile was reported by Takahashi and co-workers. The selective synthesis of pyridines, pyridones, and iminopyridines from two different alkynes were conducted via aza-zirconacycle.[10] The reaction of $Cp_2ZrEt_2$ with the first alkyne and nitrile gave aza-zirconacyclopentadiene. The aza-zirconacycle reacted with the second alkyne and $NiCl_2(PPh_3)_2$ to give the corresponding penta-substituted pyridine (Scheme 7). The reaction of CuCl, aza-zirconacyclopentadiene, and propargyl bromide gave tetrasubstituted pyridine derivatives in excellent yields (Scheme 8).

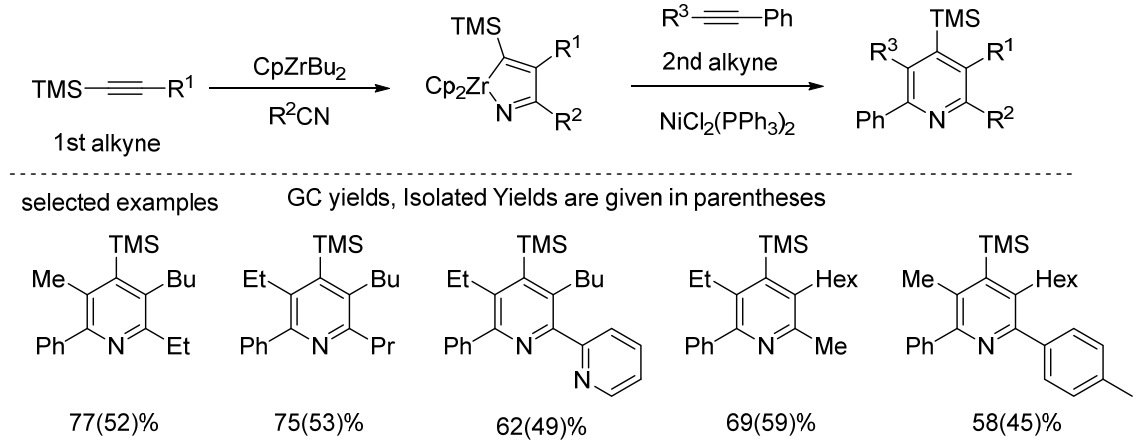


Scheme 7. $Cp_2ZrBu_2$/$NiCl_2(PPh_3)$-mediated substituted pyridine synthesis.

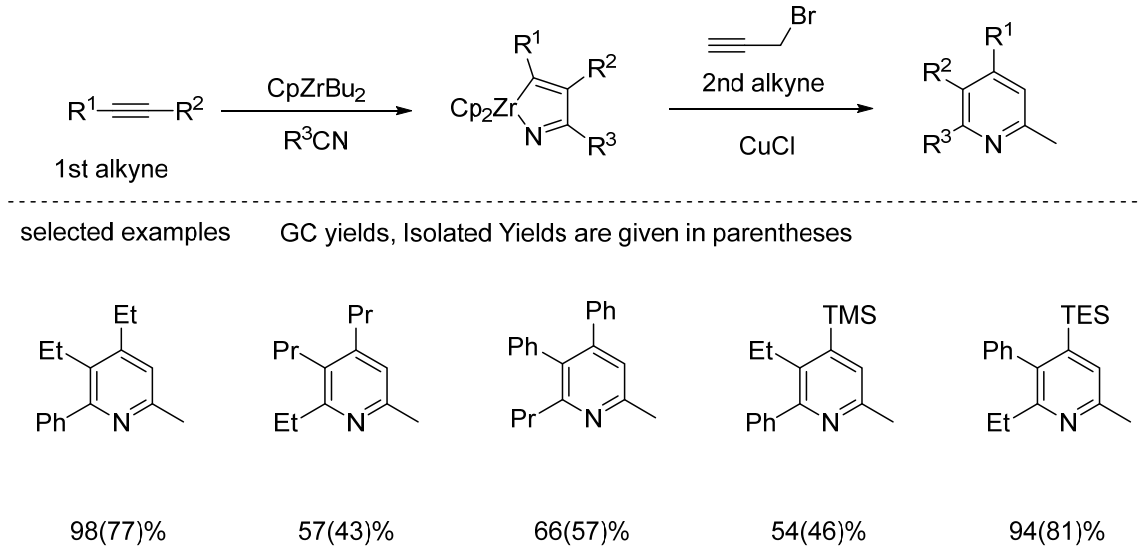


Scheme 8. Substituted pyridine synthesis mediated by $Cp_2ZrBu_2$/CuCl.

A subsequent study showed that aza-zirconacyclopentadiene can be used in one-pot pyridine synthesis.[7] For example, the reaction of a aza-zirconacyclopentadiene derived from 3-hexyne and acetonitrile with 4-octyne gave the corresponding pyridine in 86% yield (Scheme 9).

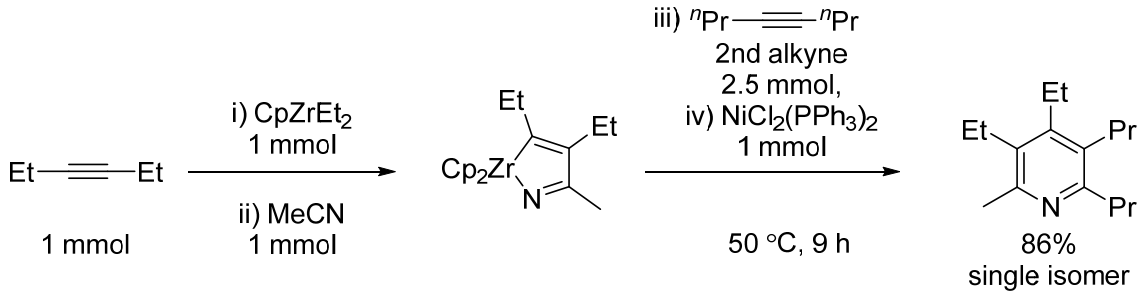


Scheme 9. One-pot pyridine synthesis.

## 2.4 Niobium-catalyzed pyridine synthesis

Niobium complexes consisting of low-valent Nb(III) and a Lewis acid have good reactivities.[12] In 2013, Satoh and Obora reported a low-valent-Nb-catalyzed pyridine synthesis.[13] The reaction of *tert*-butyl acetylene (1 mmol) and benzonitrile (3 mmol) in the presence of a catalytic amount of $NbCl_5$ (20 mol%), zinc (20 mol%), and $Ph_2Si(OMe)_2$ (60 mol%) as an additive in toluene at 80 °C gave the 2,3,6-trisubstitued pyridine in 80% yield (Scheme 10). A mechanistic experiment indicated that cycloaddition proceeds via a five-membered niobacyclic intermediate (Scheme 11).

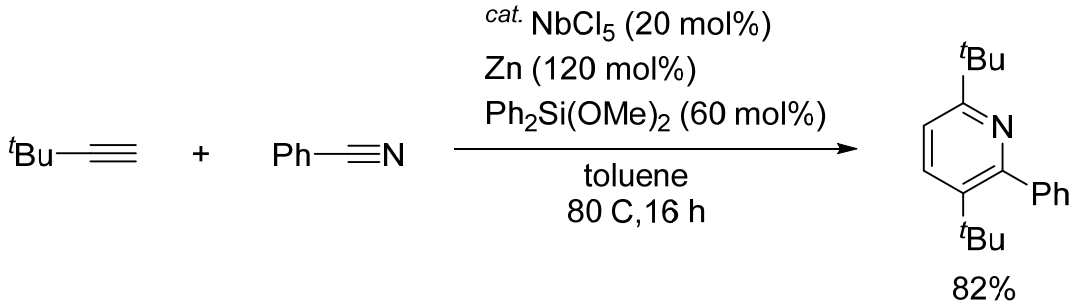


Scheme 10. Low-valent-Nb(III)-catalyzed [2+2+2] cycloaddition of two terminal alkynes and nitrile.

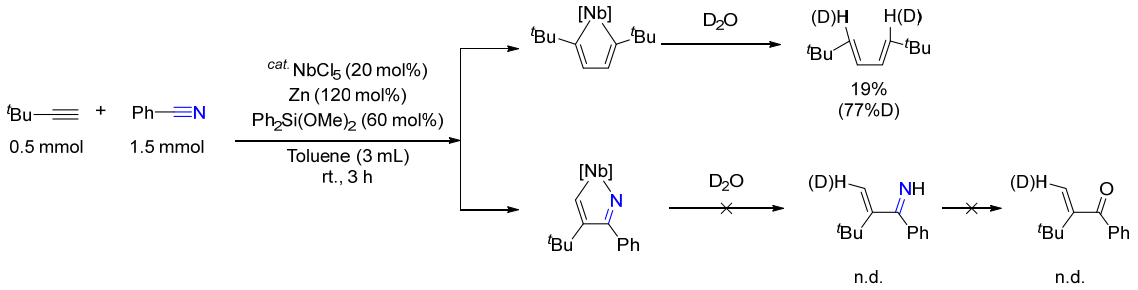


Scheme 11. investigation of formation of niobacyclic intermediates.

## Group 8 metals (Fe,Ru) catalyzed pyridine synthesis

2.5 Iron-catalyzed pyridine synthesis

In 2011, Louie et al. reported that $Fe(OAc)_2$/sterically hindered pyridylbisimine ligands catalyzed [2+2+2] cycloadditions of alkynenitriles and alkynes (Scheme 12).[14] The reaction of alkynenitrile with 5-decyne in the presence of a catalytic amount (1 mol%) of $Fe(OAc)_2$ and pyridylbisimine ligand (13 mol%), and Zn (20 mol%) in THF at room temperature gave the desired pyridine in 70% yield This system afforded various substituted pyridines.

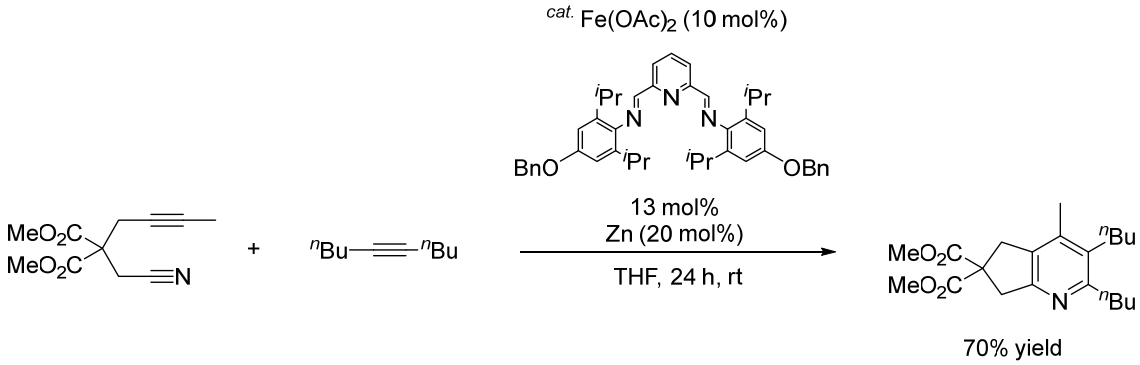


Scheme 12. $Fe(OAc)_2$/pyridylbisimine ligand-catalyzed reaction of alkynenitrile and alkyne.

Wan et al. reported the Fe-catalyzed regioselective cycloaddition of a diyne and nirile,[15] and the pyridine derivative was obtained in excellent yield in the presence of $FeI_2$ (5 mol%), dppp (10 mol%), and Zn (10 mol%) (Scheme 13). The use of easily accessible

phosphine ligand generates highly active catalyst for the [2+2+2] cycloaddition.

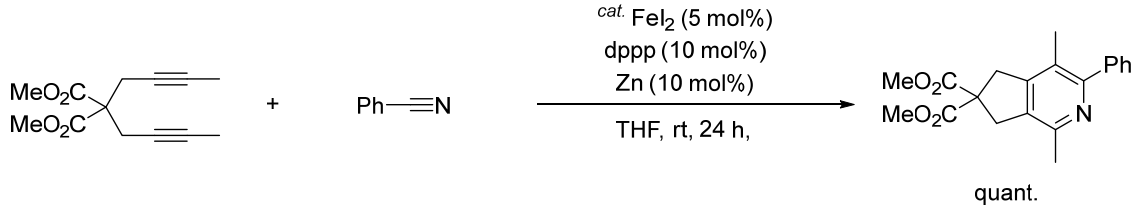


Scheme 13. Fe/dppp-catalyzed cycloaddition of diyne and benzonitrile.

Fe-catalyzed regioselective cycloaddition of a diyne and cyanamide reported Wan and co-workers.[16] 2-Aminopyridine was obtained in excellent yield. In typical procedure, a mixture of diyne (0.75 mmol), cyanamide and $PPh_3$(10 mol %) in THF was heated at 135 °C for 24 h in the presence $FeI_2$ (5 mol%) and dppp (10 mol%) reduced by Zn (10 mol%). The corresponding 2-aminopyridine was obtained in 92% yield (Scheme 14).

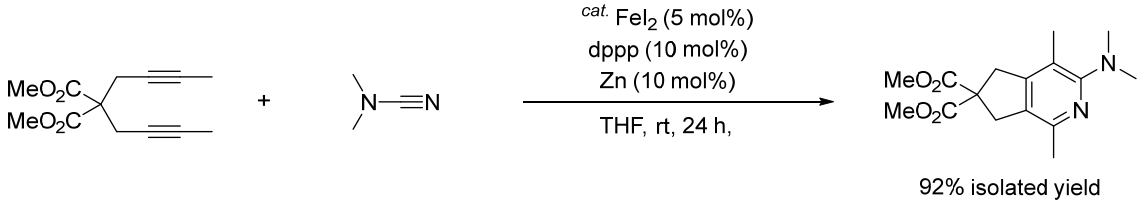


Scheme 14. Fe/dppp-catalyzed cycloaddition of diyne and cyanamide.

In 2014, Renaud et al. reported pyridine ring construction by using air-stable Fe(ll) complex and phosphine ligand.[17] The combination of 10 mol% [CpFe(naphth)][$PF_6$] and 10 mol% generates an active catalyst, which can be used for the [2+2+2] cycloaddition of diyne and acetonitrile (Scheme 15). The desired pyridine was obtained in 81%.

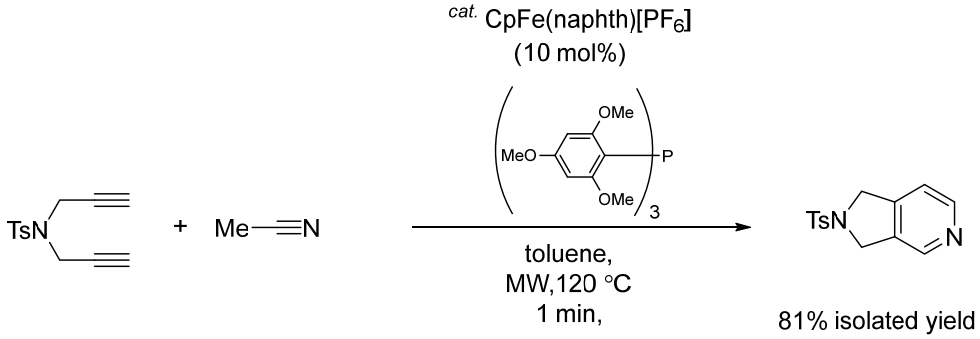


Scheme 15. Fe-catalyzed [2+2+2] cycloaddition of diyne and nitrile.

In 2017, Louie's group reported a Fe/$^{Mes}$PDAI-catalyzed [2+2+2] pyridine synthesis.[18] Terminal alkyne and cyanamide were reacted in toluene at room temperature for 24 h in the presence of $FeI_2$ (5 mol%), $^{Mes}$PDAI (10 mol%), and Zn (10 mol%). The reaction gave

the corresponding 2,4-disubstituted 2-aminopyridine regio- and chemo-selectively (Scheme 16). A mechanistic experiment showed that using an excess of cyanamide caused formation of a catalytically inactive Fe complex (Scheme 17).

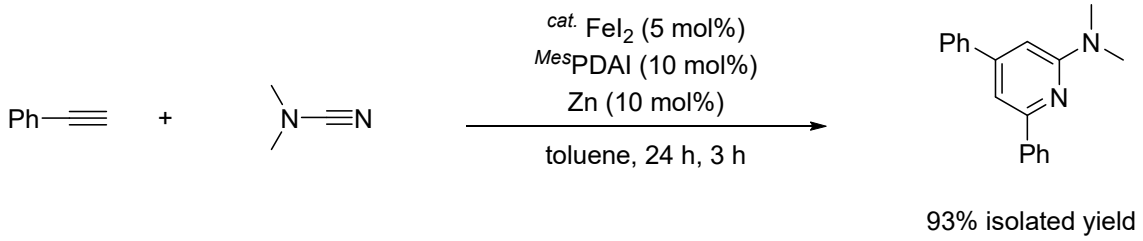


Scheme 16. Fe/$^{Mes}$PDAI-catalyzed cycloaddition of terminal alkyne and cyanamide.

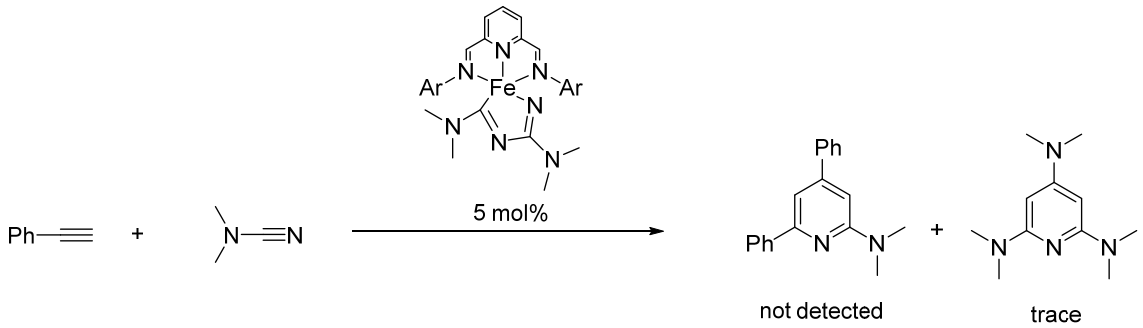


Scheme 17. Mechanistic exploration of formation of catalytically inactive species.

An Fe/PDAI-catalyzed cycloaddition was used to synthesize an estrogen receptor ligand. Cycloaddition and subsequent deprotection gave the estrogen ligand in 70% overall yield (Scheme 18).

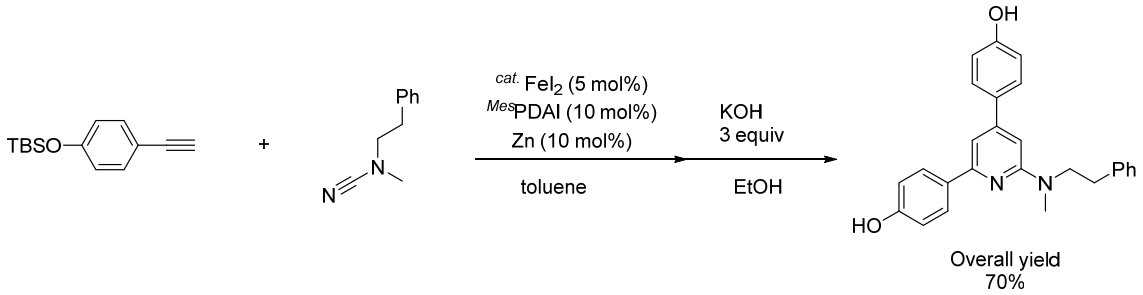


Scheme 18. Synthesis of estrogen ligand via Fe-catalyzed [2+2+2] cycloaddition.

## 2.6 Ruthenium-catalyzed pyridine synthesis

In 2011 Deiters and co-workers reported Ru-catalyzed [2+2+2] cycloaddition of diyne and an electron-deficient thiazocarbonitrile.[19] The reaction of diyne and nitrile in the presence of 5 mol% Cp*RuCl(cod) (Cp* = 1,2,3,4,5-pentamethyl-cyclopentadienyl) in dichloroethane gave the desired pyridine derivatives in 95% yield (Scheme 19).

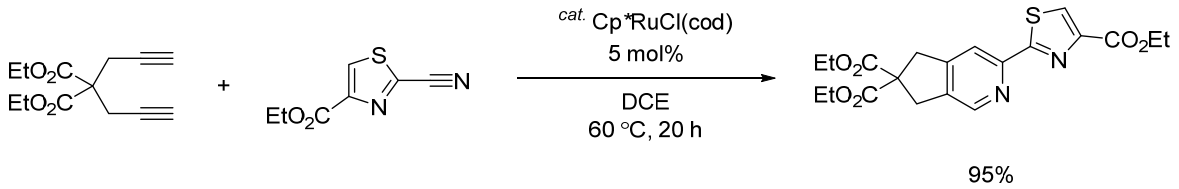


Scheme 19. Ru-catalysed [2+2+2] cycloaddition of diyne and thiazolecarbonitrile.

In 2012, Perez-Castells and co-workers reported Hoveyda-Grubbs 2nd catalyst serve as efficient activity for [2+2+2] cycloaddition diyne and nitirles.[20] In a typical procedure, diyne reacted with malononitrile using Ru-catalyst (5 mol%) at 90 °C for 15 min gave the corresponding pyridine (Scheme 20).

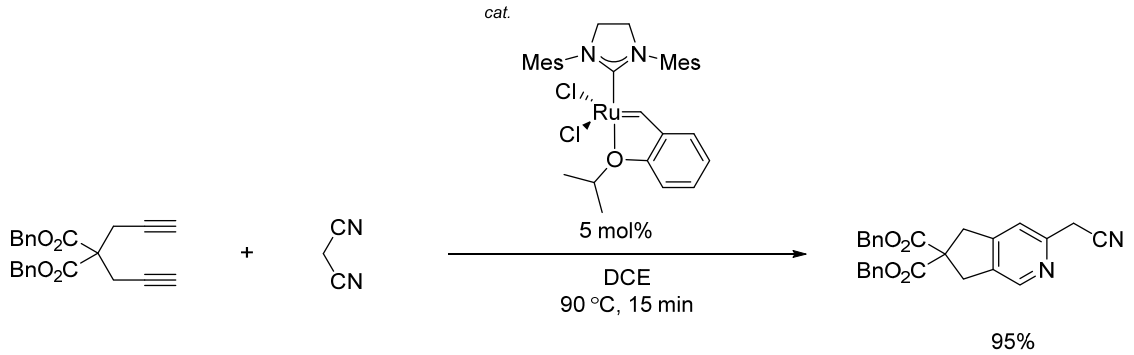


Scheme 20. Ru-carbene catalyzed [2+2+2] cycloaddition of diyne with malononitrile.

In 2017, Michelet et al. reported the Ru-catalyzed [2+2+2] cycloaddition of diynes and cyanamide (Scheme 21).[21] The Cp*Ru(MeCN)$_3$PF$_6$ catalyst showed high catalytic activity in 2-aminopyridine synthesis. When this reaction was performed with 1 mol% of Cp*Ru(MeCN)$_3$PF$_6$, diyne (0.5 mmol), and cyanamide (1 mmol) at room temperature for 5 min under Ar, the corresponding 2-aminopyridine was obtained in 95% yield. The reaction proceeds under additional ligand and additive-free conditions.

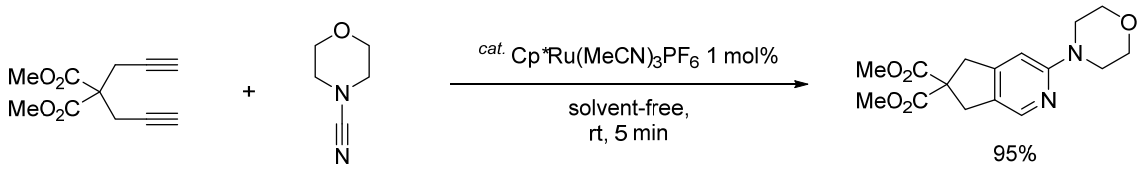


Scheme 21. Synthesis of 2-aminopyridine derivatives by Ru-catalyzed [2+2+2] cycloaddition.

Michelet group also reported applications of Cp*Ru(MeCN)$_3$PF$_6$-catalyzed [2+2+2]cycloaddition.[22] A mixture of diyne (0.5 mmol) and cyanamide was heated at 50 °C for 2 h. As a result, the corresponding 2-aminopyridine was obtained in 82% yield. In addition, a gram-scale synthesis of [2+2+2] cycloaddition was demonstrated (Scheme 22).

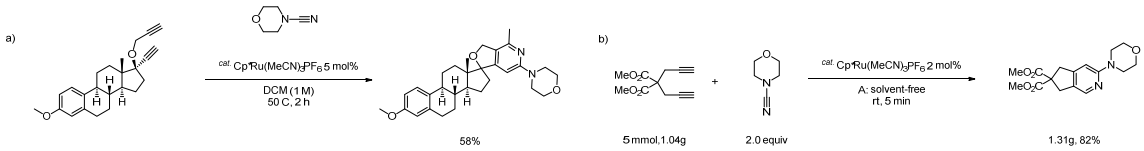


Scheme 22. Application of (a) late-stage functionalization and (b) gram-scale synthesis.

Recently, In 2018, Michelet and Ratovelomanana-Vidal group reported Ru-catalyzed synthesis of azafluorenone.[23] Typically, azafluorenone were obtained by the reaction of benzoyl bridged diyne with cyanamide (3 equiv) in the presence of Cp*Ru(MeCN)$_3$PF$_6$ (2 mol%) as catalyst. The reaction proceeded smoothly under solvent-free conditions and gave the desired pyridine in 87% yield (Scheme 23).

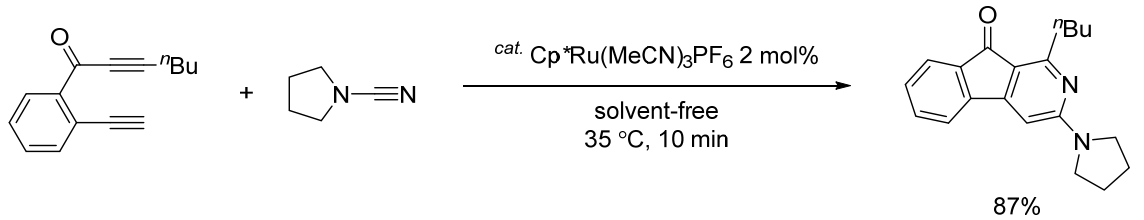


Scheme 23. Synthesis of 2-azafluorenone by Ru-catalysed [2+2+2] cycloaddition.

Ratovelomanana-Vidal group reported Cp*Ru(MeCN)$_3$PF$_6$ under microwave irradiation was found to be an effective catalyst for the synthesis of 2-aminopyridines.[24] The reaction of diyne and cyanamide with [Cp*Ru(MeCN)$_3$]PF$_6$ under 50 W microwave irradiation in MeTHF at 50 °C for 10 min gave the desired 2-aminopyridine quantitatively (Scheme 24).

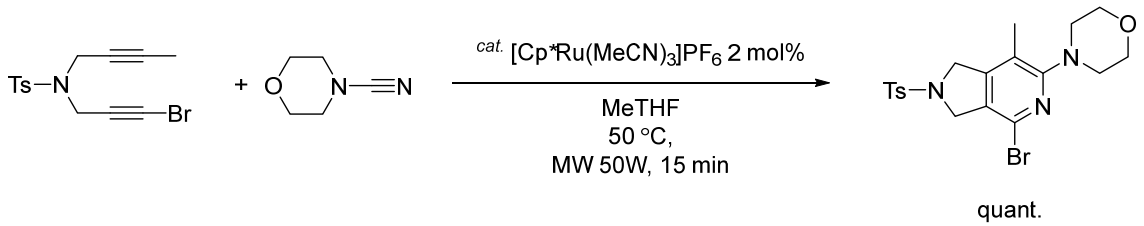


Scheme 24. Synthesis of 2-azafluorenone by Ru-catalysed [2+2+2] cycloaddition.

In 2017, Goswami and Chowdhury developed chemo- and regio- selective [2+2+2] cycloaddition.[25] The reaction of diyne and N-cyanoindole was carried out under open-flask and solvent-free conditions (Scheme 25). The desired 1-(2-pyridyl)indoles was obtained in 93% yield. This protocol provides a method of synthesis of indole N-substituted pyridines to use readily accessible catalyst under low catalyst loading and solvent- free conditions.

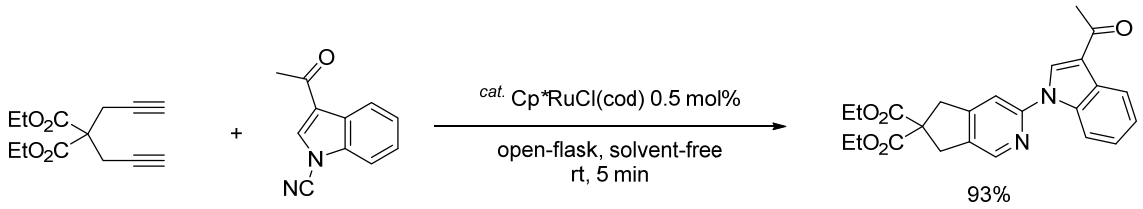


Scheme 25. Synthesis of 1-(2-pyridyl) indole scaffolds by Ru-catalysed [2+2+2] cycloaddition.

Later, Goswami group reported the synthesis of 2-aryloxypyridine and 2,2'/ 2,3'-diaryloxybipyridine.[26] The reaction of diyne and phenyl cyanate with Cp*RuCl(cod) (2 mol%) under solvent-free condition at room temperature gave the corresponding 2-aryloxypyridine in 90% yield (Scheme 26). This reaction also led to the formation of 2,2' and 2,3'-diaryloxybipyridines from the reaction of tetraynes with aryl cyanates.

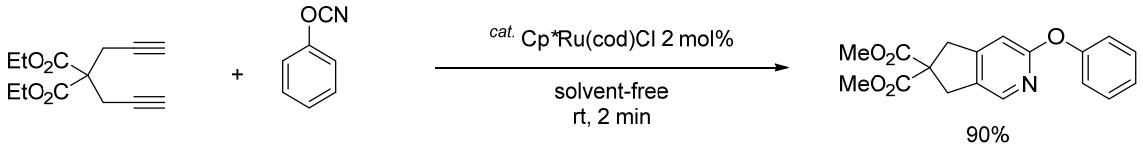


Scheme 26. The synthesis of 2-aryloxypyridine by Ru-catalyzed [2+2+2] cycloaddition.

Goswami et al. reported an additive-dependent 2-alkynylpyridine synthesis.[27] Cp*RuCl(cod) (3 mol%) and AgOTf (3 mol%) in dimethoxyethane at room temperature catalyzed the selective [2+2+2] cycloaddition of diyne and alkynenitrile. The reaction proceeds smoothly to give the corresponding 2-alkynylpyridine in excellent yield (Scheme 27). When the reaction was performed without AgOTf, the benzene derivative was obtained in 62% yield (Scheme 28).

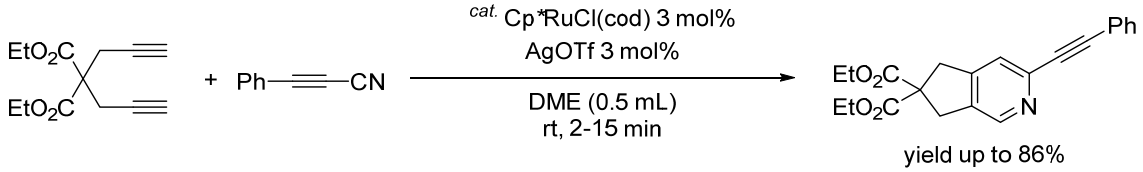


Scheme 27. Synthesis of 2-alkynylpyridines via Ru-catalyzed [2+2+2] cycloaddition of diyne and alkynenitrile.

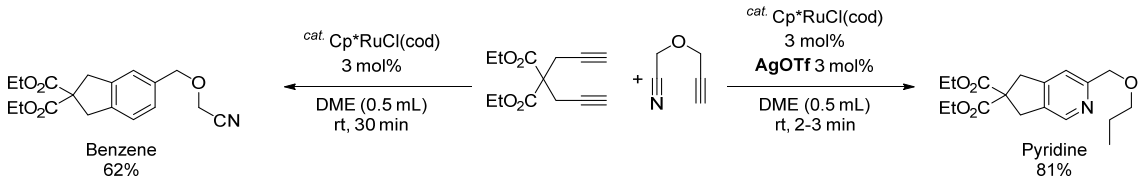


Scheme 28. Additive-controlled chemoselective [2+2+2] cycloaddition to give pyridine or benzene.

The [2+2+2] cycloaddition of an alkynyltriazene and nitrile in the presence of 5 mol% [Cp*Ru] was reported in 2019 by Cramer's group.[28] In this reaction, the cycloaddition proceeds regioselectively with Cp*Ru(MeCN)$_3$PF$_6$ (10 mol%)/Bu$_4$NI (16 mol%) (Scheme 29). The Cp*Ru(MeCN)$_3$PF$_6$ system was effective in the reactions of triazenyldiynes and various nitriles to give pyridyl triazenes with good regioselectivity. The product regioselectivity arises from introduction of the triazenyl group and yields a more sterically hindered product.

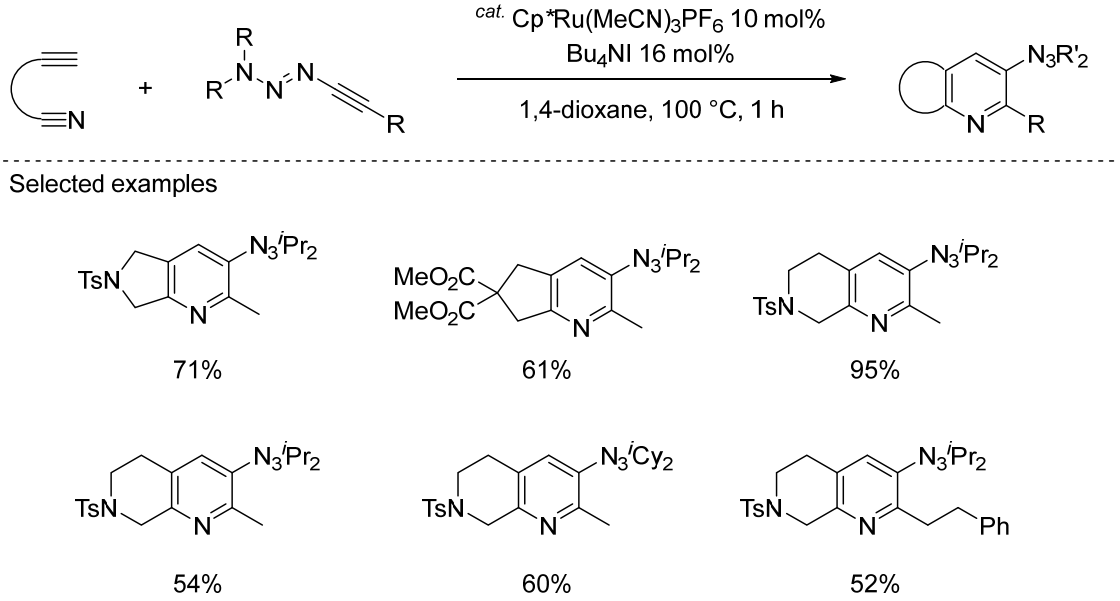


Scheme 29. Synthesis of pyridylriazenes from nitriles and alkynyltriazine.

To date, several examples of Ru-catalyzed selenopyridine have been reported (Scheme 30)[29.30] Both Cp*RuCl(cod) and Cp*Ru(MeCN)$_3$PF$_6$ complex catalyst system gave excellent yields, respectively. Goswami reported an efficient catalytic system for selenopyridine synthesis under short reaction time and external ligand or additive free condition. Ratovelomanana-Vidal et al. demonstrated synthesis of various diaryl selenium derivatives and post-functionalization of cycloadduct.

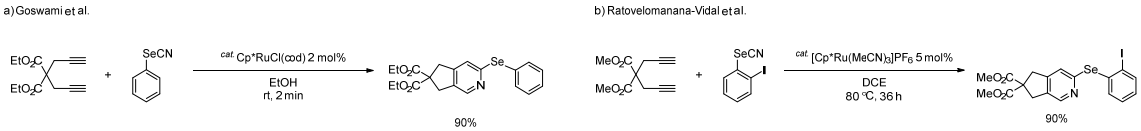


Scheme 30 Synthesis of selenopyridines by Ru-catalysed diyne and selenocyanates.

## Group 9 metal catalyzed pyridine synthesis

2.7 Cobalt-catalyzed pyridine synthesis

Co complexes show high catalytic activities in [2+2+2] cycloadditions, and pyridine synthesis via various Co-catalyzed [2+2+2] reactions has been reported. $CpCoL_2$ [Cp = cyclopentadienyl; L = CO, $PR_3$, cod (cyclooctadiene)] systems have enabled enantio- and regio-selective pyridine synthesis and have featured in several reviews.[31]

In 2010, Mclver and Deiters reported a tricyclic alkaloid core structures using $CpCo(CO)_2$ under microwave irradiation (300 W).[32] The diyne and cyano alcohol gave the fused bicyclic pyridine rings in 90% yield (Scheme 31).

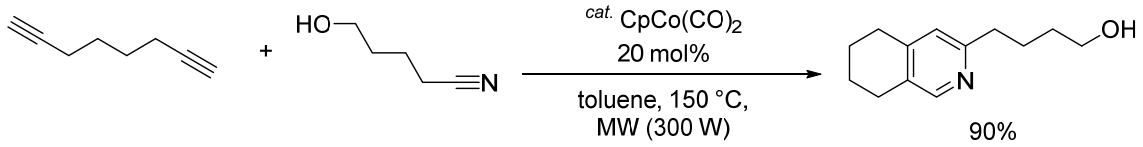


Scheme 31. Co-mediated [2+2+2] cyclotrimerization.

The optimized conditions have been applied to the synthesis of citrinadin A and B core. The alkaloid core structures derived the overall yield from diyne was 30% and 28%, respectively. (Scheme 32).

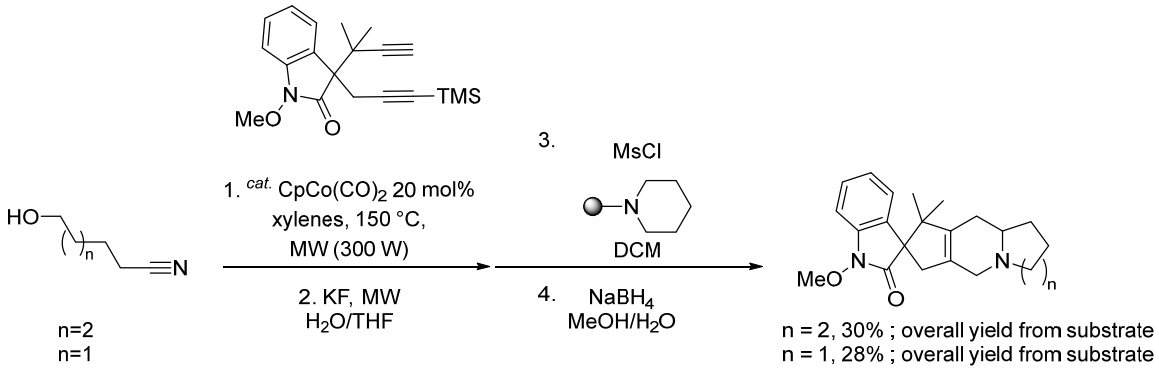


Scheme 32. Construction of the scaffolds of Citrinadin A and B

In 2010, Siegel and co-workers developed Co-mediated [2+2+2] cycloaddition for total synthesis of (+)-complanadine A (Scheme 33).[33]

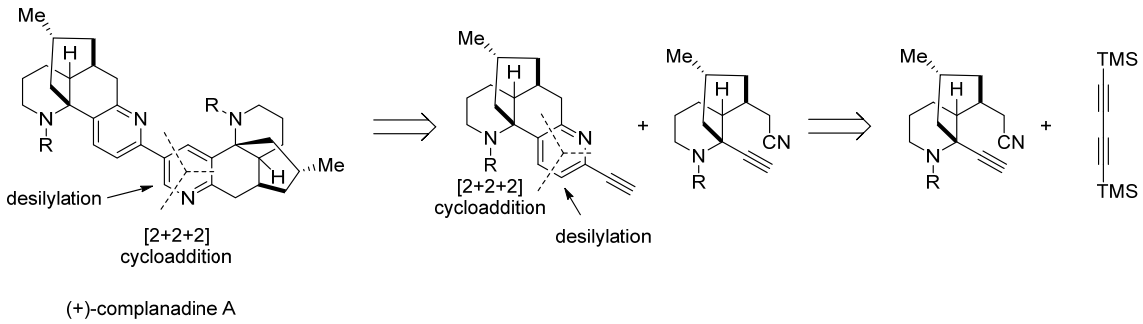


Scheme 33. Retrosynthetic analysis for Complanadine A.

The first ring construction succeeded regioselectively in the presence of $CpCo(CO)_2$ at 140 °C in THF (Scheme 34). For example, the desired pyridine was obtained in 79%. The second ring construction required excess amount of $PPh_3$ (8 equiv) by using formyl group derivative (Scheme 35).

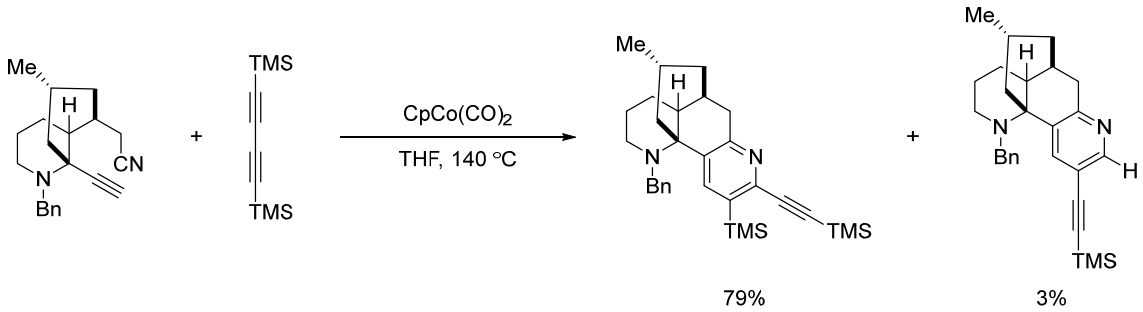


Scheme 34. Co-mediated first pyridine ring construction.

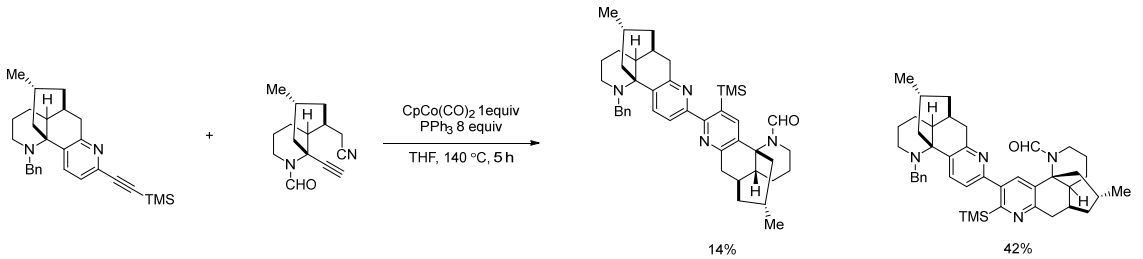


Scheme 35. Co-mediated second [2+2+2] cycloaddition.

Siegel group reported the synthesis of Lycodine derivatives and the controlled-formation of 2,3'-bipyridyl core.[34] The effect of Lewis-basic additives was examined. The use of $PPh_3$ proved to be best reactivity and regioselectivity. The use of $PPh_3$ led to selective formation of 2,3'-bipyridyl core, whereas additive-free condition led to form 2,2'-bipyridyl core (Scheme 36).

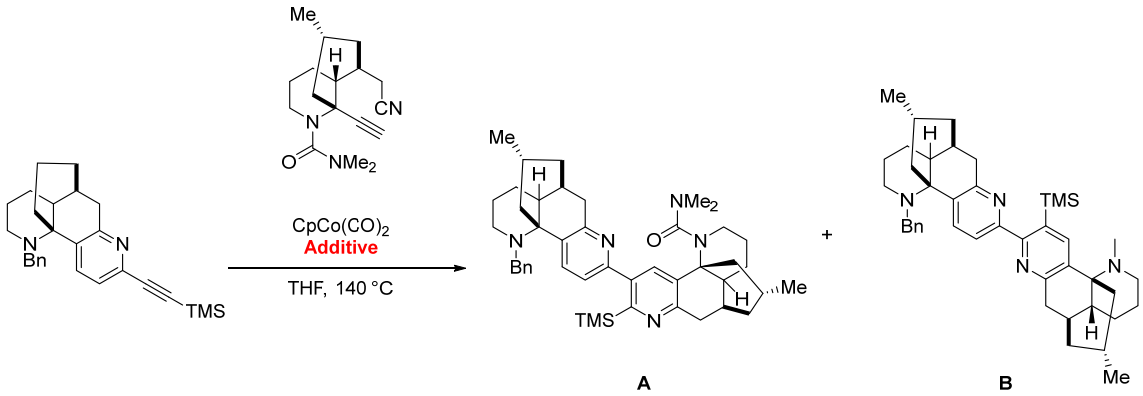


| Additive | ratio (**A**: **B**) | yield | Additive | ratio (**A** : **B**) | yield |
|---|---|---|---|---|---|
| no additive | 1 : 4 | 50% | $AsPh_3$ | 1 : 1.3 | 35% |
| $PPh_3$ | 1 : 1.1 | 44% | P(o-toluyl) | 1 : 2 | 32% |
| DMAP | 1.5 : 1 | 20% | DPPE | - | 0% |
| P(2-furyl) | - | 0% | | | |

Scheme 36. Screening of Lewis basic additives.

In 2011, Sugiyama and Okamoto reported Co-catalyzed [2+2+2] cycloaddition of α ω -diyne with nitrile.[35] The dppe (1,2-bis(diphenylphosphino)ethane), $CoCl_2 \cdot 6H_2O$ and Zn system was found to be an effective catalyst for pyridine synthesis in excellent yields at room temperature to 50 °C in NMP(*N*-methylpyrrolidone) (Scheme 37).

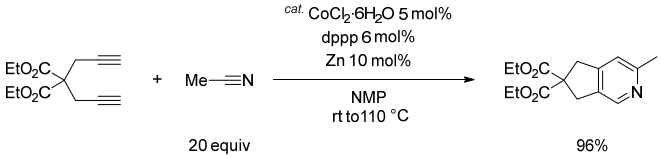


Scheme 37. Annulated pyridine synthesis via Co/dppp-catalyzed cycloaddition.

In 2012, Gandon et al. reported Co-catalyzed cycloaddition between yne–ynamides and nitriles.[36] The use of [CpCo(CO)(dmfu)] (dmfu = dimethyl fumarate) as a pre-catalyst enabled the use of cyanoformates as a CN substrate. Cycloaddition of an yne–ynamide and nitrile was performed with 10 mol% [CpCo(CO)(dmfu)] at 110 °C in toluene (Scheme 38). The corresponding 3-aminopyridine was obtained in 72% yield. A wide range of functional groups survived the reaction conditions. Replacing the yne–ynamide substitution pattern switched the product regioselectivity from 3-aminopyridine to 4-aminopyridine. Density functional theory (DFT) calculations indicate that a formal [4+2] cycloaddition is responsible for 3-aminopyridine formation.

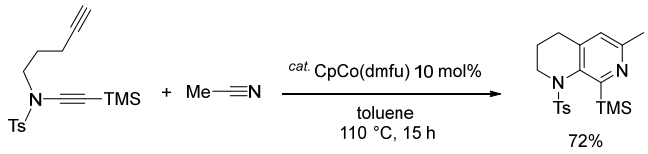


Scheme 38. [CpCo(CO)(dmfu)]-catalyzed [2+2+2] cycloaddition of acetonitrile with yne–ynamide to give 3-aminopyridine.

In 2013, Hapke reported the use of [CpCo($H_2C$=CHSi$Me_3$)] (5 mol%) as an efficient catalyst for [2+2+2] cycloaddition.[37] It is noteworthy that they described various $CpCo^I$ complexes synthesis either olefin-phosphite ligands and two phosphite ligands. In one example, 1,6-heptadiyne was allowed to react with benzonitirle in the presence of Co complex in THF at 50 °C for 15 h to give the cycloaddition product in excellent yield (Scheme 39).

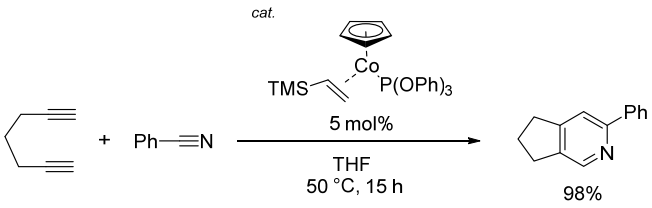


Scheme 39 [CpCo($H_2C$=CHSi$Me_3$)]-catalyzed [2+2+2] cycloaddition of diyne and benzonitrile.

In 2013, Hapke reported synthesis air stable- and recyclable $CpCo^I$-complex and their catalytic use of [2+2+2] cycloaddition.[38] To solution of Co-complex catalyst, diyne and benzonitrile were added. The mixture was stirred at 100 °C for 3h, and then the desired pyridine was obtained in excellent yield (scheme 40).

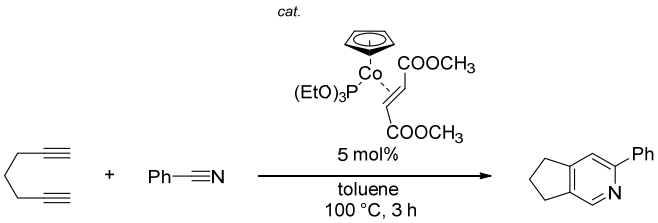


Scheme 40. indenyl Co-catalyzed [2+2+2] cycloaddition of diyne and benzonitrile.

Hapke group also demonstrated catalytic activities various Co-catalyzed asymmetric [2+2+2] cycloaddition.[39] The photochemical cycloaddition of the diynes and nitriles catalyzed by [CpCo(cod)] was found to serve as an efficient synthetic route to the construction of the heterobiaryls (Scheme 41a). The use of [CpCo(trans-$MeO_2CHC$=$CHCO_2Me$){P($OEt$)$_3$}] under microwave conditions were shown to be effective to the access of (Scheme 41b). Furthermore, the five-membered ring backbone substituents affect the configurational stability of biaryl axis.

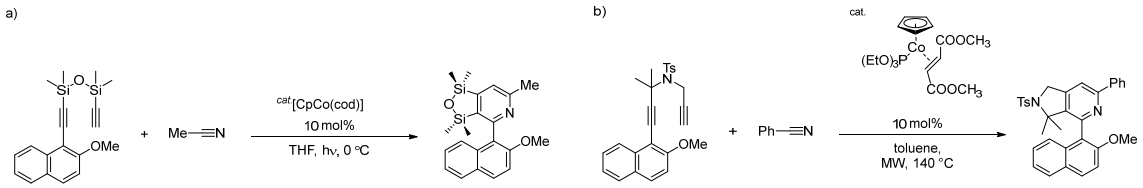


Scheme 41. Representative examples of Co-catalyzed [2+2+2] cycloaddition of diynes and benzonitrile.

In an extension of these works, Hapke et al. reported the development of Co-indenyl complex-catalyzed asymmetric [2+2+2] cycloadditions.[40] For example, the reaction of a naphthyldiyne with nitrile was performed in the presence of Co complex in THF at room temperature for 24 h under photochemical conditions. The desired arylpyridine was obtained in 86% yield and with 64% ee (Scheme 42). In another example, chiral indenyl Co catalyst succeed in enantioselective synthesis of heterobiaryl in 80% ee.

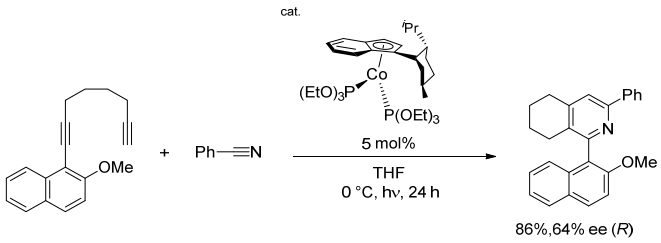


Scheme 42. Enantioselective synthesis of hetrobiaryl.

In 2017, Kawatsura et al. reported Co-catalyzed synthesis of trifluoromethyl-substituted ethyl picolinate derivatives.[41] In typical procedure, the reaction of trifluolomethyl-substituted internal alkyne and ethyl cyanoformate was carried out by using $CoI_2$ 20 mol% and dcype 40 mol% (1,2-bis(dicyclohexylphoshino)ethane) in THF for 16 h. The desired substituted picolinate was obtained in 94% (Scheme 43).

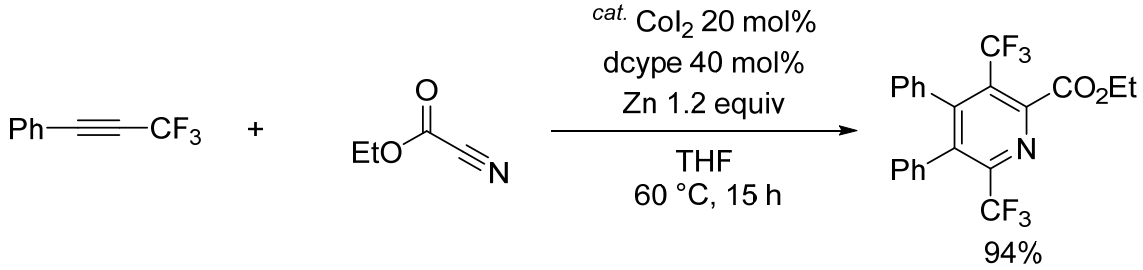


Scheme 43. Co- catalyzed [2+2+2] cycloaddition of trifluoromethyl substituted internal alkyne and cyanoformate.

2.8 Rhodium-catalyzed pyridine synthesis

The early work on Rh based [2+2+2] cycloadditions of alkynes and nitriles was performed by Tanaka et al.[42] In 2013, Gandon et al. reported [2+2+2] cycloaddition of diyne and sulfonimines.[43] In the presence of 2.5 mol% $[Rh(hexadiene)Cl]_2$ and diphosphine ligand (5 mol%), and $AgSbF_6$ (5 mol%), the reaction of diyne and oxime at 80 °C for 48 h gave the corresponding pyridine in 77% yield and 92% *ee* (Scheme 44).

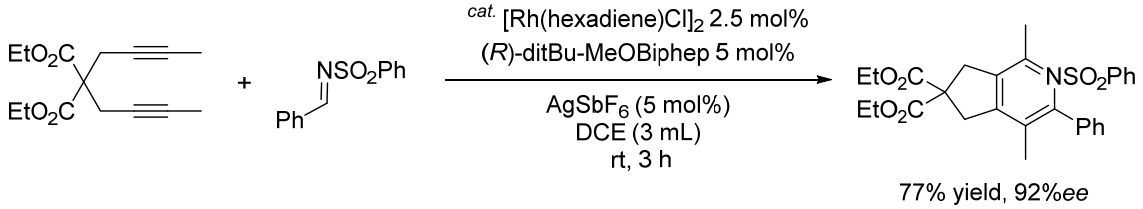


Scheme 44. Rh-catalyzed [2+2+2] cycloaddition of diyne and sulfonimine.

In 2013, Wan et al. reported the synthesis of pyridine derivatives via [2+2+2] cycloaddition of diyne and oxime.[44] In typical procedure, a mixture of diyne with oxime in the presence of 5 mol% $[Rh(cod)_2]BF_4$ combined with 6 mol% dppf(1,1'-Bis(diphenylphosphino)ferrocene) and 4Å molecular sieves (200 mg) was heated at 80 °C for 48 h. The corresponding pyridine was obtained in 69% yield (Scheme 45).

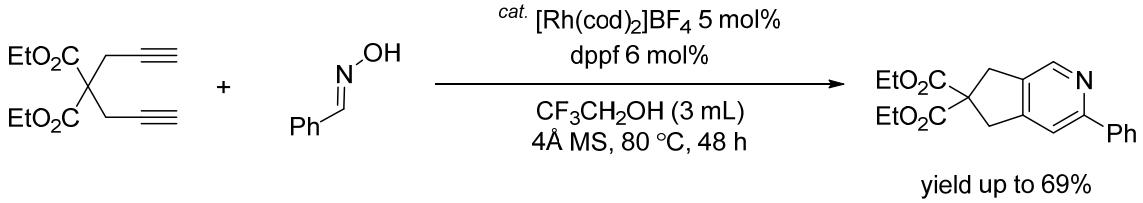


Scheme 45. Rh-catalyzed [2+2+2] cycloaddition of diyne and oxime.

In 2016, Tanaka et al. developed cationic Rh(I)/(*S*)-$H_8$-BINAP complex-catalyzed atroposelective [2+2+2] cycloadditions (Scheme 46).[45] For example, the reaction of a diyne with a nitrile was performed in the presence of $Rh(cod)_2BF_4$ (10 mol%) and (S)-$H_8$−BINAP (10 mol%) in dichloromethane at room temperature for 16 h. This produced the desired arylpyridine in 80% yield and with 99% ee. The optimized reaction tolerated a range of diynes and nitriles (up to 89% yield and 98%*ee*). Decreased enantioselectivity was observed when ortho methoxy and methoxycarbonyl substituents were present on the phenyl group of the diynes. It should be noted that when the ortho substituents were alkyl groups, the regioselectivity switched to give achiral 6-arylpyridines in high yield. The proposed reaction mechanism is shown in Scheme 47.

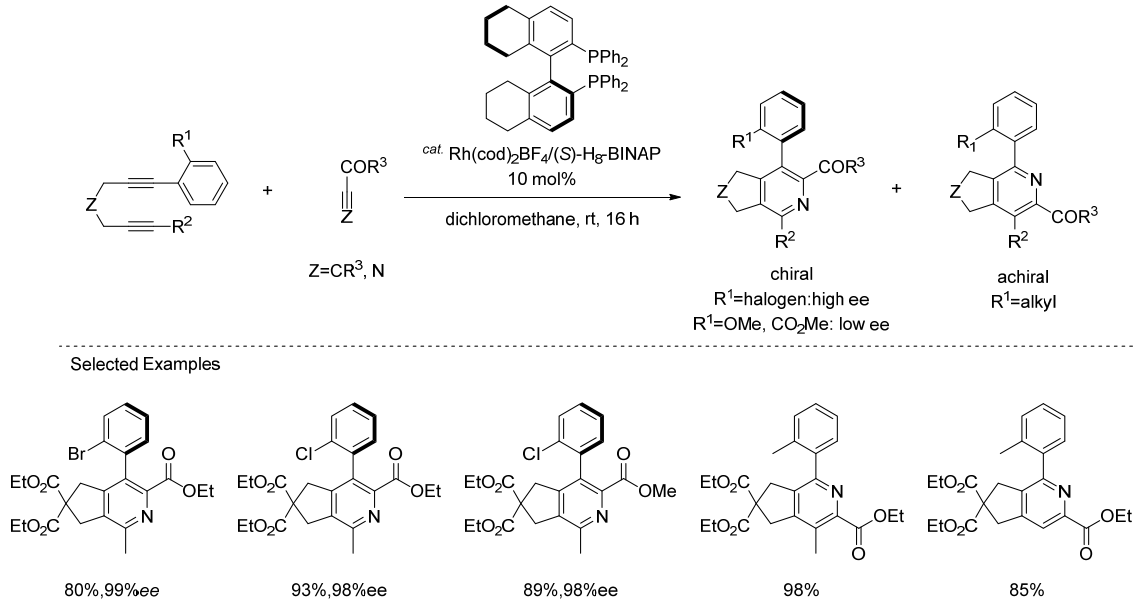


Scheme 46. Rh-catalyzed atroposelective [2+2+2] cycloaddition of diyne and nitrile.

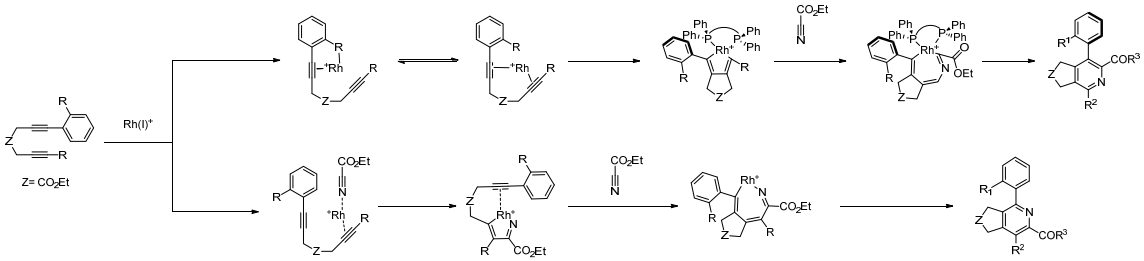


Scheme 47. Two possible reaction pathways: (a) chiral 3-arylpyridine and (b) achiral 6-arylpyridine synthesis.

2.9 Iridium-catalyzed pyridine synthesis

In 2012, Takeuchi et al. reported Ir/dppf- or BINAP-catalyzed reactions of various aliphatic nitriles.[46] Typically, penta-substituted pyridines were obtained by the reaction of 2,7-nonadiyne with benzonitrile (3 equiv) in the presence of $[Ir(cod)Cl]_2$ (1 mol%) and dppf (2 mol%). Reaction in refluxing benzene for 1 h gave the desired pyridine in 91% yield (Scheme 48). DFT calculations indicate that formal [4+2] cycloaddition is responsible for the formation of 3-aminopyridine. The enantioselective synthesis of pyridine was achieved by kinetic resolution of racemic nitrile (Scheme 49).

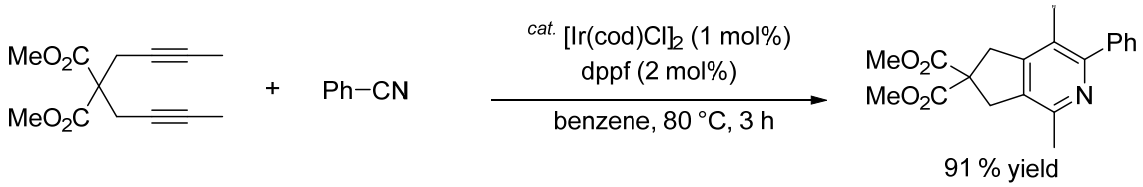


Scheme 48. Ir/BINAP-catalyzed [2+2+2] cycloaddition of diyne and nitrile.

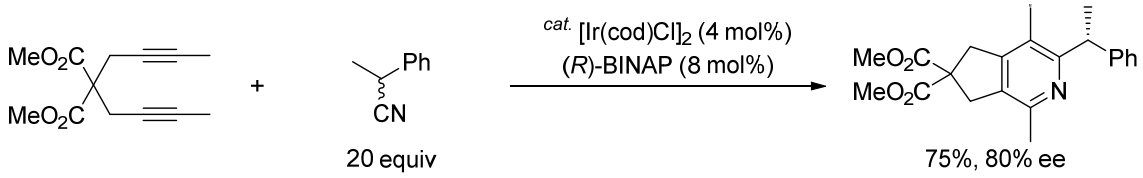


Scheme 49. Enantioselective cycloaddition of diyne and nitrile.

Takeuchi and co-workers showed that the same Ir/biphosphine catalytic system could be used for the cycloaddition of an α,ω-diyne and acyl cyanide.[47] The $[Ir(cod)Cl]_2$/*rac*-BINAP combination generates a highly active catalyst, which was used for regioselective [2+2+2] cycloaddition of diyne and acyl cyanide to give the desired acylpyridine in 99% yield (Scheme 50). Although it is difficult to introduce functional groups at the 2-position of pyridine, [2+2+2] cycloaddition of α,ω-diynes with aliphatic, aromatic, or heteroaromatic acyl cyanides gave 2-acylpyridines.

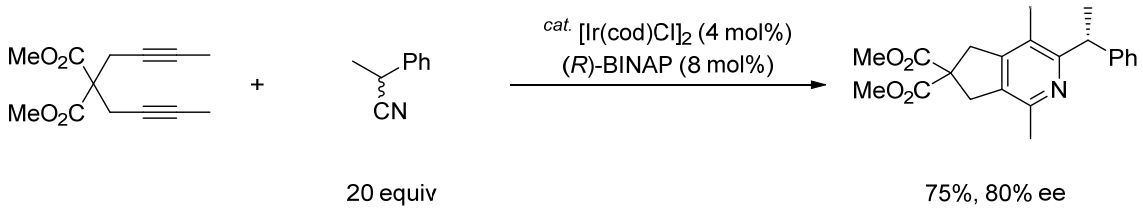


Scheme 50. Synthesis of 2-acylpyridine catalyzed by $[Ir(cod)Cl]_2$/*rac*-BINAP.

In an extension of these works, synthesis of multisubstituted azatriohenylene reported by Takeuchi group.[48] In typical procedure, a mixture of biaryl-linked diyne and nitrile was added to $[Ir(cod)Cl]_2$ (1 mol%) and dppf (2 mol%) in toluene. The corresponding azatriphenylene was obtained in 91% yield (Scheme 51). Various nitrile and functionalized biaryl-linked diyne can be applied to [2+2+2] cycloaddition.

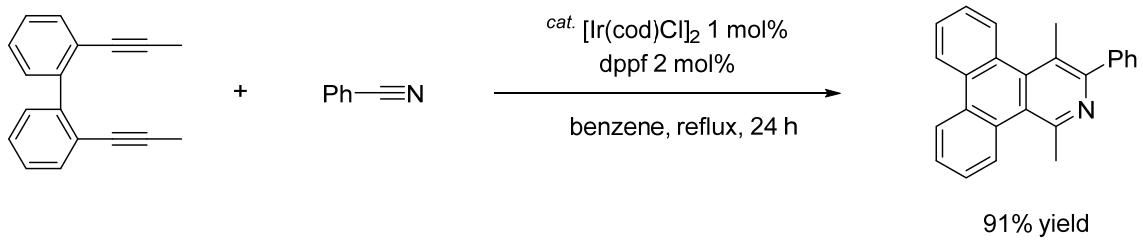


Scheme 51. Ir-catalyzed [2+2+2] cycloaddition of biaryl-linked diyne with nitrile.

## Ni- and group 11 metals (Cu, Au)-mediated /catalyzed pyridine synthesis

2.10 Nickel-catalyzed pyridine synthesis

In 2011, Louie et al. disclosed the reaction mechanism of the Ni-NHC-catalyzed [2+2+2] cycloaddition of diynes and nitriles.[49] For example, the reaction of diyne with cyanamide in the presence of $Ni(cod)_2$ (5 mol%) and IPr [IPr = 1,3-bis(2,6-diisopropylphenyl) imidazolidine] (10 mol%) gave the 2-aminopyridine in 99% yield (Scheme 52). The proposed catalytic cycle, which is based on a subsequent mechanistic study, is shown in Scheme 53.[50] This reaction is initiated by selective binding of the nitrile over alkyne (A). Subsequent IPr ligand loss and oxidative heterocoupling of an alkyne and the nitrile occur at the Ni center (B). Insertion of a second alkyne leads to the nickelacyclic cycloheptatriene intermediate (C). Reductive elimination and IPr coordination complete the catalytic cycle and produce the corresponding pyridine derivative.

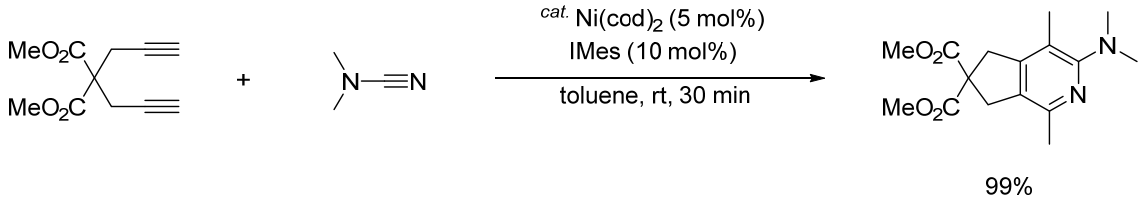


Scheme 52. Ni/$IPr_2$-catalyzed 2-aminopyridine synthesis.

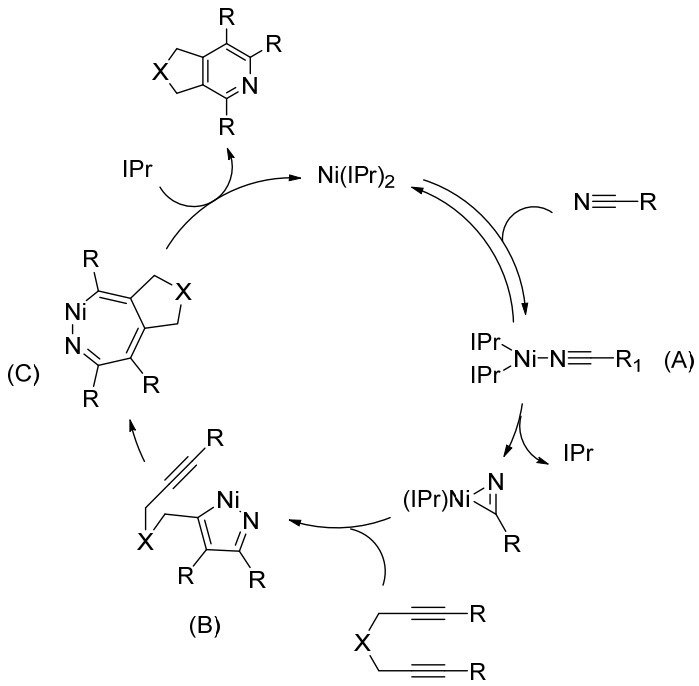


Scheme 53. Proposed catalytic cycle in the Ni catalyzed [2+2+2] cycloaddition

Louie's group later reported the use of catalytic amounts of $Ni(cod)_2$ and SIPr [SIPr = 1,3-bis(2,6-diisopropylphenyl)imidazolidine] in 3,5-disubstituted 2-iminopyridine synthesis (Scheme 54).[51] In a typical procedure, a mixture of 1-pentyne and *N*-butyl-*N*-tosylcyanamide was added to $Ni(cod)_2$ (5 mol%) and SIPr (10 mol%) in toluene. The mixture was stirred at room temperature for 4 h. The corresponding 2-aminopyridine was obtained in 68% yield and 3-aminopyridine was obtained in 5% yield as a by-product.

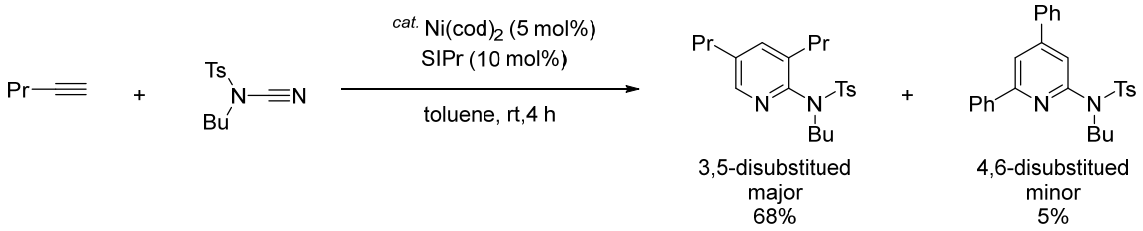


Scheme 54. Ni/SIPr-catalyzed 3,5-disubstituted 2-aminopyridine synthesis.

In 2016, Ogoshi et al. reported Ni-catalyzed synthesis of dihydropyridine by [2+2+2] cycloaddition of imines with alkynes.[52] The combination of imine, $Ni(cod)_2$ (2 mol%), and IMes (2 mol%) generates a highly active catalyst, which can be used for regioselective [2+2+2] cycloaddition with alkynes (Scheme 55). The stoichiometric reaction imine and 2-methyl-1-hexen-3-yne gave aza-niclelacycle in 77% isolated yield (Scheme 56). The five-membered aza-nickelacycle would be considered as a key intermediate of the [2+2+2] cycloaddition.

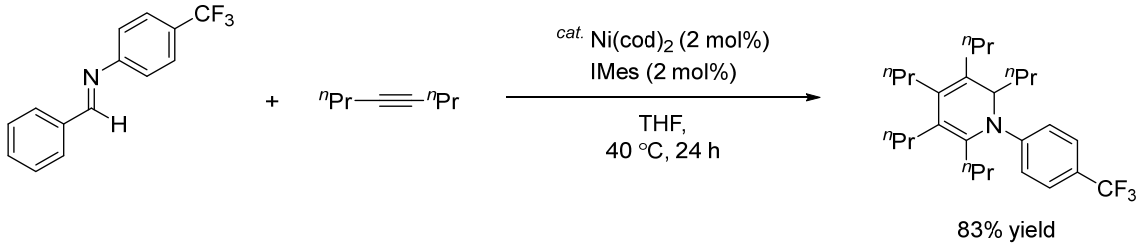


Scheme 55. Ni/IMes-catalyzed [2+2+2] cycloaddition of imine and alkyne.

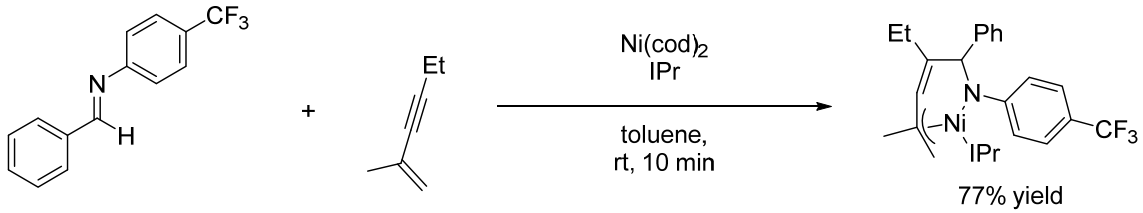


Scheme 56. The isolation of ( $\eta^2$-*N*–aryl imine) nickel (0) complex.

In 2016, Liu et al. reported the synthesis of fused pyridines by using a combination of Ni and a Lewis acid.[53] The combination of $Ni(cod)_2$ (5 mol%), $PBu_3$ (10 mol%), and $BPh_3$ (20 mol%) generates a highly active catalyst, which can be used for regioselective [2+2+2] cycloaddition of alkynenitriles with alkynes (Scheme 57). Mechanistic experiments indicated that $BPh_3$ assisted formation of an aza-nickelacycle.

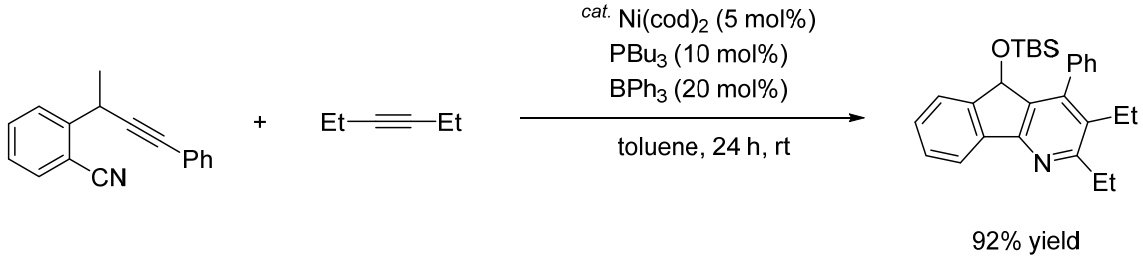


Scheme 57. Ni/$BPh_3$-catalyzed [2+2+2] cycloaddition of alkyne and cyanamide.

In 2017, Liu et al. reported a $NiCl_2$(DME)/dppp/Zn catalytic system for [2+2+2] cycloaddition of functional alkynenitriles with alkynes.[54] Typically, δ-carbolines are derived from ynamide-nitrile with 3-hexyne in the presence of a catalytic amount (10 mol%) of $NiCl_2$(DME). The addition of dppp (10 mol%) and Zn (1 equiv) and subsequent reaction in 1,4-dioxane at room temperature for 2.5 h gives the desired δ-carboline in 96% yield (Scheme 58). It has been proposed that the Lewis acid coordinates with an imine group, which facilitates the reductive elimination step (Scheme 59).

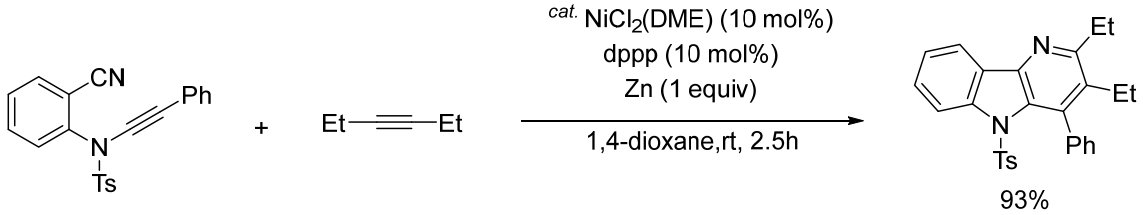


Scheme 58. Ni-catalyzed [2+2+2] cycloaddition of alkynenitrile with alkyne.

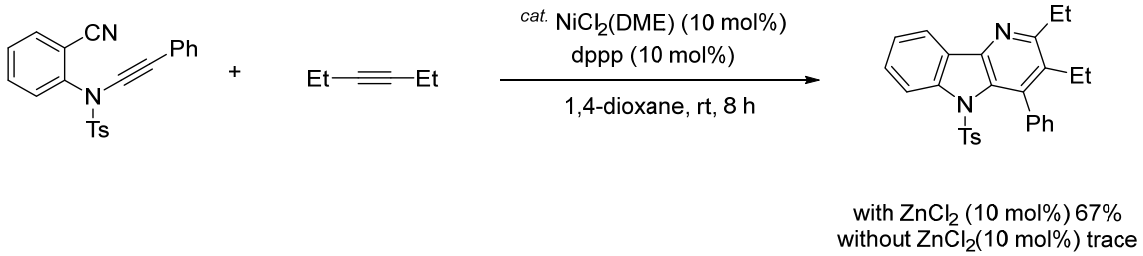


Scheme 59. Control experiment to explore role of $ZnCl_2$.

## 2.11 Copper-catalyzed pyridine synthesis

In 2013, Chen's group reported $Cu(OTf)_2$catalyzed [2+2+2] pyridine synthesis.[55] The combination of $Cu(OTf)_2$ (10 mol%) diaryliodoniums, and benzonitrile generates anactive catalyst, which can be used for regioselective [2+2+2] cycloaddition with alkynes. The corresponding pyridine was obtained in 83% yield (Scheme 60).

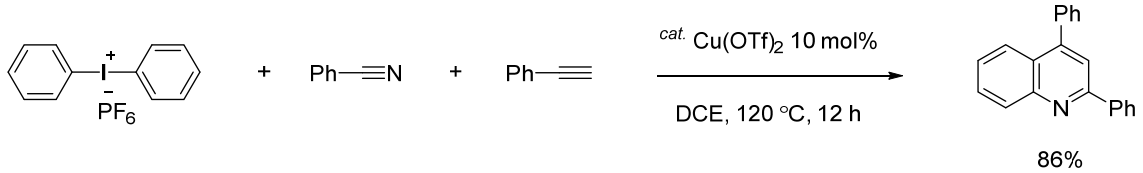


Scheme 60. Cu-catalyzed three-component cycloaddition for substituted quinolines

In 2017, [2+2+2] cycloaddition for pyridine reported Chen's group also reported CuBr-catalyzed pyridine synthesis via cycloaddition.[56] In a typical procedure, a solution of the vinylliodonium salt and benzonitrile was heated at 130 °C in the presence of $Cu(OTf)_2$ for 12 h, the corresponding pyridine was obtained in 92% yield (Scheme 61). The alkenylation of nitrile with vinyliodonium salts catalyzed by CuBr and react with alkynes.

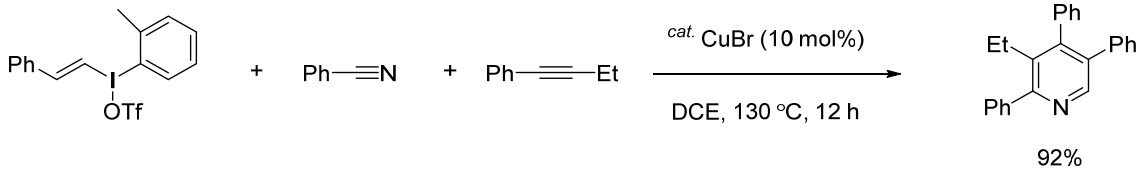


Scheme 61. Cu-catalyzed pyridine synthesis vinyliodonium, nitrile, and alkynes.

## 2.12 Gold-catalyzed pyridine synthesis

Liu et al. reported a Au-complex-catalyzed [2+2+2] pyridine synthesis (Scheme 62).[56] In this method, [$Ph_3PAuNTf_2$] serves as a π-acid in the reaction to alkynes. Cycloaddition of ynamides and nitriles was achieved with good chemoselectivity (pyridine/pyrimidine). Scheme 63 shows the reaction mechanism. The reaction is initiated by Au coordination with an ynamide. Then a second ynamide attacks the Au(I)–π-alkyne to generate a 1-azaallenium species. Subsequent reaction with a nitrile produces the desired 2,4-diaminopyridine.

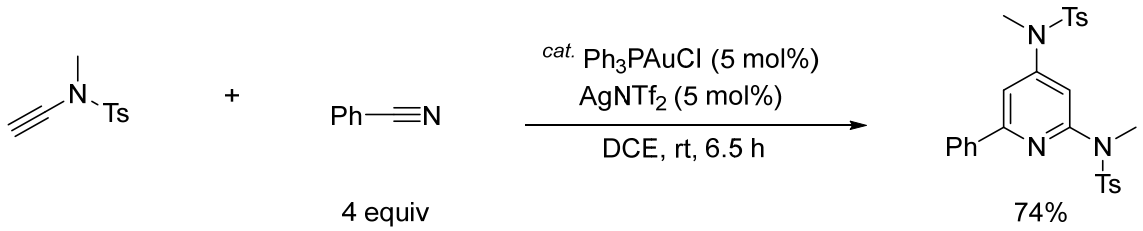


Scheme 62. Au-catalyzed [2+2+2] cycloaddition of ynamide and nitrile.

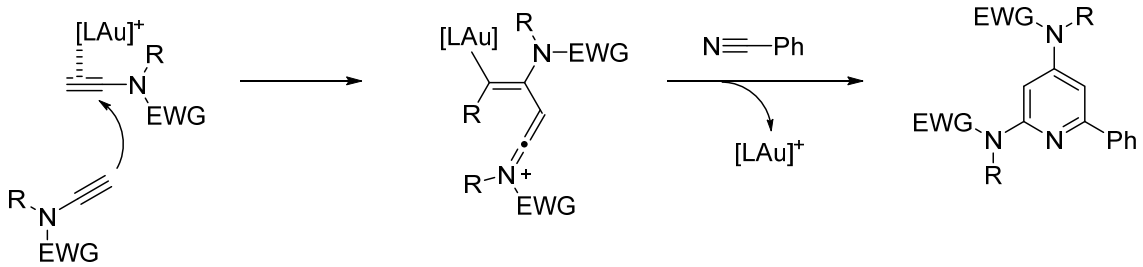


Scheme 63. A plausible reaction mechanism for pyridine synthesis.

## 3. Synthesis of pyrimidines

### Early-transition metal mediated/catalyzed pyrimidine synthesis

3.1 Zirconium-mediated/catalyzed pyrimidine synthesis

In 2013, Liu and co-authors reported a zirconium-mediated synthesis of pyrimidines (Scheme 64).[58] In a typical procedure, a zirconocene–butadiyne complex derived from 1,4-bis(*tert*-butyldimethylsilyl)buta-1,3-diyne (0.5 mmol) was reacted with benzonitrile (1.5 mmol) at 80 °C for 5 h in toluene. The desired pyrimidine was obtained in 81% yield. The reaction of an aliphatic nitrile with the zirconocene–butadiyne complex gave enynyl ketones after hydrolysis. This indicates formation of azazirconacycle (Scheme 65).

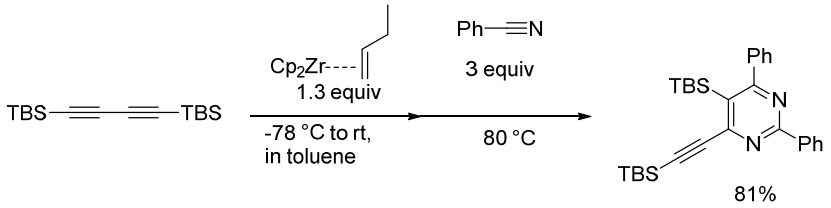


Scheme 64. Zr/butadiyne-complex-mediated [2+2+2] cycloaddition for pyrimidine synthesis.

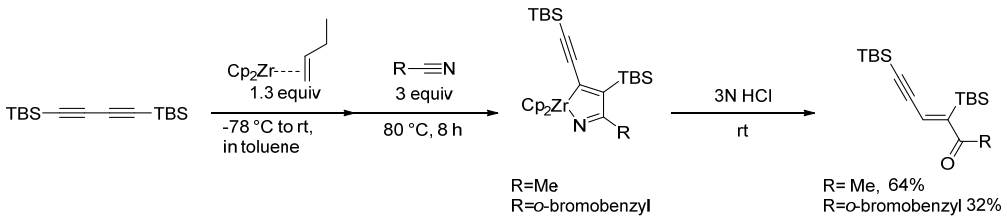


Scheme 65. Formation of enynyl ketones by hydrolysis of aza-zirconacycle.

More recently, Agapie and co-workers reported synthesis and use of a Zr–bisphenoxide ligand complex to catalyze pyrimidine synthesis (Scheme 66).[59] The redox-active complex $Zr^{IV}$–$Anth^{red}$ was derived by photolytic reduction. This transformation proceeds in the presence of 5 mol% of the $Zr^{IV}$–$Anth^{red}$ complex and leads to pyrimidines.

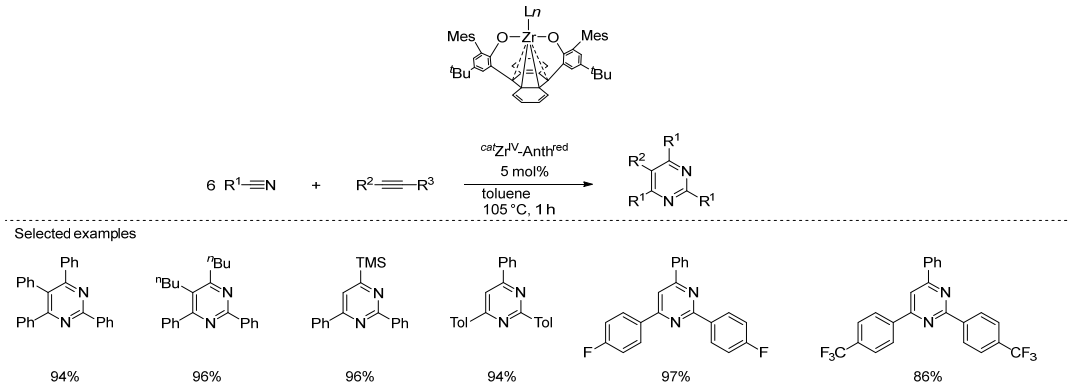


Scheme 66. Zr/anthracene-based ligand complex-catalyzed [2+2+2] cycloaddition of nitriles and alkynes to pyrimidines.

3.2 Niobium-mediated/catalyzed pyrimidine synthesis

In 2012, Obora and co-workers reported $NbCl_5$-mediated pyrimidine synthesis via cycloaddition.[60] In a typical procedure, a solution of alkyne (1 mmol) and benzonitrile (2 mL) was heated at 60 °C by adding $NbCl_5$ (0.2 mmol) in six portions, one every 2 h, over 22 h, the corresponding pyrimidine was obtained in 86% yield (Scheme 67).

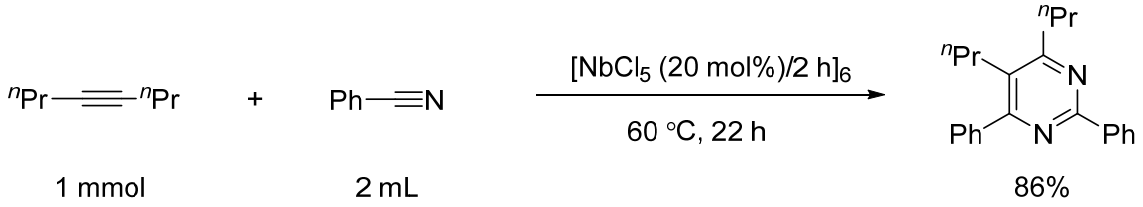


Scheme 67. $NbCl_5$ mediated pyrimidine synthesis.

In 2017, Fuji and Obora reported $FeCl_3$-assisted $NbCl_5$-catalyzed [2+2+2] pyrimidine synthesis.[61] In the presence of $NbCl_5$ (20 mol%) and $FeCl_3$ (2 equiv), the reaction of 3-hexyne and benzonitrile gave the corresponding pyrimidine in 83% yield (Scheme 68). FT-IR analysis was performed to clarify the roles of $NbCl_5$ and $FeCl_3$. The affinity of $NbCl_5$ toward the nitrile is higher than that of $FeCl_3$. The initial nitrile activation is assisted by $NbCl_5$ then $FeCl_3$ serves as a sacrificial reagent (Scheme 69).

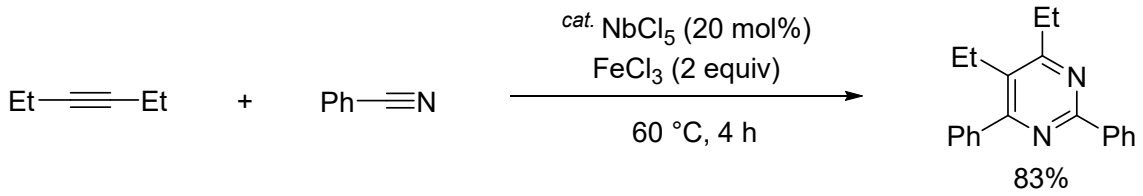


Scheme 68. Nb-catalyzed [2+2+2] cycloaddition of alkyne and nitrile.

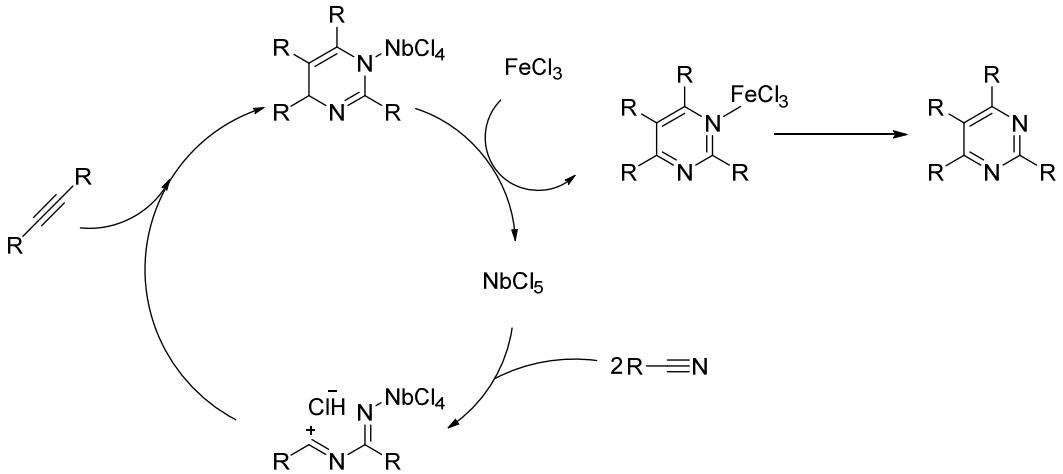


Scheme 69. Plausible mechanism of catalytic pyrimidine synthesis.

## Late-transition metal mediated/catalyzed pyrimidine / quinazoline synthesis

3.3 Iron-catalyzed pyrimidine synthesis

An Fe/$^{iPr}$PDAI system was found to be an effective catalyst for the [2+2+2] cycloaddition of alkynenitriles and cyanamides (Scheme 70).[62] The reaction of alkynenitrile and cyanamide with $FeI_2$ (5 mol%), $^{iPr}$PDAI (10 mol%), and Zn (30 mol%) in toluene at 40 °C gave the corresponding 2-aminopyrimidine in 90% yield.

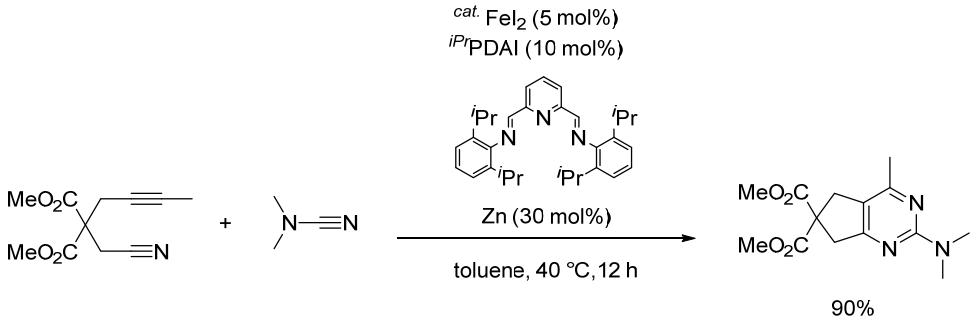


Scheme 70. Fe/$I^{Pr}$PDAI-catalyzed 2-aminopyridine synthesis.

3.4 Copper-catalyzed quinazoline synthesis

In 2013, Chen group reported Cu-catalyzed synthesis of quinazoline derivertives.[63] In a typical procedure, a solution of diphenyliodonium and benzonitrile was heated at 130 °C in the presence of $Cu(OTf)_2$ for 12 h and the corresponding quinazoline was obtained in 84% yield (Scheme 71).

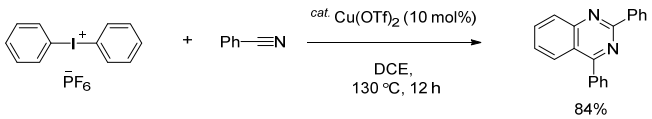


Scheme 71. Cu-catalyzed quinazoline synthesis via [2+2+2] cycloaddition.

3.5 Gold-catalyzed pyrimidine synthesis

In 2014, Liu et al. reported a Au-catalyzed 4-aminopyridine synthesis.[64] The reaction of *N*-methyl-*N*-(phenylethynyl)methanesulfonamide and benzonitrile in the presence of $Ph_3AuCl/AgNTf_2$ (5 mol%) in 1,2-dicholomethane at 75 °C for 4 h gave the corresponding 4-aminopyridine in 95% yield (Scheme 72).

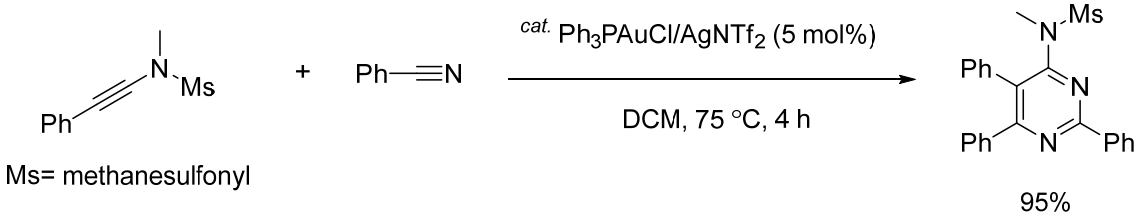


Scheme 72. Synthesis of 4-pyrimidines catalyzed by $Ph_3AuNTf_2$.

A DFT computational study indicated that Au(I)-alkyne species are more active than the Au(I)–nitrile intermediate in nucleophilic attack of the second nitrile (Scheme 73).[65]

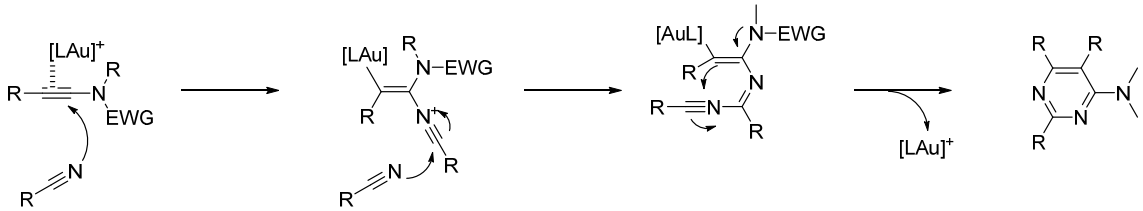


Scheme 73. Proposed reaction mechanism of Au-catalyzed pyridine synthesis.

## 4. Synthesis of triazines

Because of the low reactivity of nitriles, the catalyst-free trimerization of a C–N triple bond requires extremely harsh conditions such as high pressures (35 000–50 000 atm) and high temperatures (350–500 °C).[66] Strong acids e.g., $H_2SO_4$ and $Tf_2O$ or a base, e.g., NaH or EtONa, promote nitrile trimerization.[67] The reaction of bis(silyl-substituted) methyllithium and a hydrogen-free nitrile is shown in (Scheme 74).[68] The reaction of benzonitrile (10 mmol) in the presence bis(silyl-substituted) methyllithium (1.3 mmol) results in formation of the desired triazine in 91% yield. Because of the presence of an α-hydrogen, alkylnitriles do not give the corresponding triazines.

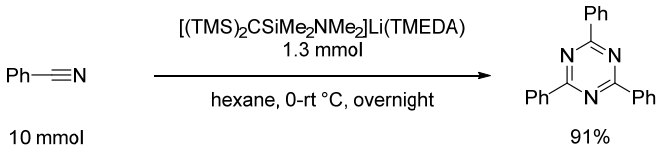


Scheme 74. Bis(silyl-substituted)-methyllithium-mediated triazine synthesis.

In 2012, Hulliger et al. reported that $ZnCl_2$ catalyzes the synthesis of 2,4,6-trisubstitued triazines at 250–300 °C. The products are obtained in good yields.[69] For example, the reaction of bromobenzonitrile and $ZnCl_2$ (molar ratio 5:1) at 270 °C for 60 h gave the corresponding 2,4,6-tris(4-bromophenyl)-1,3,5-triazine in 69% yield (Scheme 75).

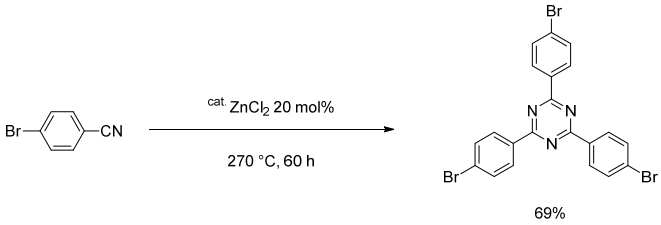


Scheme 75. $ZnCl_2$-catalyzed triazine synthesis.

In 1988, Sanders and co-workers reported that yttrium (III) triflate or lanthanum triflate catalyzed ammonia-assisted nitrile trimerization.[70] In the presence of 1 mol% $Y(OTf)_3$, the reaction of a 1:1 molar mixture of benzonitrile and ammonia at 200 °C for 24 h gave the corresponding triazine in 100% yield (Scheme 76).

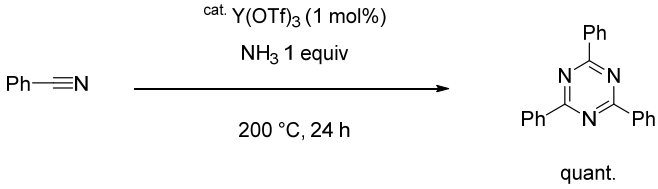


Scheme 76. Yttrium (III) trifluoromethanesulfonate-catalyzed triazine synthesis.

In 2002, Shen et al. reported $SmI_2$-catalyzed nitrile cyclotrimerization in the presence of amine co-catalysts.[71] In a typical procedure, a mixture of $SmI_2$ (2.5 mol%), hexylamine (20 mol%), and benzonitrile was stirred at 80 °C for 3 h. The desired triazine was obtained in 96% yield (Scheme 77). Various arylnitriles gave the corresponding *s*-triazines. The proposed reaction mechanism is shown in Scheme 78. The amine co-catalyst assists formation of an amidine intermediate.

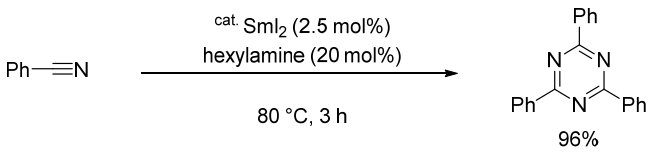


Scheme 77. $SmI_2$/amine-catalyzed synthesis of *s*-triazine.

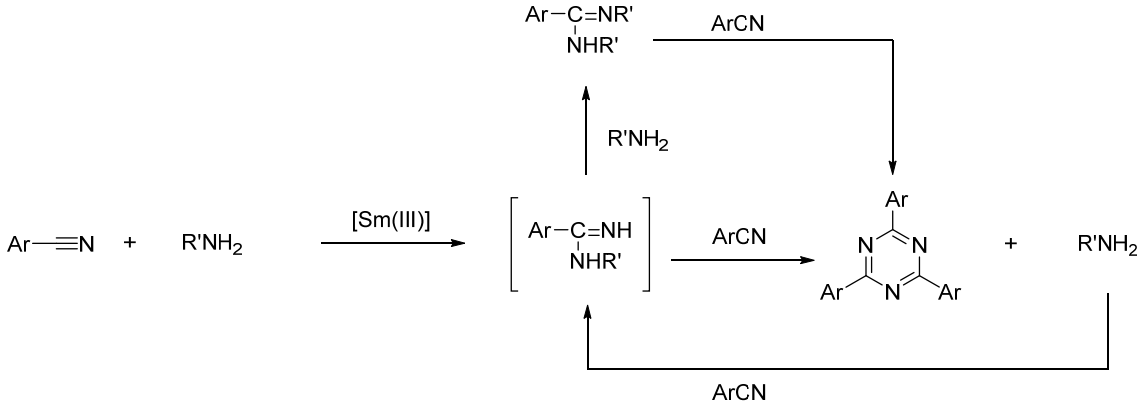


Scheme 78. Plausible reaction mechanism for Sm(II) complex/*n*-hexylamine catalysis.

## *Part B*

## *N, N* -Dimethylformamide-protected single-sized metal nanoparticles and their use as catalysts for organic transformations

1. General mechanism of synthesis of DMF-stabilized metal nanoparticles.

DMF is a well-known as high boiling point and polar solvent in organic chemistry.[1] Because of its structure, the use of DMF has been explored in a wide range of applications, e.g., as a reagent in colloidal synthesis. Because of the high oxidation potential of DMF (1.9 V vs SHE),[2] it can reduce metal salts and form NPs in the solution phase.[3] In early studies of DMF-based reduction of metal precursors and nanocrystal synthesis, Liz-Marzán and coworkers used PVP as a capping agent.[4] DMF based reduction method advantage, Metal ion reduction rate depends on DMF decomposition. The reduction rate can be controlled by a various parameter (temperature and metal precursor concentration) various Metal NPs/NCs can be obtained with narrow size distribution.[3] The proposed reduction mechanism is shown in eq 1; carbamic acid is readily oxidized to $CO_2$ and $(CH_3)_2NH$.[2,3]

(1)

In other reduction pathways, formic acid generated from DMF decomposition serves as a reductant for the metal precursor; CO or $H_2$ reduces metal ions (eq 2).

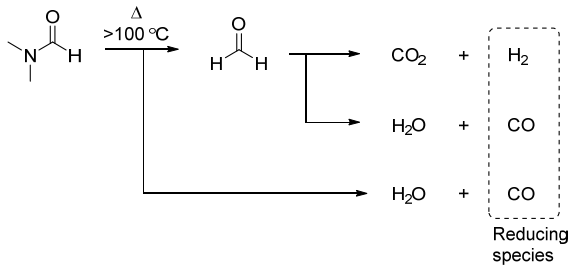


(2)

DMF also acts as a protectant in surfactant-free synthesis. Surfactant-free Au NPs was first synthesized by Li and coworkers as fluorescent quantum dots.[4] Since 2011, Kawasaki and our group have reported external-surfactant- and stabilizer-free syntheses of various M NPs and their use as organic transformation catalysts.[5]

2. DMF-stabilized metal nanoparticles and nanoclusters for organic transformations

2.1.Palladium

DMF-stabilized Pd NCs were synthesized from $PdCl_2$. Our group reported the synthesis and cross-coupling catalytic activities of DMF-protected Pd NCs. The Pd NCs showed high catalytic activities in the Suzuki–Miyaura cross-coupling and Mizoroki–Heck reactions (eqs. 3 and 4).[6] High turnover numbers (TONs) were achieved, i.e., $4.5 \times 10^5$ and $6.0 \times 10^8$.The DMF-stabilized Pd NCs showed higher TONs than polymer micelles stabilized Pd NPs up to $2.8 \times 10^5$. The DMF-stabilized Pd NCs were recyclable. The Pd NCs were separated from the substrates and products by simple extraction with hexane/DMF (Scheme 2). The Pd NCs were recycled at least five times without significant loss of activity.

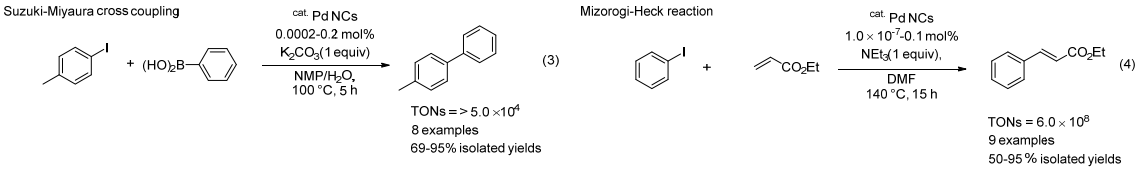


**Scheme 2 Procedure for recycling Pd NCs**

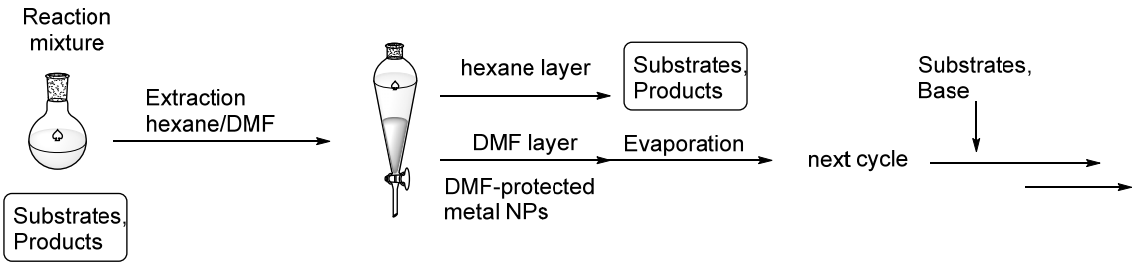


In 2013, DMF-stabilized Pd NCs were used to catalyze the Migita–Kosugi–Stille coupling reaction (eq 5).[7] Reactions of aryl halides with tributylphenyl-/tributyl-vinylstannane gave the corresponding cross-coupling products. The Pd NCs gave high TONs (up to $3.5 \times 10^4$).

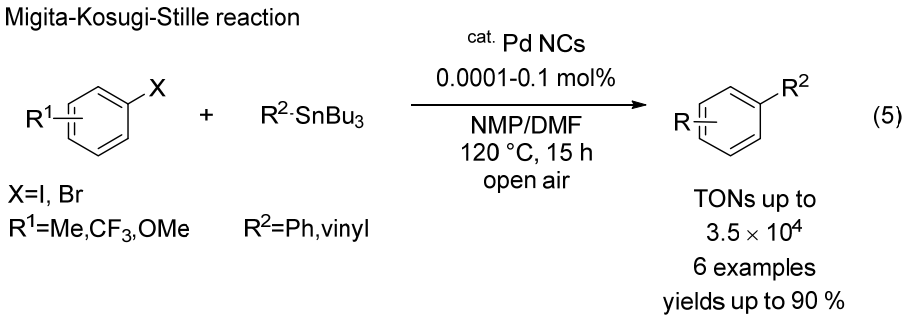

Indole derivatives are key motifs in many bioactive compounds. The reaction of 2-haloanilines with alkynes, namely the Larock indole synthesis, is a useful method for accessing indole motifs. DMF-stabilized Pd NCs successfully catalyzed the synthesis of 2,3-disubstituted indoles from 2-iodoanilines and internal alkynes under external-ligand-free conditions at low catalyst loadings (0.3 mol%) (eq 6).[8] The Pd NC catalyst can be reused at least three times.

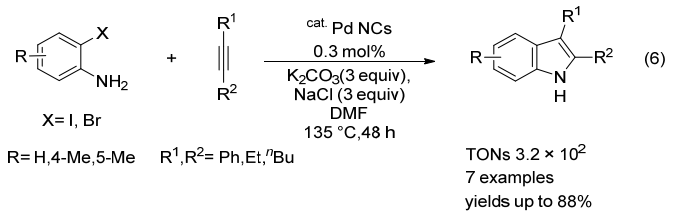


Sanda and our group achieved Sonagashira–Hagihara (eq 7) and Mizoroki–Heck coupling (eq 8) polymerization by using DMF-stabilized Pd NCs as the catalyst.[9]

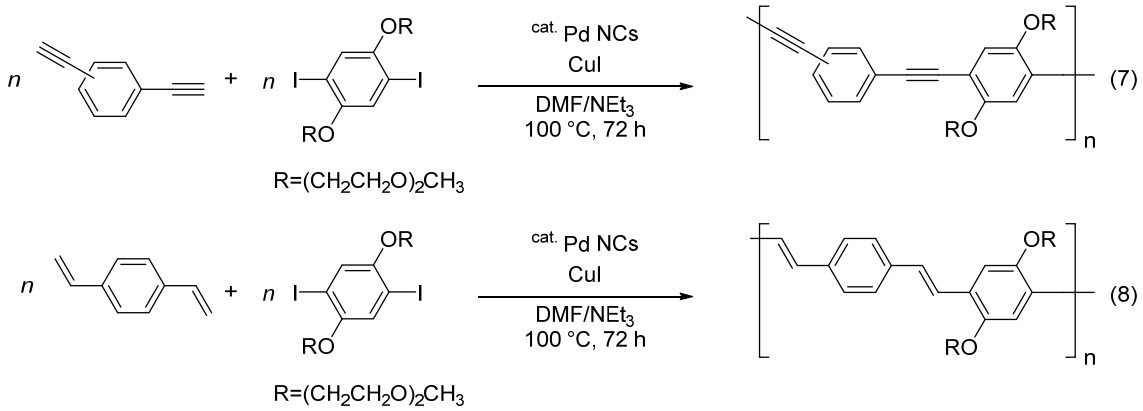


The catalytic reaction provided poly(phenyleneethynylene)s and poly(phenylenevinylene) of moderate molecular weights ($M_n$ 6700 and 5900). These results are similar to those achieved with conventional $PdCl_2(PPh_3)_2$ and $Pd(PPh_3)_4$ complex catalysts. The ligand-free Pd NC polymerization system avoids contamination of the growing polymer by ligand-derived phosphorus impurities.

2.2.Gold

Kawasaki and coworkers investigated the catalytic activities and specific properties of Au NPs.[10] The DMF-stabilized Au NCs consisted on average of 13 Au atom clusters. FT-IR and $^1$H-NMR spectroscopic investigations showed a strongly coordinated DMF layer around the Au NCs. These DMF-stabilized Au NCs catalyzed reduction of 4-nitrophenol to 4-aminophenol by $NaBH_4$ (eq 9). An induction time (~3000 s) was observed, which indicates that the DMF layer hindered access to catalytically active site. Thermally aged Au NCs had a shorter induction time (~100 s at 80 °C for 8 h).

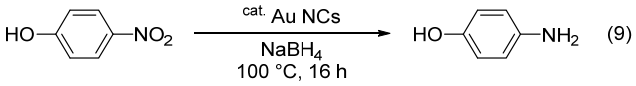

(9)

Lang et al. reported DMF-stabilized Au NPs of three different sizes (1.0, 2.5, and 5.5 nm).[11] The solution temperature and nucleation time were used to control the particle size. The catalytic activities of these three Au NPs in the Ullmann homocoupling reaction were evaluated (eq 10).

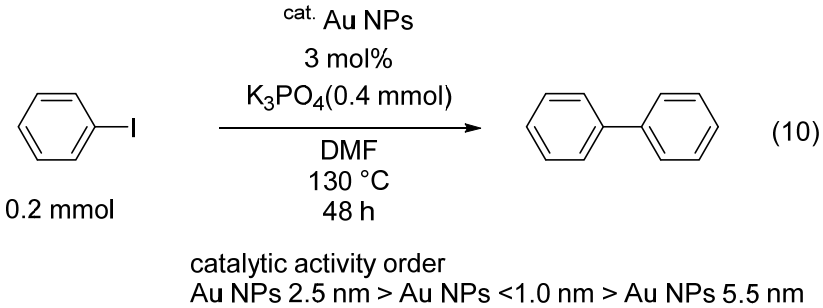

(10)

The order of the catalytic activities was Au (2.5 nm) > Au (<1 nm) > Au (5.5 nm). These Au NPs were stable. They were recycled fewer than three times and their catalytic activity gradually decreased.

2.3.Copper

DMF-stabilized Cu NPs were prepared from $CuCl_2$. The particle size was determined by TEM and DLS (2–7 nm). The catalytic activity in Ullmann-type cross-coupling of aryl halides with phenol derivatives under ligand-free conditions was evaluated (eq 11);[12] the reaction of iodobenzene (1.5 mmol) with 3,5-dimethyphenol (1.0 mmol) was used as a model reaction. When this reaction was performed in the presence of DMF-protected Cu NPs (0.2 mol%) and $Cs_2CO_3$ (2.0 mmol) in DMF at 110 °C for 24 h. the corresponding product was obtained in 92% yield. The DMF-stabilized Cu NPs showed high catalytic activity (TONs up to $2.2 \times 10^4$). The Cu NPs can be reused three times.

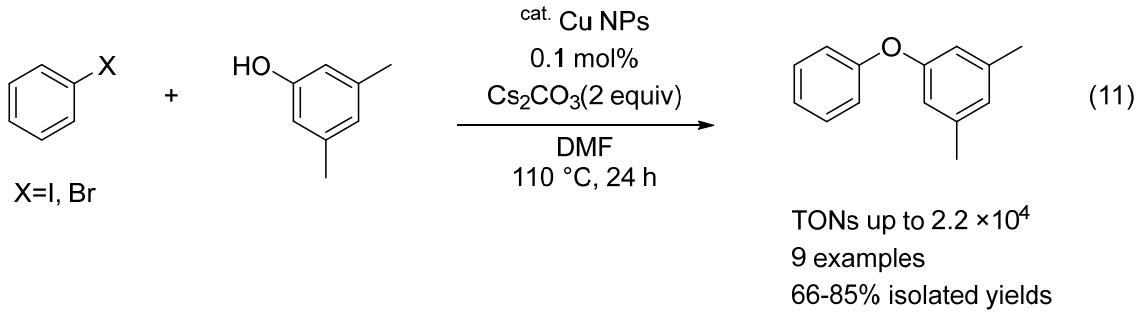


The Sonogashira–Hagihara coupling reaction is a powerful tool for obtaining acetylenes. The DMF-stabilized Cu NPs showed high catalytic activity in this reaction (eq 12).[13] In a typical procedure, a mixture of iodobenzene (0.5 mmol), phenylacetylene (0.75 mmol), and $PPh_3$ (10 mol%) in DMF (1 mL) was heated at 135 °C for 24 h in the presence of DMF-stabilized Cu NPs (0.2 mol%). The corresponding product was obtained in 96% yield. The presence of $PPh_3$ or bipyridine (bpy) was necessary for this reaction. TEM observations from a reaction mixture showed that the Cu NPs retained their single-nano-sized structure after the catalytic reaction. The DMF-stabilized Cu NPs are themselves inactive, but they act as a catalyst precursor when $PPh_3$ and bpy are used as additives. Some of the DMF dissociates from the Cu NPs, and in situ- generated $PPh_3$-stabilized Cu NPs catalyze the Sonogashira cross-coupling.

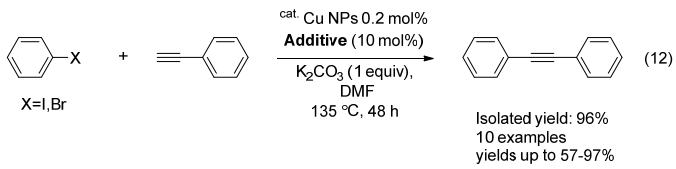


| Additive | | | | |
|---|---|---|---|---|
| none | $PPh_3$ | $PCy_3$ | dppe | bpy |
| 7% | >99% | trace | trace | >99% |

## 2.4.Iron

Iron oxide NPs were prepared from $Fe(acac)_3$ under open-air conditions. The DMF-stabilized Fe oxide NPs were characterized by XANES and XPS. The Fe oxide NPs were identified as α-$Fe_2O_3$. The $Fe_2O_3$ NPs were efficient catalysts in hydrosilylation of alkenes (eq 13).[14] Various alkenes and primary/secondary hydrosilanes were used under these conditions and the corresponding hydrosilylation products were obtained in moderate to good yields. Alkenes with various functional groups were tolerated in this reaction. The $Fe_2O_3$ NPs were recycled multiple times. Catalyst pre-activation process was not needed prior to their reuse. The $Fe_2O_3$ NPs maintained nanosized particles even after fifth run.

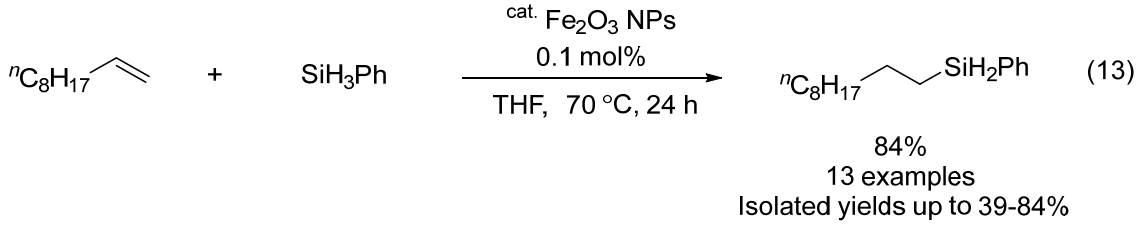


2.5.Iridium

DMF-stabilized Ir NCs were prepared from $IrCl_3$. The particle diameter was determined to be 1–1.5 nm from HR-TEM images. Ir complexes are generally efficient catalysts in alkylations with alcohols, which involve a hydrogen-borrowing reaction.[15] In particular, methylation is a widely used modification in medicinal chemistry. Methylation uses hazardous reagents, e.g., $(CH_3O)_2SO_4$ and MeI. Methylation using methanol as the C1 source is a challenging transformation. However, methanol oxidation requires harsh conditions. DMF-stabilized Ir NCs showed high catalytic activity in promoter-free methylation of anilines by alcohols.[16] In a typical procedure, the reaction of 1-phenyl-1-ethanol with methanol (2 mL) in the presence of Ir NCs (0.1 mol%) and $Cs_2CO_3$ gave the desired dimethylated product in 94% yield with high alcohol selectivity (eq 14). $[Cp^*IrCl_2]_2$ and $[IrCl(cod)]_2$ known to be a good catalyst for a-methylation resulted in lower 25%, 21% yields. Monomethylation at the β-carbon (eq 15) and *N*-alkylation of anilines (eq 16) were achieved under modified conditions. The DMF-stabilized Ir NCs have high catalytic activity in *N*-methylation. A high TON was achieved for *N*-methylation of anilines (up to 310000).

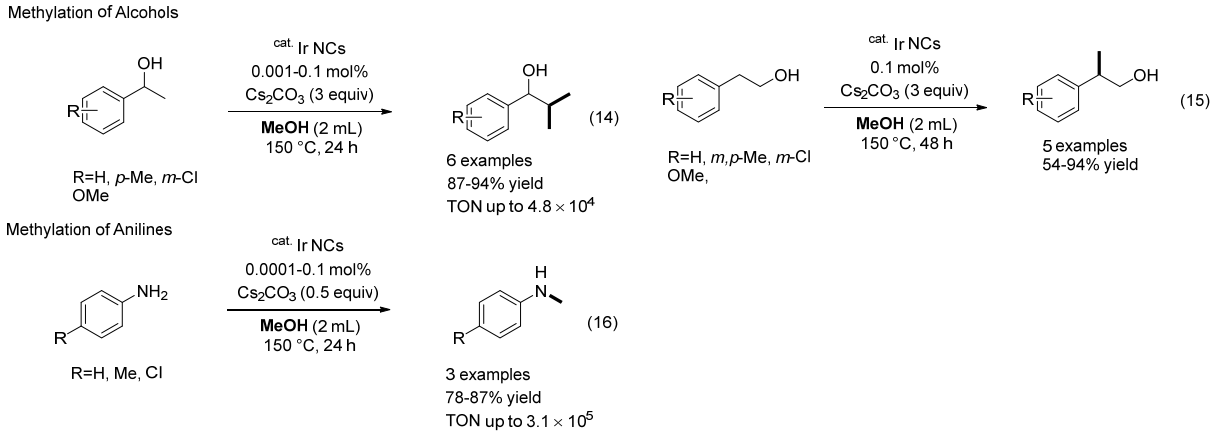

In these metal nanoparticle syntheses, DMF served as a stabilizer, reductant, and solvent. In the DMF-stabilized M NPs and NCs, the DMF molecules surrounded the surface of the metal center. The DMF stabilized M NPs/NCs are thermally stable (at 150 °C) as thiolate stabilized M NCs. Whereas strongly binding ligand (thiolates, phosphines) also acts catalyst poison, surface capping DMF does not hinder catalytic reactions. The resulting M NPs were stable for a long time, which hampered aggregation during catalytic reactions. The DMF-stabilized M NPs showed high catalytic activities (TONs and selectivities). Partial liberation of DMF molecules from the surfaces of the M NPs opened active sites to serve as the active catalyst in various organic transformations such as cross-coupling reactions, hydrogen borrowing reactions, and alkene hydrosilylation reactions. In addition, the use of M NPs enabled catalyst recycling in various reaction systems by using liquid–liquid extraction. Finally, control of the M NP properties (shape, size, and capping state) will provide new and specific reactivities. Innovative transformations could be achieved by alloying NPs (e.g., Pd–Cu)[17] to modify the catalytic properties of M NPs. can control and improve catalytic activities, as has been shown by photoluminescence properties. Further advances in combining M NPs and NCs will play a key role in future progress in organic chemistry. The author hope that to explore further applications of stable, practical, and highly active catalytic DMF-stabilized M NPs in organic chemistry.

# Reference

## General introduction


(1) M. Poliakoff, J. M. Fitzpatrick, T. R. Farren, P. T. Anastas, *Science* **2002**, *297*, 807–810.

(2) a) R. A. Sheldon, *Green Chem.* **2017**, *19*, 18–43.; b) R. A. Sheldon, *Green Chem.* **2007**, *9*, 1273–1283.

(3) a) A. Roglans, A. P. Quintana, M. Solà, *Chem. Rev.* **2021**, *121*, 1894-1979; b) L. D. de Almeida, H. Wang, K. Junge, X. Cui, M. Beller, *Angew. Chem. Int. Ed.* **2021**, *60*, 550–565; c) L. J. Gooßen, L. Huang, M. Arndt, K. Gooßen, H. Heydt, *Chem. Rev.* **2015**, *115*, 2596–2697.

(4) a) R. H. Grubbs, A. G. Wenzel, *Handbook of Metathesis, Volume 1: Catalyst Development and Mechanism*, Wiley, **2015;** b) K. Grela, *Olefin Metathesis: Theory and Practice*, Wiley, **2014**; c) R. R. Schrock, A. H. Hoveyda, *Angew. Chem. Int. Ed.* **2003**, *42*, 4592－4633.

(5) a) R. R. Schrock, *Acc. Chem. Res.* **2014**, *47*, 2457-2466; b) K. Nomura, M. M. Abdellatif, *Polymer* **2010**, *51*, 1861－1881; c) R. H. Grubbs, A. G. Wenzel, *Handbook of Metathesis, Volume 3: Polymer Synthesis*, Wiley, **2015**

(6) a) R. R. Arvizo, S. Bhattacharyya, R. A. Kudgus, K. Giri, R. Bhattacharya, P. Mukherjee, *Chem. Soc. Rev.* **2012**, *41*, 2943–2970; b) A. Corma, J. Navas, M. J. Sabater, *Chem. Rev.* **2018**, *118*, 1410-1459; c)$. Fratoddi, R. Matassa, L. Fontana, I. Venditti, G. Familiari, C. Battocchio, E. Magnano, S. Nappini, G. Leahu, A. Belardini, R. Li Voti, and C. Sibilia, *J. Phy. Chem. C* **2017,** *121*, 18110-18119.

(7) G. Li, R. Jin, *Acc. Chem. Res.* **2013**, *46*, 1749–1758; b) Y. Du, H. Sheng, D. Astruc, M. Zhu, *Chem. Rev.* **2020**, *120*, 526–622.

(8) M. Haruta, T. Kobayashi, H. Sano, N. Yamada, *Chem. Lett.* **1987**, *16*, 405–408; b) A. Taketoshi, M. Haruta, *Chem. Lett.* **2014**, *43*, 380–387; c) T. Ishida, M. Haruta, *Angew. Chem. Int. Ed.* **2007**, *46*, 7154–7156.

(9) (a) K. An, G. A. Somorjai, *ChemCatChem* **2012**, *4*, 1512–1524; b) A. Heuer-Jungemann, N. Feliu, I. Bakaimi, M. Hamaly, A. Alkilany, I. Chakraborty, A. Masood, M. F. Casula, A. Kostopoulou, E. Oh, K. Susumu, M. H. Stewart, I. L. Medintz, E. Stratakis, W. J. Parak, A. G. Kanaras, *Chem. Rev.* **2019**, *119*, 4819–4880; c) N. T. K. Thanh, N. Maclean, S. Mahiddine, *Chem. Rev.* **2014**, *114*, 7610–7630; d) T. S. Rodrigues, M. Zhao, T.-H. Yang, K. D. Gilroy, A. G. M. da Silva, P. H. C. Camargo, Y. Xia, *Chem. Eur. J.* **2018**, *24*, 16944–16963.

(10) a) H. Kawasaki, *Nanotechnology Reviews* **2013**, *2*, 5–25. b) Z. Niu, Y. Li, *Chem. Mater.* **2014**, *26*, 72–83.

Part A

(1) J. A. Joule, K. Mills, *Heterocyclic chemistry,* Wiley, Chichester, **2010**.

(2) a) E. Vitaku, D. T. Smith, J. T. Njardarson, *J. Med. Chem.* **2014**, *57*, 10257-10274. b) N. Manevski, L. King, W. R. Pitt, F. Lecomte, F. Toselli, *J. Med. Chem.* **2019**, *62*, 10955-10994.

(3) a) P. Singla, V. Luxami, K. Paul, *Eur. J. Med. Chem.* **2015**, *102*, 39-57. b) S. Cascioferro, B. Parrino, V. Spano, A. Carbone, A. Montalbano, P. Barraja, P. Diana, G. Cirrincione, *Eur. J. Med. Chem.* **2017**, *142*, 523-549.

(4) W. Reppe, O. Schlichting, K. Klager, T. Toepel, *Justus Liebigs Annalen der Chemie* **1948**, *560*, 1-92.

(5) a) G. Dominguez, J. Perez-Castells, *Chem. Soc. Rev.* **2011**, *40*, 3430-3444. b) P. R. Chopade, J. Louie, *Adv. Synth. Catal.* **2006**, *348*, 2307-2327.

(6) a) F. Kröhnke, *Synthesis* **1976**, *1976*, 1-24. b) R. Lavilla, *J. Chem. Soc. Perkin Trans. 1* **2002**, 1141-1156. c) *Comprehensive Organic Name Reactions and Reagents*, pp. 2241-2243. d) M. D. Hill, M. Movassaghi, *Chem. Eur. J.* **2008**, *14*, 6836-6844.

(7) a) B. Heller, M. Hapke, *Chem. Soc. Rev.* **2007**, *36*, 1085-1094. b) Ò. Torres, A. Roglans, A. Pla-Quintana, J. M. Luis, M. Solà, *J. Organomet. Chem.* **2014**, *768*, 15-22. c) K. Sakata, S. Shimada, R. Takeuchi, *Organometallics* **2020**, *39*, 2091-2101.

(8) R. Tanaka, A. Yuza, Y. Watai, D. Suzuki, Y. Takayama, F. Sato, H. Urabe, *J. Am. Chem. Soc.* **2005**, *127*, 7774-7780

(9) V. A. Rassadin, E. Nicolas, Y. Six, *Chem. Commum.* **2014**, *50*, 7666-7669.

(10) T. Takahashi, F.-Y. Tsai, M. Kotora, *J. Am. Chem. Soc.* **2000**, *122*, 4994-4995.

(11) T. Takahashi, F. Y. Tsai, Y. Li, H. Wang, Y. Kondo, M. Yamanaka, K. Nakajima, M. Kotora, *J. Am. Chem. Soc.* **2002**, *124*, 5059-5067.

(12) Y. Satoh, Y. Obora, *Eur. J. Org. Chem.* **2015**, *2015*, 5041-5054.

(13) Y. Satoh, Y. Obora, *J. Org. Chem.* **2013**, *78*, 7771-7776.

(14) B. R. D'Souza, T. K. Lane, J. Louie, *Org. Lett.* **2011**, *13*, 2936-2939.

(15) C. Wang, X. Li, F. Wu, B. Wan, *Angew. Chem. Int. Ed.* **2011**, *50*, 7162-7166.

(16) C. Wang, D. Wang, F. Xu, B. Pan, B. Wan, *J. Org. Chem.* **2013**, *78*, 3065-3072.

(17) V. Richard, M. Ipouck, D. S. Merel, S. Gaillard, R. J. Whitby, B. Witulski, J. L. Renaud, *Chem Commun* **2014**, *50*, 593-595.

(18) N. A. Spahn, M. H. Nguyen, J. Renner, T. K. Lane, J. Louie, *J. Org. Chem.* **2017**, *82*, 234-242.

(19) Y. Zou, Q. Liu, A. Deiters, *Org. Lett.* **2011**, *13*, 4352-4355.

(20) S. Medina, G. Dominguez, J. Perez-Castells, *Org. Lett.* **2012**, *14*, 4982-4985.

(21) F. Ye, M. Haddad, V. Ratovelomanana-Vidal, V. Michelet, *Org. Lett.* **2017**, *19*, 1104-1107.

(22) F. Ye, F. Boukattaya, M. Haddad, V. Ratovelomanana-Vidal, V. Michelet, *New J. Chem.* **2018**, *42*, 3222-3235.

(23) F. Ye, C. Tran, L. Jullien, T. Le Saux, M. Haddad, V. Michelet, V. Ratovelomanana-Vidal, *Org. Lett.* **2018**, *20*, 4950-4953.

(24) C. Tran, M. Haddad, V. Ratovelomanana-Vidal, *Synlett* **2019**, *30*, 1891-1894.

(25) H. Chowdhury, A. Goswami, *Adv. Synth. Catal.* **2017**, *359*, 314-322.

(26) P. Kalaramna, D. Bhatt, H. Sharma, A. Goswami, *Adv. Synth. Catal.* **2019**, *361*, 4379-4385.

(27) D. Bhatt, N. Patel, H. Chowdhury, P. V. Bharatam, A. Goswami, *Adv. Synth. Catal.* **2018**, *360*, 1876-1882.

(28) J. F. Tan, C. T. Bormann, F. G. Perrin, F. M. Chadwick, K. Severin, N. Cramer, *J. Am. Chem. Soc.* **2019**, *141*, 10372-10383.

(29) P. Kalaramna, D. Bhatt, H. Sharma, A. Goswami, *Eur. J. Org. Chem.* **2019**, *2019*, 4694-4700.

(30) C. Tran, M. Haddad, V. Ratovelomanana-Vidal, *Synlett* **2019**, *30*, 1891-1894.

(31) a) C. Saá, J. Varela, *Synlett* **2008**, *2008*, 2571-2578. b) J. A. Varela, C. Saa, *Chem. Rev.* **2003**, *103*, 3787-3801.

(32) A. L. McIver, A. Deiters, *Org. Lett.* **2010**, *12*, 1288-1291.

(33) C. Yuan, C. T. Chang, A. Axelrod, D. Siegel, *J. Am. Chem. Soc.* **2010**, *132*, 5924-5925.

(34) C. Yuan, C. T. Chang, D. Siegel, *J. Org. Chem.* **2013**, *78*, 5647-5668.

(35) S. Okamoto, Y. Sugiyama, *Synthesis* **2011**, *2011*, 2247-2254.

(36) P. Garcia, Y. Evanno, P. George, M. Sevrin, G. Ricci, M. Malacria, C. Aubert, V. Gandon, *Chem. Eur. J.* **2012**, *18*, 4337-4344.

(37) I. Thiel, H. Jiao, A. Spannenberg, M. Hapke, *Chem. Eur. J.* **2013**, *19*, 2548-2554.

(38) I. Thiel, A. Spannenberg, M. Hapke, *ChemCatChem* **2013**, *5*, 2865-2868.

(39) F. Fischer, A. F. Siegle, M. Checinski, C. Fischer, K. Kral, R. Thede, O. Trapp, M. Hapke, *J. Org. Chem.* **2016**, *81*, 3087-3102.

(40) F. Fischer, A. F. Siegle, M. Checinski, C. Fischer, K. Kral, R. Thede, O. Trapp, M. Hapke, *J. Org. Chem.* **2016**, *81*, 3087-3102.

(41) M. Kawatsura, T. Ishikawa, T. Sonehara, S. Murakami, M. Minakawa, *Synlett* **2016**, *27*, 2029-2033.

(42) K. Tanaka, *Heterocycles* **2012**, *85*, 1017-1043.

(43) M. Amatore, D. Leboeuf, M. Malacria, V. Gandon, C. Aubert, *J. Am. Chem. Soc.* **2013**, *135*, 4576-4579.

(44) F. Xu, C. Wang, D. Wang, X. Li, B. Wan, *Chem.Eur. J.* **2013**, *19*, 2252-2255.

(45) K. Kashima, K. Teraoka, H. Uekusa, Y. Shibata, K. Tanaka, *Org. Lett.* **2016**, *18*, 2170-2173.

(46) G. Onodera, Y. Shimizu, J. N. Kimura, J. Kobayashi, Y. Ebihara, K. Kondo, K. Sakata, R. Takeuchi, *J. Am. Chem. Soc.* **2012**, *134*, 10515-10531.

(47) T. Hashimoto, K. Kato, R. Yano, T. Natori, H. Miura, R. Takeuchi, *J. Org. Chem.* **2016**, *81*, 5393-5400.

(48) R. Takeuchi, S. Fujisawa, Y. Yoshida, J. Sagano, T. Hashimoto, A. Matsunami, *J. Org. Chem.* **2018**, *83*, 1852-1860.

(49) R. M. Stolley, M. T. Maczka, J. Louie, *Eur. J. Org. Chem.* **2011**, *2011*, 3815-3824.

(50) R. M. Stolley, H. A. Duong, J. Louie, *Organometallics* **2013**, *32*, 4952-4960.

(51) Y. Zhong, N. A. Spahn, R. M. Stolley, M. H. Nguyen, J. Louie, *Synlett* **2015**, *26*, 307-312.

(52) Y. Hoshimoto, T. Ohata, M. Ohashi, S. Ogoshi, *Chem. Eur. J.* **2014**, *20*, 4105-4110.

(53) X. You, X. Xie, G. Wang, M. Xiong, R. Sun, H. Chen, Y. Liu, *Chem. Eur. J.* **2016**, *22*, 16765-16769.

(54) G. Wang, X. You, Y. Gan, Y. Liu, *Org. Lett.* **2017**, *19*, 110-113.

(54) Y. L. Chen, P. Sharma, R. S. Liu, *Chem. Commun.* **2016**, *52*, 3187-3190.

(55) Y. Wang, C. Chen, J. Peng, M. Li, *Angew. Chem. Int. Ed.* **2013**, *52*, 5323-5327.

(56) J. Sheng, Y. Wang, X. Su, R. He, C. Chen, *Angew. Chem. Int. Ed.* **2017**, *56*, 4824-4828.

(57) Y. L. Chen, P. Sharma, R. S. Liu, *Chem. Commun.* **2016**, *52*, 3187-3190.

(58) X. You, S. Yu, Y. Liu, *Organometallics* **2013**, *32*, 5273-5276.

(59) C. H. Low, J. N. Rosenberg, M. A. Lopez, T. Agapie, *J. Am. Chem. Soc.* **2018**, *140*, 11906-11910.

(60) Y. Satoh, K. Yasuda, Y. Obora, *Organometallics* **2012**, *31*, 5235-5238.

(61) M. Fuji, Y. Obora, *Org. Lett.* **2017**, *19*, 5569-5572.

(62) T. K. Lane, M. H. Nguyen, B. R. D'Souza, N. A. Spahn, J. Louie, *Chem. Commun.* **2013**, *49*, 7735-7737.

(63) X. Su, C. Chen, Y. Wang, J. Chen, Z. Lou, M. Li, *Chem Commun*. **2013**, *49*, 6752-6754.

(64) S. N. Karad, R. S. Liu, *Angew. Chem. Int. Ed.* **2014**, *53*, 9072-9076.

(65) H. Liang, S. Bi, Y. Liu, Y. N. Tang, C. Liu, *Org. Biomol. Chem.* **2016**, *14*, 2637-2644.

(66) a) T. L. Cairns, A. W. Larchar, B. C. McKusick, *J. Am. Chem. Soc.* **1952**, *74*, 5633-5636. b) I. S. Bengelsdorf, *J. Am. Chem. Soc.* **1958**, *80*, 1442-1444.

(67) a) K. Wakabayashi, M. Tsunoda, Y. Suzuki, *Bull. Chem. Soc. Jpn.* **1969**, *42*, 2924-2930; b) A. Herrera, A. Riano, R. Moreno, B. Caso, Z. D. Pardo, I. Fernandez, E. Saez, D. Molero, A. Sanchez-Vazquez, R. Martinez-Alvarez, *J. Org. Chem.* **2014**, *79*, 7012-7024; c) R. Martínez-Alvarez, A. Herrera, P. Ramiro, M. Chioua, R. Chioua, *Synthesis* **2004**, 503-505; d) L. L. Whitfield, E. P. Papadopoulos, *J. Heterocycl. Chem.* **1981**, *18*, 1197-1201; e) W. M. Zhang, S. J. Liao, Y. Xu, Y. P. Zhang, *Synth. Commun.* **1997**, *27*, 3977-3983.

(68) X. Chen, S.-D. Bai, L. Wang, D.-S. Liu, *Heterocycles* **2005**, *65*, 1425-1430.

(69) R. Berger, J. Hauser, G. Labat, E. Weber, J. Hulliger, *CrystEngComm* **2012**, *14*, 768-770.

(70) J. H. Forsberg, V. T. Spaziano, S. P. Klump, K. M. Sanders, *J. Heterocycl. Chem.* **1988**, *25*, 767-770.

(71) F. Xu, X.-H. Zhu, Q. Shen, J. Lu, J.-Q. Li, *Chin. J. Chem.* **2010**, *20*, 1334-1339.

(72) M. Amatore, C. Aubert, *Eur. J. Org. Chem.* **2015**, 265-286.Part B

# Part B

(1) J. Muzart, *Tetrahedron* **2009**, *65*, 8313–8323.

(2) T. S. Rodrigues, M. Zhao, T.-H. Yang, K. D. Gilroy, A. G. M. da Silva, P. H. C. Camargo, Y. Xia, *Chem. Eur. J.* **2018**, *24*, 16944–16963.

(3) I. Pastorizo-Santos, L. M. Liz-Marzán, *Adv. Funct. Mater.* **2009**, *19*, 679–688.

(4) X. Liu, C. Li, J. Xu, J. Lv, M. Zhu, Y. Guo, S. Cui, H. Liu, S. Wang, Y. Li, *J. Phys. Chem. C* **2008**, *112*, 10778–10783.

(5) H. Kawasaki, *Nanotechnol. Rev.* **2013**, *2*, 5–25.

(6) M. Hyotanishi, Y. Isomura, H. Yamamoto, H. Kawasaki, Y. Obora, *Chem. Commun.* **2011**, *47*, 5750–5752.

(7) H. Yano, Y. Nakajima, Y. Obora, *J. Organomet. Chem.* **2013**, *745-746*, 258–261.

(8) K. Onishi, K. Oikawa, H. Yano, T. Suzuki, Y. Obora, *RSC Adv.* **2018**, *8*, 11324–11329.

(9) S. Asada, A. Nito, Y. Miyagi, J. Ishida, Y. Obora, F. Sanda, *Macromolecules* **2017**, *50*, 4083–4087.

(10) H. Yamamoto, H. Yano, H. Kouchi, Y. Obora, R. Arakawa, H. Kawasaki, *Nanoscale* **2012**, *4*, 4148–4154.

(11) W. Yao, W. J. Gong, H.-X. Li, F.-L. Li, J. Gao, J.-P. Lang, *Dalton Trans.* **2014**, *43*, 15752–15759.

(12) Y. Isomura, T. Narushima, H Kawasaki, T. Yonezawa, Y. Obora, *Chem. Commun.* **2012**, *48*, 3784–3786.

(13) H. Oka, K. Kitai, T. Suzuki, Y. Obora, *RSC Adv.* **2017**, *7*, 22869–22874.

(14) R. Azuma, S. Nakamichi, J. Kimura, H. Yano, H. Kawasaki, T. Suzuki, R. Kondo, Y. Kanda, K. Shimizu, K. Kato, Y. Obora, *ChemCatChem* **2018**, *10*, 2378–2382.

(15) Y. Obora, *ACS Catal.* **2014**, *4*, 3972–3981.

(16) K. Oikawa, S. Itoh, H. Yano, H. Kawasaki, Y. Obora, *Chem. Commun.* **2017**, *53*, 1080–1083.

(17) M. Chiba, M. N. Thanh, Y. Hasegawa, Y. Obora, H. Kawasaki, T. Yonezawa, *J. Mater. Chem.* **2014**, *3*, 514–520.

**Chapter 2.** Thiolate-protected $Au_{25}$ $(SC_2H_4Ph)_{18}$ nanoclusters as a catalyst for intermolecular hydroamination of terminal alkynes

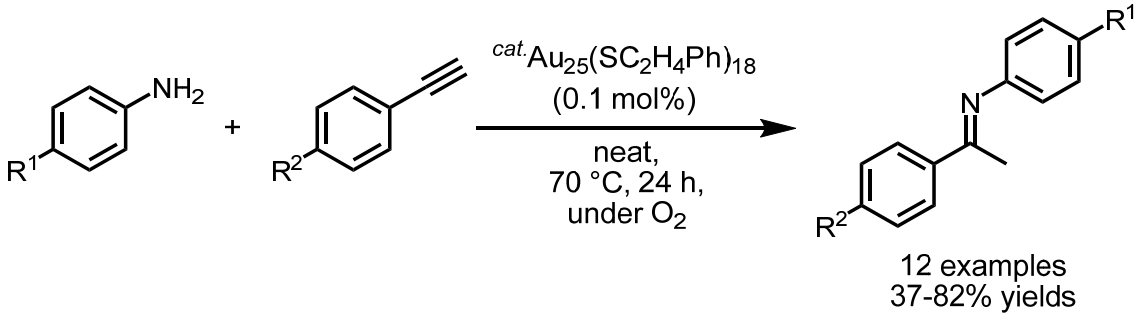

## Introduction

Imines are important building blocks for a variety of organic reactions. They have high reactivity toward various nucleophiles, such as in aza-Henry or Mannich-type reactions, nucleophilic addition, asymmetric hydrogenation, and cycloaddition.[1] Nitrogen-containing products are widely used as the scaffolds of synthetic drugs or natural products. Traditional imine synthesis is an equilibrium reaction, and hydroamination is one of the most atom economical and sustainable imine formation methods.[2]

In late-transition metal (Pd, Ru, Ir, Rh, Pt, and Au) catalyzed hydroamination of alkynes, C–C triple bond activation is generally the key step.[2,3] Au(I) catalysts have π-acidic properties, and various gold-activated reactions have been investigated for hydroamination.[4] Mizushima and Tanaka reported intermolecular hydroamination of alkynes with acidic promoters (eq 1 in Scheme 1).[5a] He and Brouwer reported hydroamination of 1,3-dienes. The noncoordinating anion effect was observed (eq 2 in Scheme 1).[5b] Generation of more electrophilic gold active species is necessary. Co-acidic and stable counter anions are required for application of the catalysts. Additives that can be easily removed from the desired products are desirable.

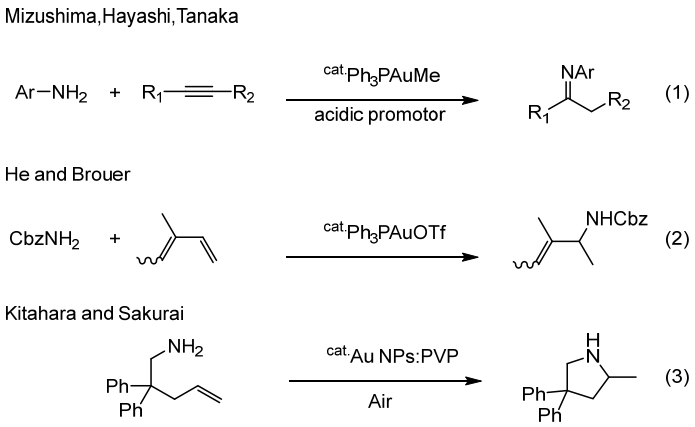


Scheme 1 Hydroamination of multiple bonds activated by gold catalysts

Among the attempts to activate Au complex, considerable attention has been focused on gold nanoparticles owing to their unique properties.[6] Haruta found significant differences in the catalytic activities of bulk metals and small particles(<10 nm).[7] Ligand-protected nanoclusters, such as thiolate, phosphine, and dendrimer protected clusters, have been studied in detail, and they are suitable as models for catalytic reaction investigation because it is easy to produce nanoparticles of a specific size.[8] Atomically precise Au nanoclusters with very small particle sizes (1–2 nm) are known to have high catalytic activity[9] for CO oxidation, Sonogashira cross-coupling, hydrogenation, alcohol oxidation, and hydroamination reactions. In 2010, Sakurai and Kitahara reported gold nanoclusters (NCs) stabilized by poly(N-vinyl-2-pyrrolidone) (Au NCs :PVP, mean size

= 1.3 nm) as versatile catalysts for intramolecular cycloaddition of primary amines to unactivated alkenes (eq 3 in Scheme 1).[10] They proposed that $O_2$ is initially adsorbed on the gold surface to form electron-deficient reactive sites. From the results of density functional theory calculations, absorption of $O_2$ provides superoxo-like species and Lewis acidic sites for Au NCs. Substrate alkene activation is favorable, whereas a high activation barrier prevents amine activation. Corma reported that nano-gold supported on chitosan is an efficient catalyst for hydroamination of terminal alkynes in the absence of an acid promoter. Nanocatalysts possess the potential to replace conventional reaction promoters.[11] Thiolate-protected Au NCs catalyze the C–N bond formation reaction. Jin et al. reported that the thiolate-protected Au NCs $Au_{38}(SC_2H_4Ph)_{24}$ catalyzes three component (amine, aldehyde, and alkyne, A3) coupling reactions.[12] Recently, our research group reported that $Au_{25}(SC_2H_4Ph)_{18}$ gives the corresponding propargylamines in good to excellent yields under $O_2$.[12b]

## Result and discussion

In this study, $Au_{25}(SC_2H_4Ph)_{18}$ serve as an efficient catalyst for hydroamination of alkynes. Notably, the hydroamination yield is different under $O_2$ and Ar atmospheres. $Au_{25}(SC_2H_4Ph)_{18}$ NCs are activated under an $O_2$ atmosphere and catalyze intermolecular hydroamination of terminal alkyne.

Table 1. $Au_{25}(SC_2H_4Ph)_{18}$-catalyzed hydroamination of terminal alkynes

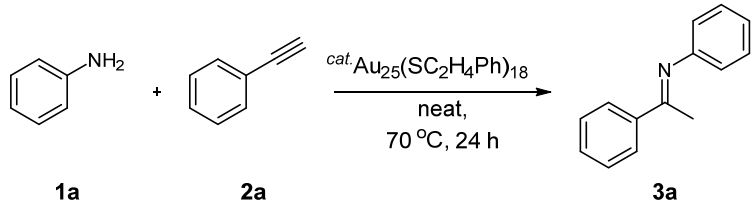


| Entry | Conditions[a] | Yield (%)[b] |
|---|---|---|
| 1 | Standard | 80(63) |
| 2 | Toluene solvent | Trace |
| 3 | Toluene solvent | 42 |
| 4 | Ratio of **1a**:**2a** = 1:1 | 62 |
| 5 | Ratio of **1a**:**2a** = 3:1 | 54 |
| 6 | Under air (balloon) | 58 |
| 7 | Under Ar (balloon) | 52 |

[a]Standard conditions: **1a** (0.5 mmol) was allowed to react with **2a** (1.5 mmol) in the presence of the $Au_{25}(SC_2H_4Ph)_{18}$ catalyst (0.1 mol % based on the amount of **1a**) at 70 °C for 24 h. [b]NMR yields based on **1a**. The isolated yield is given in parenthesis.

The reaction of aniline (**1a**) (0.5 mmol) with phenylacetylene (**2a**) (1.5 mmol) was performed in the presence of $Au_{25}(SC_2H_4Ph)_{18}$ (0.1 mol%) under an $O_2$ balloon at 70 °C for 24 h, giving **3a** in 80% NMR yield and 63% isolated yield (entry 1, Table 1). Side reactions were not observed and remaining starting material was recovered. The highest catalytic activity and yield of **3a** were achieved when the reaction was performed in the absence of a solvent. The use of representative nonpolar and polar solvents was ineffective under these conditions. (entries 1–3, Table 1). Reaction of **1a** with **2a** at a **1a**:**2a** molar ratio of 3:1 gave **3a** in high yield (54%). However, reaction with equimolar amounts of **1a** and **2a** gave in the higher yield (62%). The use of excess amine resulted in a decrease in the catalytic activity (entry 5). The reaction proceeded under open air and argon atmospheres (entries 6 and 7). However, the catalytic reaction performed better with $O_2$ rather than with air or inert gas. An amount of $O_2$ in the system gave a good yield (Figure 1).

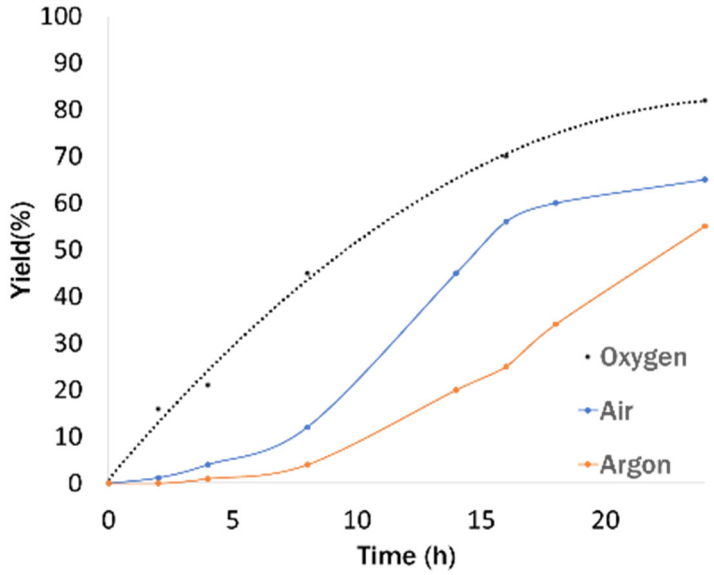


Figure 1 Plots of the reaction yields under (a) $O_2$ (black curve), (b) air (blue curve), and (c) argon (orange curve) atmospheres.

Thereafter, various substituted anilines and phenylacetylenes were studied for the hydroamination under these conditions (Figure 2). Using aniline derivatives bearing electron-rich substituents gave the corresponding ketimines **3b**–**3d** in good to moderate yields. Anilines bearing fluoro/chloro substituents were found to be less effective. Anilines bearing methoxy and *tert*-butyl groups gave the corresponding imines **3g** and **3h** in good yields. Heteroaromatic terminal alkynes were also tolerated in this reaction (**3k** and **3l**). The use of 3-aminopridine with phenylacetylene was not suitable for this reaction and desired product was obtained only in low yield (<10%) under these conditions. The reaction of **1a** with terminal aliphatic alkyne such as 1-octyne was sluggish. Unfortunately, internal alkynes (e.g. diphenylacetylene, 4-octyne) and aliphatic amines (e.g hexylamine, cyclohexylamine) did not give the desired products and starting materials were recovered.

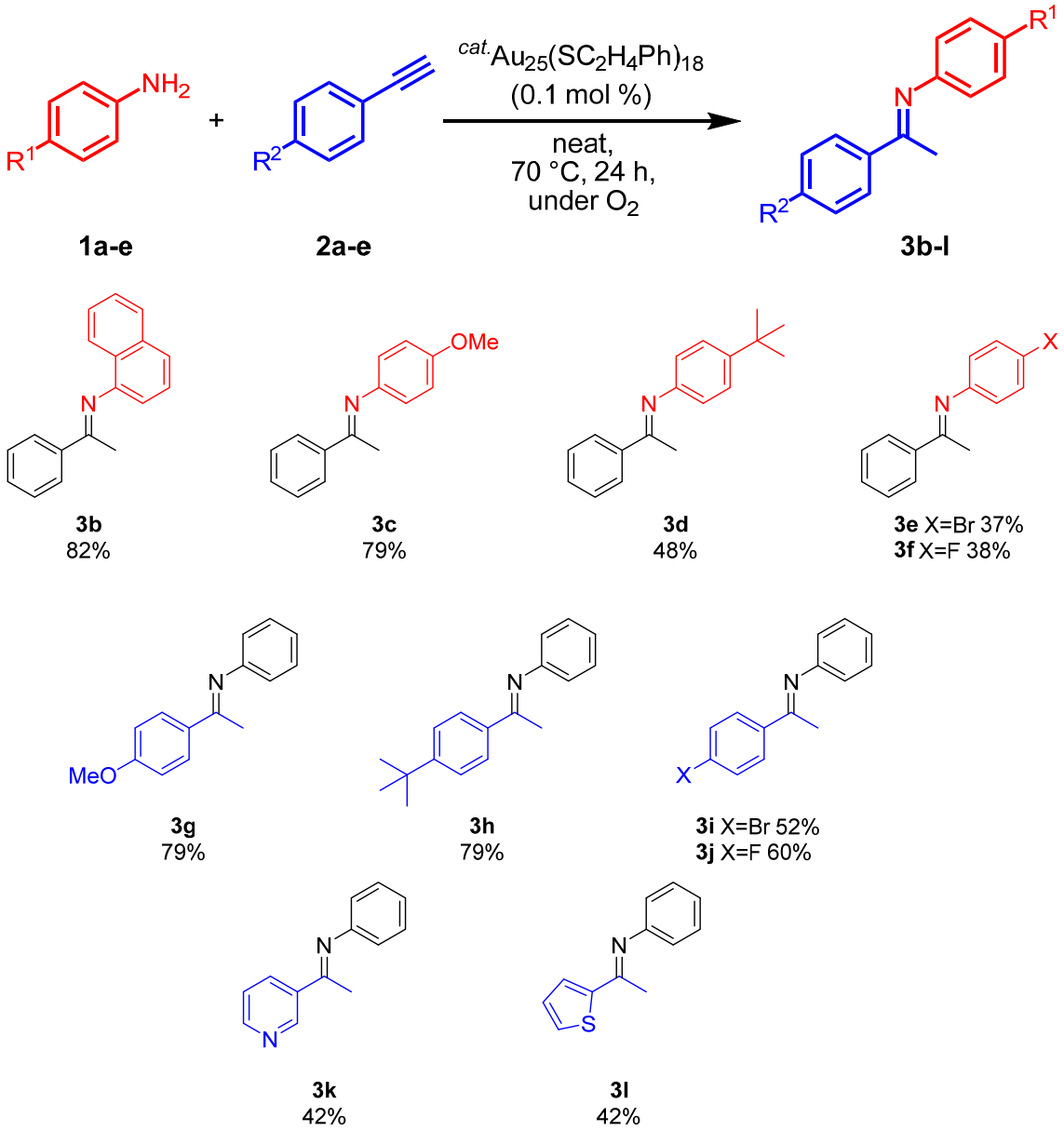


**Figure 2** Reaction of various anilines and phenylacetylenes

A plausible reaction mechanism based on the most general pathway is shown in Scheme 2.[2] Initially, $Au_{25}(SC_2H_4Ph)_{18}$ NCs generate Lewis acidic sites. Terminal alkynes are activated by electron deficient (Lewis acidic) sites. An oxygen atmosphere results in nanoclusters oxidation.[13] $Au_{25}(SC_2H_4Ph)_{18}$ has an electron rich $Au_{13}$ core and delocalized valence electrons. The $Au_{12}$ shell is positively charged owing to electron transfer from gold to sulfur. In the presence of molecular oxygen, it has been proposed that electron transfer from the $Au_{13}$ core to absorbed oxygen occurs.[14] This coordination

of $O_2$ has been well investigated by research of CO oxidation and the olefin epoxidation mechanism.[15] Overall, cationic activated $Au_{25}(SC_2H_4Ph)_{18}$ promotes activation of the alkyne triple bond. After attack of the aniline, the hydroamination product is released from the enamine intermediate.

The catalyst recyclability is important for its use in industrial and chemical research. Metal nanoparticles are possible recoverable and recyclable catalysts.[16] The author investigated the reusability of the catalyst. The reaction was performed under the standard conditions. Catalyst separation and recovery were performed by filtration and extraction (Figure 3). For five reusing experiments, the desired product **3a** was obtained in 38%–78% yield (Figure 4). The catalyst tolerated multiple cycles. To understand the significant loss in the catalytic activity, the particle size was measured by dynamic light scattering (DLS). After 1st run, the particle was retained their size (1-2 nm). Aggregated clusters (210 nm) were found after the fifth run (Figure 5). The decrease in the yield can be attributed to gradual decomposition of $Au_{25}(SC_2H_4Ph)_{18}$. A study of the stability of $Au_{25}(SR)_{18}$ agrees with our results.[17]

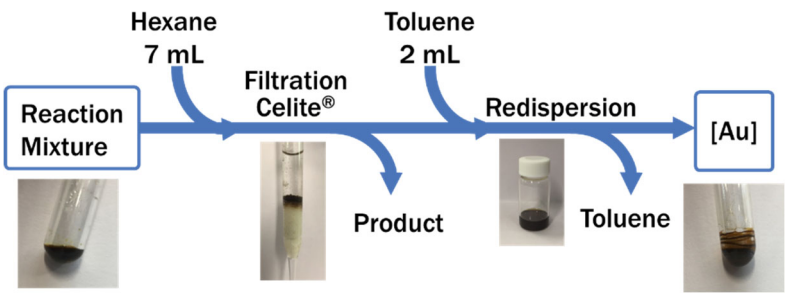


**Figure 3 Catalyst reusing process.**

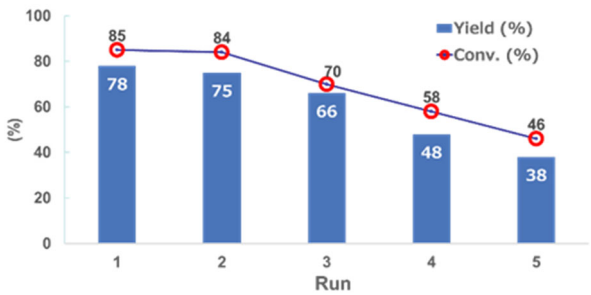


**Figure 4.** Reusing of the $Au_{25}(SC_2H_4Ph)_{18}$ catalyst five times

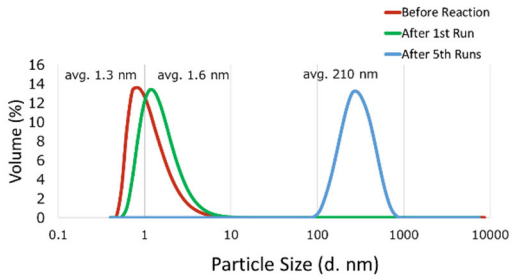


**Figure 5.** DLS average Au NCs sizes before the reaction (red curve), after first run (green curve), and after five runs (blue curve)

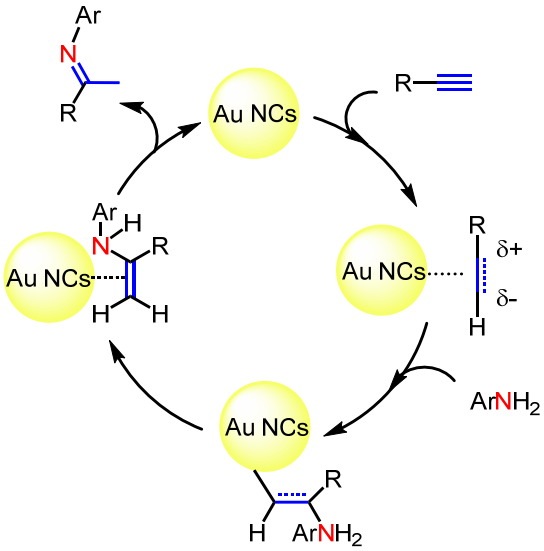


**Scheme 2: A plausible reaction mechanism of $Au_{25}(SC_2H_4Ph)_{18}$ catalyzed hydroamination**

## Conclusion

The author has demonstrated that the $Au_{25}(SC_2H_4Ph)_{18}$ catalyst has high catalytic activity for hydroamination of terminal alkynes. Abundant molecular oxygen plays an important role in gold activation. This catalytic system can be easily separated from the product and provides access to imines. The $Au_{25}(SC_2H_4Ph)_{18}$ catalyst can be reused.

## Experimental

General

GC analysis was performed with a Shimadzu GC-2010 a flame ionization detector (FID) using a 0.22 mm × 25 m capillary column (BP-5 SGE). $^{1}H$ and $^{13}C$ NMR were measured at 400 and 100 MHz, respectively, in $CDCl_3$ with tetrametylsilane as the internal standard (0 and 77 ppm). The products were characterized by $^{1}H$ NMR, $^{13}C$ NMR, and GC-MS(EI).

**Preparation of the $Au_{25}(SC_2H_4Ph)_{18}$ catalyst**

The $Au_{25}(SC_2H_4Ph)_{18}$ nanoclusters were synthesized according to a previously reported method.[18] $HAuCl_4 \cdot 4H_2O$ (2 mmol) was dissolved in 150 ml tetrahydrofuran (THF) solution containing tetraoctylammonium bromide (2.4 mmol) at room temperature. After stirring for 15 min, 2-phenylethanethiol (10 mmol) was added and the solution was stirred for 15 min 2 h. A cold aqueous solution (25 ml) containing $NaBH_4$ (20 mmol) was then rapidly added to the solution, and the solution was then stirred at room temperature. After 15 h, the THF solvent was evaporated, and the remaining red brown powder was washed with methanol to remove excess thiol and other byproducts. The $Au_{25}(SC_2H_4Ph)_{18}$ clusters were extracted from the dried sample using acetonitrile.

**General Procedure and the analytical data of some typical compounds**

The reaction of aniline (**1a**) with phenylacetylene (**2a**) was performed as follows. The prepared 1 mM $Au_{25}(SC_2H_4Ph)_{18}$ nanocluster solution in toluene (0.5 mL) was added to a Schlenk flask and the solvent was evaporated. **1a** (0.5 mmol) and **2a** (1.5 mmol) were then added and the solution was stirred for 24 h at 70 °C under $O_2$ (balloon). The chemical yield of imine **3a** was determined by integrating the $^{1}H$ NMR spectrum with respect to an internal standard (1,3,5-trimethoxybenzene). **3a** was isolated by column chromatography (25 μm silica gel, *n*-hexane:ethylacetate = 99:1).

Characterization of the compounds

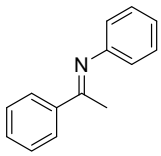

**3a** Phenyl-(1-phenylethylidene)amine, yellow solid. m.p. 40-41 °C; $^{1}H$-NMR (400 MHz, $CDCl_3$) δ: 7.98-7.96 (2H, m), 7.45-7.44 (3H, m), 7.34 (2H, t, $J$ = 7.7 Hz), 7.08 (1H, t, $J$ = 7.2 Hz), 6.79 (2H, d, $J$ = 7.9 Hz), 2.22 (3H, s);$^{13}C$-NMR (100 MHz $CDCl_3$) δ: 165.48 (C), 151.65 (C), 139.42 (C), 130.46 (CH), 128.94 (CH), 128.36 (CH), 127.14 (CH), 123.20 (CH), 119.36 (CH), 17.38 ($CH_3$); GC-MS (EI) m/z (relative intensity) 195 (53) $[M]^+$, 180 (100), 118 (12)

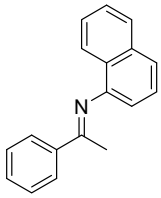

**3b** Naphthyl-(1-phenylethylidene)amine, yellow solid. m.p. 85-86 °C; $^{1}H$-NMR (400 MHz $CDCl_3$) δ: 8.12-8.10 (2H, m), 7.84-7.77 (2H, m), 7.60-7.40 (7H, m), 6.78 (1H, d, $J$ = 7.2 Hz), 2.19 (3H, s); $^{13}C$-NMR (100 MHz $CDCl_3$) δ: 166.42 (C), 147.93 (C), 139.20 (C), 134.15 (C), 130.64 (CH), 128.43 (CH), 127.94 (CH), 127.28 (CH), 126.08 (CH), 125.90 (C), 125.88 (CH), 125.37 (CH), 123.55 (CH), 123.21 (CH), 113.44 (CH), 17.66 ($CH_3$);GC-MS (EI) m/z (relative intensity) 246 (12), 245 (62) $[M]^+$, 231 (20), 230 (100), 128 (6), 127 (53)

**3c** 4-Methoxy-*N*-(1-phenylethylidene)benzenamine, pale yellow solid. m.p. 85-86 °C; $^{1}$H-NMR (400 MHz $CDCl_3$) δ: 7.98-7.95 (m, 3H), 7.45-7.44 (m, 3H), 6.92-6.74(m, 2H), 3.82 (s, 3H), 2.25 (s, 3H); $^{13}$C-NMR (100 MHz $CDCl_3$) δ: 165.73 (C), 155.91 (C), 144.80 (C), 139.74 (C), 130.31 (CH), 128.32 (CH), 127.09 (CH), 120.73 (CH), 114.21 (CH), 55.47 ($CH_3$), 17.31 ($CH_3$);GC-MS (EI): m/z (relative intensity): 225 (70) $[M]^+$, 210 (100), 211 (12);

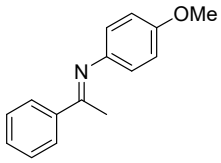


**3d** 4-*tert* Butyl-*N*-(1-phenylethylidene)benzeneamine, pale yellow solid. m.p. 80-81 °C;$^{1}$H-NMR (400 MHz $CDCl_3$) δ: 7.98-7.96 (2H, m), 7.45-7.43 (3H, m), 7.37-7.35 (2H, m), 6.74-6.73 (2H, m), 2.25 (3H, s), 1.34 (9H, s); $^{13}$C-NMR (100 MHz $CDCl_3$) δ: 165.25 (C), 148.91 (C), 145.95 (C), 139.62 (C), 130.30 (CH), 128.30 (CH), 127.12 (CH), 125.69 (CH), 119.05 (CH), 34.26 (C), 31.49 ($CH_3$), 17.36 ($CH_3$); GC-MS (EI) m/z (relative intensity) 251 (36)$[M]^+$, 236 (100), 118 (8);

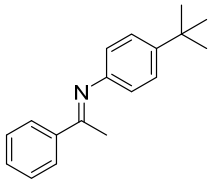


**3e**, 4-Bromo-(1-phenylethylidene)benzeneamine, pale yellow solid. m.p. 70-71 °C; $^{1}$H-NMR (400 MHz $CDCl_3$) δ: 7.96-7.94 (m, 2H), 7.45-7.44 (m, 5H), 6.92-6.74 (m, 2H), 2.25 (s, 3H) ; $^{13}$C-NMR (100 MHz $CDCl_3$) δ: 166.2 (C), 150.6 (C), 139.1 (C), 132.0 (CH), 130.7 (CH), 128.4 (CH), 127.1 (CH), 121.2 (CH), 116.2 (CH), 17.4 ($CH_3$); GC-MS (EI) m/z (relative intensity) 275 (60), 273 (59) $[M]^+$, 260 (99), 258 (100), 157 (22), 155 (23);

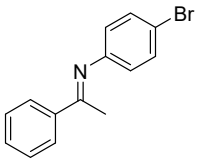


**3f** 4-Fluoro-(1-phenylethylidene)benzeneamine, yellow solid. m.p. 84-85 °C; $^{1}$H-NMR (400 MHz $CDCl_3$) δ: 7.96-7.94 (m, 2H), 7.45-7.44 (m, 5H), 6.92-6.74 (m, 2H), 2.25 (s, 3H); $^{13}$C-NMR (100 MHz $CDCl_3$) δ: 166.3 (C), 159.3 (d, $J_{C\text{-}F}$ =241 Hz), 147.6 (d, $J_{C\text{-}F}$=2.9 Hz),139.1 (C), 132.0 (CH), 130.7 (CH), 128.4 (CH), 127.1 (CH), 120.7 (CH, d, $J_{C\text{-}F}$ = 7.7 Hz), 115.6 (d, $J_{C\text{-}F}$ =22.2 Hz), 17.3 ($CH_3$); GC-MS (EI) m/z (relative intensity) 214 (8), 213 (58) $[M]^+$, 199 (14), 198 (100), 136 (15), 95 (40)

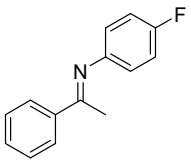


**3g** Phenyl-(4-methoxy-1-phenylethylidene)amine, white solid. m.p. 84-85 °C; $^{1}$H-NMR (400 MHz $CDCl_3$)δ: 7.99-7.96 (m,2H), 7.35-7.33(m, 2H), 7.14-7.07 (m, 3H), 6.79-6.77 (m, 2H), 3.86 (s, 3H) , 2.19 (s, 3H); $^{13}$C-NMR (100 MHz $CDCl_3$) δ : 164.51 (C), 161.51 (C), 151.90 (C), 132.19 (C), 128.91 (CH) 122.99 (CH), 119.59 (CH), 113.58 (CH), 55.38 ($CH_3$), 17.3 ($CH_3$); GC-MS (EI) m/z (relative intensity) 225 (51) $[M]^+$, 210 (100), 195 (5)

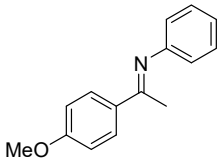

**3h** Phenyl-(4-*tert*-butyl-1-phenylethylidene)amine, yellow solid. m.p. 62-63 °C; $^{1}$H-NMR (400 MHz $CDCl_3$) δ: 7.94-7.92 (m, 2H), 7.49-7.47(m, 2H), 7.14-7.07 (m, 3H), 6.7 (m, 2H), 2.22 (s, 3H), 1.37 (s, 9H); $^{13}$C-NMR (100 MHz $CDCl_3$) δ: 165.16 (C), 153.86 (C), 151.87 (C), 136.72 (C), 128.92 (CH) 126.97 (CH), 125.30 (CH), 123.07 (CH), 119.44 (CH), 32.81 (C), 31.22 (CH3)17.25 ($CH_3$); GC-MS (EI) m/z (relative intensity) 251 (45) $[M]^+$, 236 (100), 221 (15)

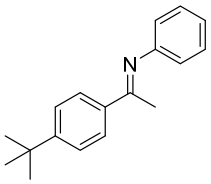


**3i** Phenyl-(4-bromo-1-phenylethylidene)amine, yellow liquid. m.p. 80-81 °C; $^{1}$H-NMR (400 MHz $CDCl_3$) δ :7.85-7.83 (m, 2H), 7.58-7.56 (m, 2H), 7.37-7.33 (m, 2H), 7.11-7.07 (m, 1H), 6.79-6.77 (m, 2H), 2.20 (s, 3H); $^{13}$C-NMR (100 MHz $CDCl_3$) δ: 164.36(C), 151.29 (C), 138.29 (C), 131.51 (C), 128.99 (CH), 128.78 (CH), 125.08 (CH), 123.43 (CH), 119.28 (CH), 17.21 ($CH_3$); GC-MS (EI) m/z (relative intensity) 273 (52) $[M]^+$, 257 (100), 178 (5)

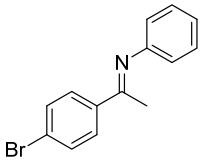


**3j** Phenyl-(4-fluoro-1-phenylethylidene)amine, pale yellow solid. m.p. 83-84 °C; $^{1}$H-NMR (400 MHz $CDCl_3$) δ: 7.99-7.96 (m,2H), 7.35-7.33(m, 2H), 7.14-7.07 (m, 3H), 6.79-6.77 (m, 2H), 2.21 (s, 3H); $^{13}$C-NMR (100 MHz $CDCl_3$) 166.4(C, d, $J_{C-F}$ = 250 Hz), 164.1 (C), 151.5 (C), 135.7 (C, d, $J_{C-F}$ = 3Hz), 129.3 (CH, d $J_{C-F}$ = 9 Hz) 129.0 (CH), 123.3 (CH), 119.4 (CH), 115.3 (CH, d, $J_{C-F}$ =22 Hz), 17.3 ($CH_3$); GC-MS (EI) m/z (relative intensity) 214 (9), 213 (59) $[M]^+$, 199 (14), 198 (100), 118 (10)

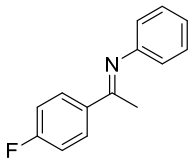


**3k** *N*-[1-(3-Pyridinyl)ethylidene]benzenamine, yellow solid. m.p. 67-68 °C; $^{1}$H-NMR (400 MHz $CDCl_3$) δ: 9.146 (d, J = 1.5 Hz, 1H), 8.70-8.69 (m, 1H), 8.33-8.30 (m, 1H), 7.39-7.35 (m, 3H), 7.11 (t, 1H J=7.6 Hz), 6.80 (d, 2H, J=7.6 Hz) , 2.23 (s, 3H); $^{13}$C-NMR (100 MHz $CDCl_3$) δ: 163.44 (C), 151.30 (CH), 150.99 (C), 148.76 (CH), 134.83 (C) 134.51 (CH), 129.06 (CH), 123.68 (CH), 123.30 (CH), 119.27 (CH) 17.22 ($CH_3$); GC-MS (EI) m/z (relative intensity) 196 (70) $[M]^+$, 181 (100), 118 (21)

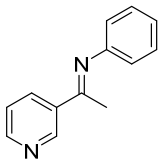


**3l** *N*-[1-(2-thienyl)ethylidene]benzenamine, pale yellow solid. m.p. 69-70 °C; $^{1}$H-NMR (400 MHz $CDCl_3$) δ: 7.47-7.44 (m, 2H), 7.35-7.31 (m, 2H), 7.09-7.07 (m, 2H), 6.83- 6.80 (m, 2H), 2.23 (s, 3H);$^{13}$C-NMR (100 MHz $CDCl_3$,)δ:160.30 (C), 150.54 (C), 146.47 (C), 129.90 (CH), 128.86 (CH), 128.49 (CH), 127.44 (CH), 123.53 (CH), 119.99 (CH), 17.44 ($CH_3$); GC-MS (EI) m/z (relative intensity) 201 (63) $[M]^+$, 186 (100), 77 (66).

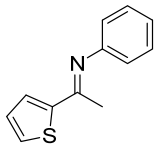

## Reference


(1) a) A. Córdova, *Acc. Chem. Res.* **2004**, *37*, 102-112; b) C. Nájera, J. M. Sansano, *Chem. Rev.* **2007**, *107*, 4584-4671; c) K. A. Jorgensen, *Angew. Chem. Int. Ed.* **2000**, *39*, 3558-3588; d) Layer, R. W. *Chem. Rev.* **1963**, *63*, 489-510; e) A. Erkkilä, I. Majander, P. M. Pihko, *Chem. Rev.* **2007**, *107*, 5416-5470.

(2) a) L. J. Gooßen, L. Huang, M. Arndt, K. Gooßen, H. Heydt, *Chem. Rev.* **2015**, *115*, 2596-2697; b) T. E. Müller,K. C. Hultzsch, M. Yus, F. Foubelo, M. Tada, M. *Chem. Rev.* **2008**, *108*, 3795-3892; c) R. Severin, S. Doye, *Chem. Soc. Rev.* **2007**, *36*, 1407-1420; d) R. D. Patil, S. Adimurthy, *Asian J. Org. Chem.* **2013**, *2*, 726-744.

(3) a) Q. Chen, L. Lv, M. Yu, Y. Shi, Y. Li, G. Pang, C. Cao, *RSC Adv.* **2013**, *3*, 18359-18366; (b) M. Tokunaga, M. Eckert, Y. Wakatsuki, *Angew. Chem. Int. Ed.* **1999**, *38*, 3222-3225; (c) W. Iali, F. La. Paglia, X. F. Goff, D. Sredojević, M. Pfeffer, J. P. Djukic, *Chem. Commun.* **2012**, *48*, 10310-10312; (d) C. G. Hartung, A. Tillack, H. Trauthwein, M. Beller, *J. Org. Chem.* **2001**, *66*, 6339-6343; (e) J. J. Brunet, N. C. Chu, O. Diallo, S. Vincendeau, *J. Mol. Catal. A Chem.* **2005**, *240*, 245-248.

(4) a) D. J. Gorin, F. D. Toste, *Nature* **2007**, *446*, 395-403; b) A. Corma, A. Leyva-Pérez, M. J. Sabater, *Chem. Rev.* **2011**, *111*, 1657-1712; c) M. Jia, M. Bandini, *ACS Catal.* **2015**, *5*, 1638-1652; d) B. Ranieri, I. Escofet, A. M. Echavarren, *Org. Biomol. Chem.* **2015**, *13*, 7103-7118; e) M. Joost, A. Amgoune, D. Bourissou, *Angew. Chem. Int. Ed.* **2015**, *54*, 15022-15045.

(5) a) E. Mizushima, T. Hayashi, M. Tanaka, *Org. Lett.* **2003**, *5*, 3349-3352; b) C. Brouwer, C. He, *Angew. Chem. Int. Ed.* **2006**, *45*, 1744-1747.

(6) a) A. Mathew, T. Pradeep, *Part. Part. Syst. Charact.* **2014**, *31*, 1017-1053; b) I. Chakraborty, T. Pradeep, *Chem. Rev.* **2017**, *117*, 8208-8271.

(7) a) M. Haruta, T. Kobayashi, H. Sano, N. Yamada, *Chem. Lett.* **1987**, *16*, 405-408; b) A. Taketoshi, M. Haruta, *Chem. Lett.* **2014**, *43*, 380-387.

(8) a) T. Tsukuda, *Bull. Chem. Soc. Jpn.* **2012**, *85*, 151-168; b) J. Fang, B. Zhang, Q. Yao, Y. Yang, J. Xie, N. Yan, *Coord. Chem. Rev.* **2016**, *322*, 1-29.

(9) a) G. Li, R. Jin, *Acc. Chem. Res.* **2013**, *46*, 1749-1758; b) X. Nie, H. Qian, Q. Ge, H. Xu, R. Jin, *ACS Nano* **2012**, *6*, 6014-6022; c) G. Li, D. E. Jiang, C. Liu, C. Yu, R. Jin, *J. Catal.* **2013**, *306*, 177-183; d) G. Li, R. Jin, *J. Am. Chem. Soc.* **2014**, *136*, 11347-11354; e) Y. Liu, H. Tsunoyama, T. Akita, T. Tsukuda, *Chem. Commun.* **2010**, *46*, 550-552; f) S. Xie, H. Tsunoyama, W. Kurashige, Y. Negishi, T. Tsukuda, *ACS Catal.* **2012**, *2*, 1519-1523.

(10) a) H. Kitahara, H. Sakurai, *Chem. Lett.* **2010**, *39*, 46-48. (b) K. Bobuatong, H. Sakurai, M. Ehara, *ChemCatChem* **2017**, *9*, 4490-4500.

(11) a) A. Corma, P. Concepción, I. Domínguez, V. Forné, M. J. Sabater, *J. Catal.* **2007**, *251*, 39-47; b) L. C. Lee, Y. Zhao, *ACS Catal.* **2014**, *4*, 688-691; c) S. Liang, L. Hammond, B. Xu, G. B. Hammond, *Adv. Synth. Catal.* **2016**, *358*, 3313-3318.

(12) a) Q. Li, A. Das, S. Wang, Y. Chen, R. Jin, *Chem. Commun.* **2016**, *52*, 14298-14301; (b) Y. Adachi, H. Kawasaki, T. Nagata, Y. Obora, *Chem. Lett.* **2016**, *45*, 1457-1459.

(13) a) M. Zhu, W. T. Eckenhoff, T. Pintauer, R. Jin, *J. Phys. Chem. C* **2008**, *112*, 14221-14224; b) M. Zhu, C. M. Aikens, M. P. Hendrich, R. Gupta, H. Qian, G. C. Schatz, R. Jin, *J. Am. Chem. Soc.* **2009**, *131*, 2490-2492.

(14) a) M. Okumura, Y. Kitagawa, M. Haruta, K. Yamaguchi, *Appl. Catal. A Gen.* **2005**, *291*, 37-44. (b) A. Roldán, J. M. Ricart, F. Illas, G. Pacchioni, *Phys. Chem. Chem. Phys.* **2010**, *12*, 10723-10729; (c) R. Pal, L. M. Wang, Y. Pei, L. S. Wang, X. C. Zeng, *J. Am. Chem. Soc.* **2012**, *134*, 9438-9445.

(15) a) Y. Zhu, H. Qian, R. Jin, *Chem. Eur. J.* **2010**, 16, 11455-11462; b) Y. Zhu, H. Qian, M. Zhu, R. Jin, *Adv. Mater.* **2010**, *22*, 1915-1920.

(16) a) D. Astruc, F. Lu, J.R. Aranzaes, *Angew. Chem. Int. Ed.* **2005**, *44*, 7852-7872; b) M. B. Li, S. K. Tian, Z. Wu, *Nanoscale* **2014**, *6*, 5714-5717; c) K. Fujita, A. Fujii, J. Sato, H. Yasuda, *Synlett*. **2016**, *27*, 1941-1944.

(17) a) C.B. Collins, M. A. Tofanelli, M. F. Crook, B.D. Phillips, C. J. Ackerson, *RSC Adv.* **2017**, *7*, 45061-45065; b) T. A. Dreier, C. J. Ackerson, *Angew. Chem. Int. Ed.* **2015**, *54*, 9249-9252; c) M. A. Tofanelli, C. J. Ackerson, *J. Am. Chem. Soc.* **2012**, *134*, 16937-16940.

(18) a)Dharmaratne, A. C.; Krick, T.; Dass, A. *J. Am. Chem. Soc.* **2009**, *131*, 13604. (b) Yamazoe, S.; Takano, S.; Kurashige, W.; Yokoyama, T.; Nitta, K.; Negishi, Y.; Tsukuda, T. *Nat. Commun.* **2016**, *7*, 10414.

**Chapter 3.** Dimethylformamide-stabilized palladium nanoclusters catalysed coupling reactions of aryl halides with hydrosilanes/disilanes

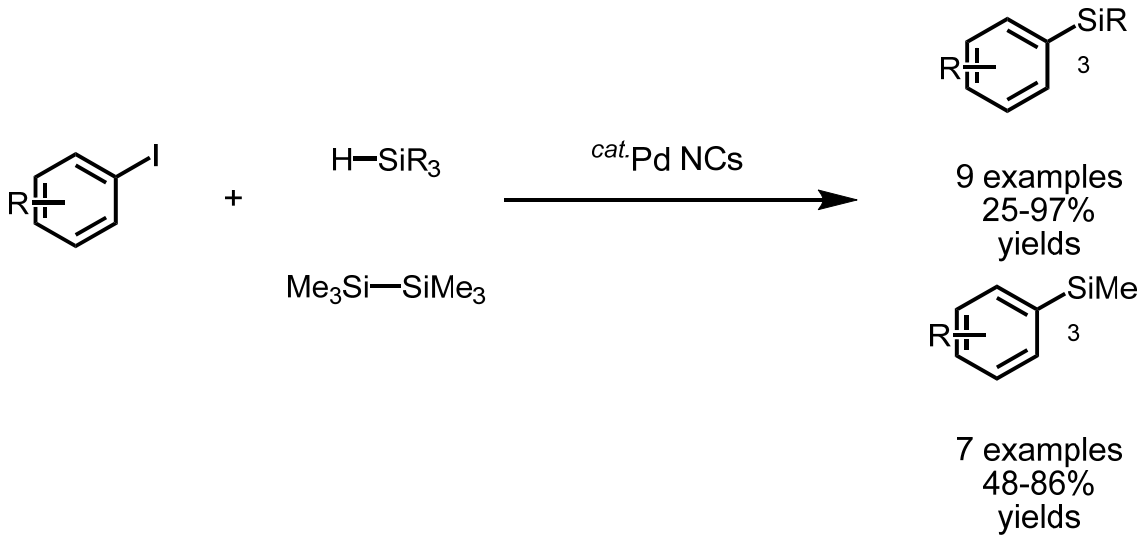

## Introduction

Arylsilanes have attracted a great deal of interest in various fields. Silicon-containing molecules have unique and specific properties and multiple uses, such as in medicine,[1] in photonics,[2] and as organic intermediates.[3] Conventional methods for arylsilane synthesis are unsatisfactory because of byproducts and side reactions.[4] Accordingly, considerable attention has focused on their selective synthesis.[5] Transition metal catalysed cross-coupling reactions between aryl halides and hydrosilanes or disilanes have emerged as selective and easy to handle protocols. However, these reactions are generally achieved using transition metal complexes, such as Pd[6] and Rh[7] complexes, with 1–5 mol % of the catalyst. In addition, hydrosilanes act as weak reducing reagents [8] and using them as coupling substrates inhibits reduction of aryl halides. Moreover, owing to the stability of the Si–Si bond, disilanes show low reactivity for silylation reagents, so the coupling reactions require bulky phosphorus ligands.[9]

Metal nanoparticles (NPs) and nanoclusters (NCs) have unique physical and chemical properties.[10] They are expected to show high catalytic performance owing to their stability, selectivity, activity, and recyclability.[11,12] On the other hand, colloidal nanocatalysts require removal of capping agent to access catalytically active surfaces. Stabilizing agents such as thiolates, phosphines, surfactants, and polymers, behaves a protective shell for reactant.[13] Obora and co-workers have reported a surfactant-free preparation of dimethylformamide (DMF)-stabilized transition-metal (Au, Fe, Ir, Cu, and Pd) NPs by the DMF reduction method.[14] Among these NPs, Pd NCs have proven to be highly effective in various palladium-catalysed cross-coupling reactions, such as Suzuki–Miyaura, Mizoroki–Heck,[15a] and Migita–Kosugi–Stille coupling reactions.[15b] DMF-stabilised $Fe_2O_3$ NPs also show high catalytic activity for hydrosilylation of unactivated terminal alkenes.[16] The Pd–Pt–$Fe_2O_3$ nanocatalyst has recently been reported for coupling aryl halides with hydrosilanes. However, the Pd monometallic catalyst shows low reactivity and causes decomposition.[17]

In this chapter, the author describes DMF-stabilised palladium NCs catalysed coupling reactions of aryl halides with hydrosilanes/disilanes to give arylsilanes with moderate to good yields. These reactions proceed at low catalyst loading under ligand and additive free conditions. In addition, the Pd NCs catalysts in both the hydrosilane/disilane reaction systems can be recycled at least five times.

## Results and disucussions

Initially, the author chose to study the cross-coupling reaction between iodobenzene (**1a**) and dimethylphenylsilane (**2a**) using LiOAc as a base in DMF at 100 °C. After 16 h, dimethyldiphenylsilane (**3a**) was obtained in moderate yield (Table 1, entry 1). When the author changed *N*-dimethylacetamide (DMAc) solvent to the reaction, the yield increased to 80% (entry 2), which indicates that there is a significant solvent effect. The reaction was not accelerated in *N*-methyl-2-pyrrolidone (NMP) and toluene (entries 4 and 5). Various bases were tested. LiOAc gave the highest yield (entries 5–7). The reaction also occurred in the absence of a base (entry 8). To test the specific solvent effect, the author prepared Pd NCs in DMF and DMAc at 100 °C for 24 h. A BF-TEM image and the particle size distribution of the DMAc-displaced Pd NCs are shown in Figure 1. The average particle size of 2 nm is the same as that of the prepared Pd NCs (Figure 1).

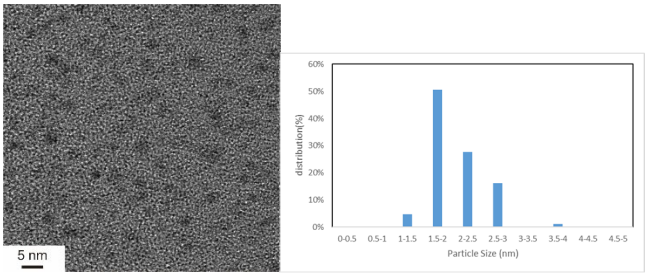


Figure 1. (a) BF-TEM image (scale bar = 5 nm) and (b) nanoparticle size distribution of the DMAc-displaced Pd NCs.

Table 1. Optimisation of the coupling reaction conditions with hydrosilane[a]

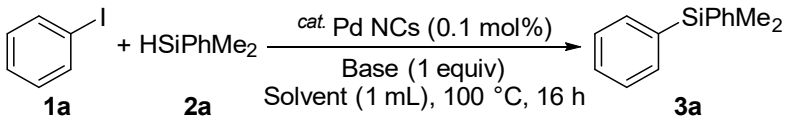


| Entry | Solvent | Base | Yield (%)[b] |
|---|---|---|---|
| 1 | DMF | LiOAc | 52 |
| 2 | DMAc | LiOAc | 80 (75) |
| 3 | NMP | LiOAc | 41 |
| 4 | Toluene | LiOAc | 7 |
| 5 | DMAc | NaOAc | 68 |
| 6 | DMAc | KOAc | 57 |
| 7 | DMAc | KO*t*Bu | 8 |
| 8 | DMAc | - | 52 |

[a]Reaction conditions: **1a** (1.0 mmol), **2a** (3.0 mmol), Pd NCs (0.1 mol %), and base (1.0 mmol) in solvent (1.0 mL) at 100 °C for 16 h. [b] the yields were determined by gas chromatography analysis. The isolated yield is shown in parenthesis.

$^1$H-NMR spectroscopy, Fourier transform-infrared (FT-IR) spectroscopy, thermogravimetric (TG) analysis, and X-ray photoelectron spectroscopy (XPS) were performed to analyse the DMAc-substituted Pd NCs. From $^1$H-NMR analysis, the formyl group proton (δ = 8.14 ppm) disappears after solvent displacement (Figure 2).

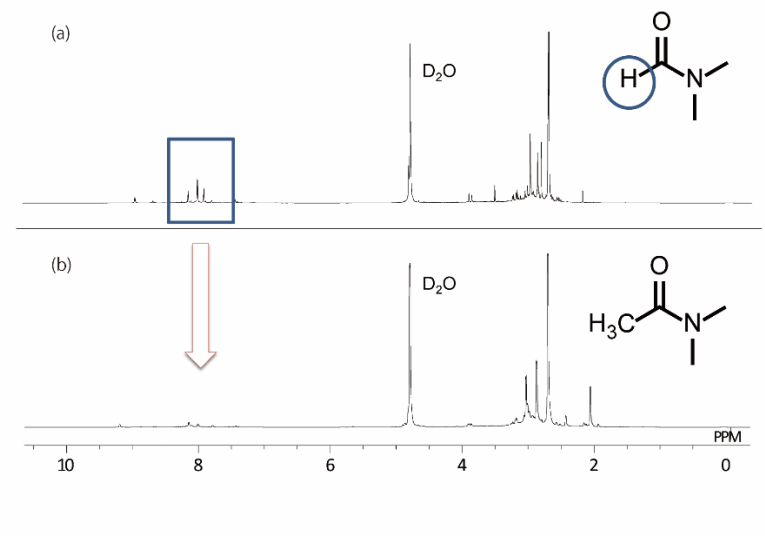


Figure 2 $^1$H NMR (400 MHz, $D_2O$, 20 ºC) spectra of (a) Pd NCs and (b) DMAc displaced Pd NCs

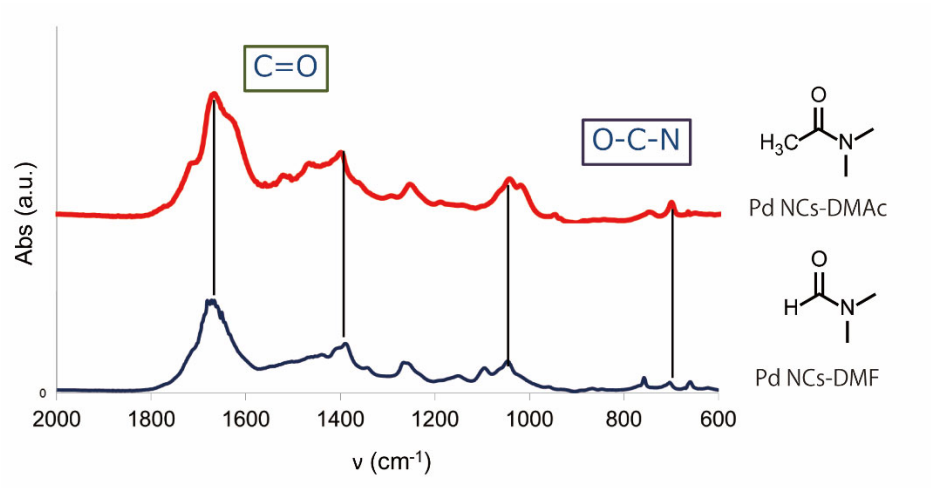


Figure 3 FT-IR measurement (red) DMAc displaced Pd NCs (blue) as prepared Pd NCs

FT-IR analysis (Figure 3) shows a peak at 1670 cm$^{-1}$, which is attributed to the *n*(C=O) stretching vibration and indicates the presence of DMF and DMAc molecules. The thermal stability of the Pd NPs was investigated by TG analysis (Figure 4). The TG curves of Pd NCs-DMF and Pd NCs-DMAc are constant between 25 °C to 200 °C. Subsequent

weight loss rates and its speeds were different for two samples. These results suggested that solvent displacement caused exchange of the surface capping agents.

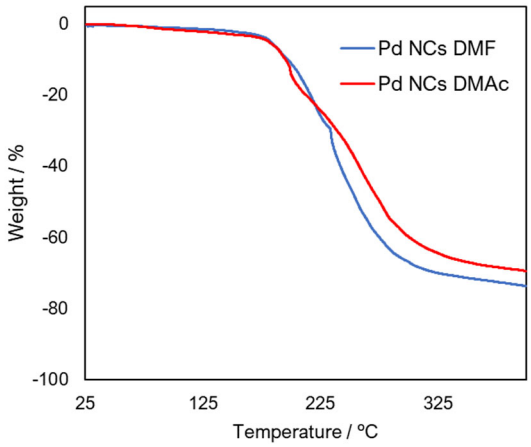


Figure 4. TG analysis of Pd NCs–DMF (blue) and Pd NCs–DMAc (red).

The surface states of the as-prepared Pd NCs and solvent-displaced Pd NCs with DMAc were determined by XPS. The binding energy positions of Pd $3d_{5/2}$ and Pd $3d_{3/2}$ are shown in Figure 5. The other main peaks (C, O, and N) are shown in Figure 6-8. Peak FWHMs are described in table 2. The main peaks of Pd at 338.8, 337.2 eV of $3d_{5/2}$ and 344.0, 342.1 of $3d_{3/2}$ was higher than that of bulk Pd (Pd $3d_{5/2}$ 335.1 eV and Pd $3d_{3/2}$ 340. 3 eV). [18,19] The Pd $3d_{5/2}$ and $3d_{3/2}$ spectrum of Pd NCs with DMF is shown in Figure 3a. The DMAc Pd NCs have a broad peak (Pd $3d_{5/2}$ 343.7,341.8 eV and Pd $3d_{3/2}$ 338.5, 336.6 eV) (Figure 5b). A significant peak shift in Pd NCs with DMAc by increase of the measurement time (Figure 5d). In contrast, the as-prepared Pd NCs remain unchanged (Figure 5c). The changes in the two samples are caused by removal of the protective molecules on the surface. With irradiation by X-ray and sample heating, the protective molecules (DMF rigid protecting layer) are removed as the number of measurements increases. With elimination of the protective surface molecules, surface palladium is reduced. These data are associated with the TG analysis results, where DMAc displacement of the Pd NCs removes the capping molecules and results in easy access to the active sites.

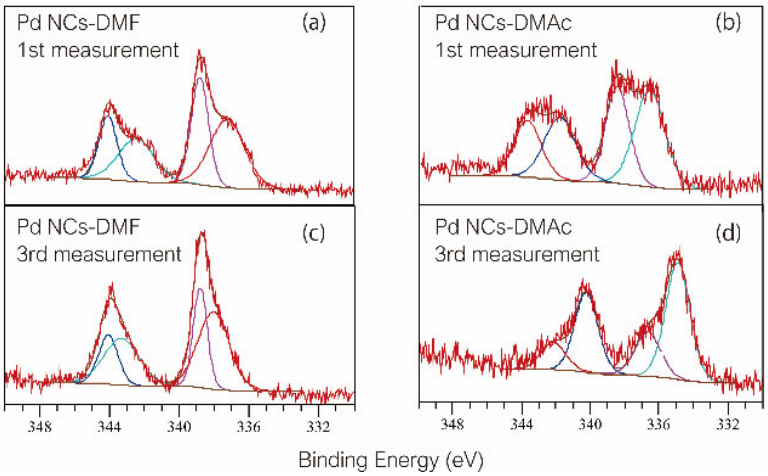


Figure 5. XPS spectra of Pd NCs with DMF (a) at first measurement, (b) at third measurement, and Pd NCs with DMA which substituted from DMF (c) at 1st and (d) at 3rd measurement.

Table 2. XPS peak positions, FWHMs

| | Binding Energy (eV) [FWHM] | | | | |
|---|---|---|---|---|---|
| Element | Pd $3d_{5/2}$ | Pd $3d_{3/2}$ | N 1s | O 1s | C 1s |
| (a) Pd NCs | 338.8 [1.2] | 344.0 [1.5] | 400.8 [2.4] | 532.8 [3.0] | 288.2[1.5] |
| | 337.2 [2.3] | 342.1 [2.2] | | 531.9 [1.5] | 286.4[1.4] |
| | | | | | 285.1[1.1] |
| (b)DMAc-substituted Pd NCs | 338.5 [1.6] | 343.7 [1.9] | 402.2 [1.5] | 532.5 [1.9] | 288.2 [1.5] |
| | 336.6 [2.1] | 341.8 [2.1] | 400.5 [2.0] | | 286.4 [1.4] |
| | | | | | 285.1 [1.1] |
| (c)Pd NCs–DMF | 338.8 [0.9] | 344.0 [1.3] | 400.7 [2.4] | 533.6 [2.9] | 288.5 [1.2] |
| at the third measurement | 338.0 [2.1] | 343.3 [2.3] | | 532.1 [1.8] | 286.3 [2.2] |
| (d)DMAc-substituted Pd NCs | 335.7 [1.8] | 342.1 [1.7] | 399.8 [2.4] | 532.0 [1.8] | 288.0 [1.4] |
| at the third measurement | 334.7 [1.4] | 340.2 [1.6] | | | 285.7 [1.4] |
| | | | | | 284.6 [1.1] |

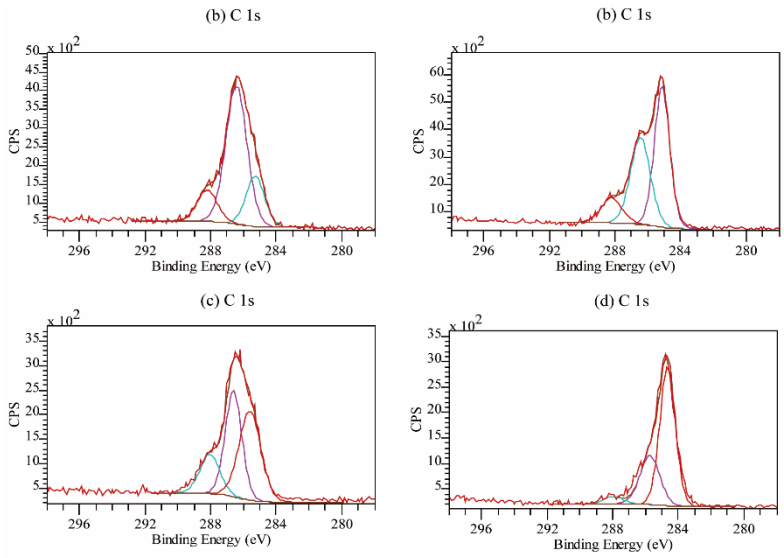


(A) Figure 6. XPS Spectra of C 1s from (i) Pd NCs, (ii) DMA-substituted Pd NCs, (iii) Pd NCs–DMF at the third measurement, and (iv) DMAc-substituted Pd NCs at the third measurement,

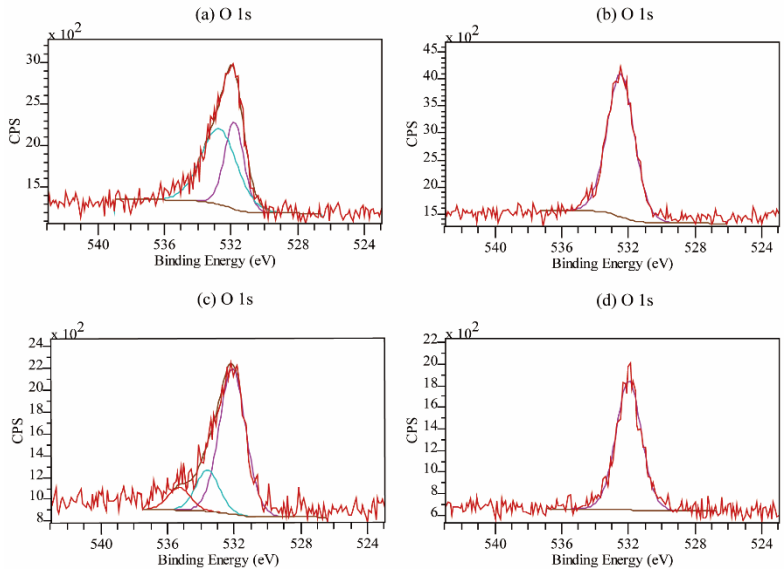


(B) Figure 7 XPS Spectra of O 1s from (i) Pd NCs, (ii) DMAc-substituted Pd NCs, (iii) Pd NCs–DMF at the third measurement, and (iv) DMAc-substituted Pd NCs at the third measurement,

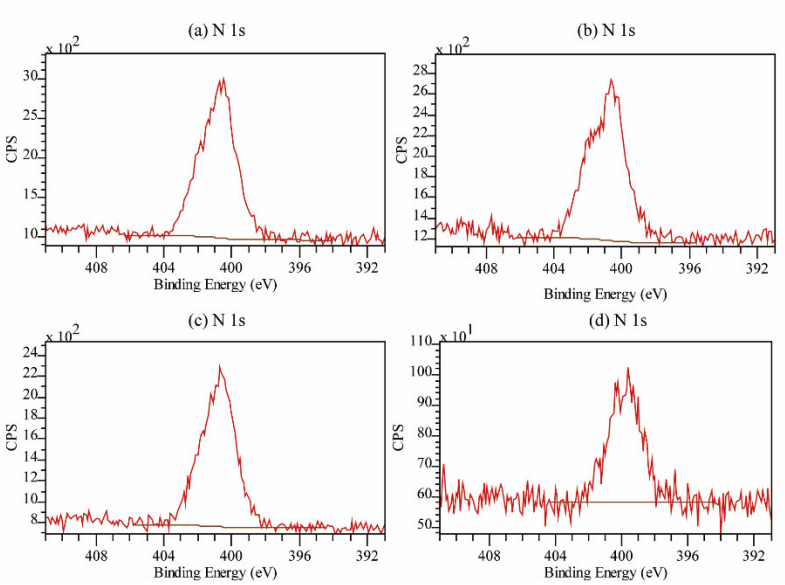


(C) Figure 8 XPS Spectra of N 1s from (i) Pd NCs, (ii) DMAc-substituted Pd NCs, (iii) Pd NCs–DMF at the third measurement, and (iv) DMAc-substituted Pd NCs at the third measurement,

Next, the author tested aryl halides bearing both electron-donating and electron-withdrawing substituents (Scheme 2). Electron-donating substrates (4-methyl and 4-methoxy, and 4-*tert*-butyl) gave excellent yields (84%, 97%, and 82% for **3b**, **3c**, and **3d**, respectively). Electron withdrawing substrates were less effective (34% and 42% for **3e** and **3f**, respectively). Various silanes were investigated. The corresponding arylsilanes diphenylmethylsilane (**3g**), triethylsilane (**3h**), and triethoxysilane (**3i**) were obtained in 38%, 32%, and 25% yield, respectively.

Scheme 2. Scope of various substrates

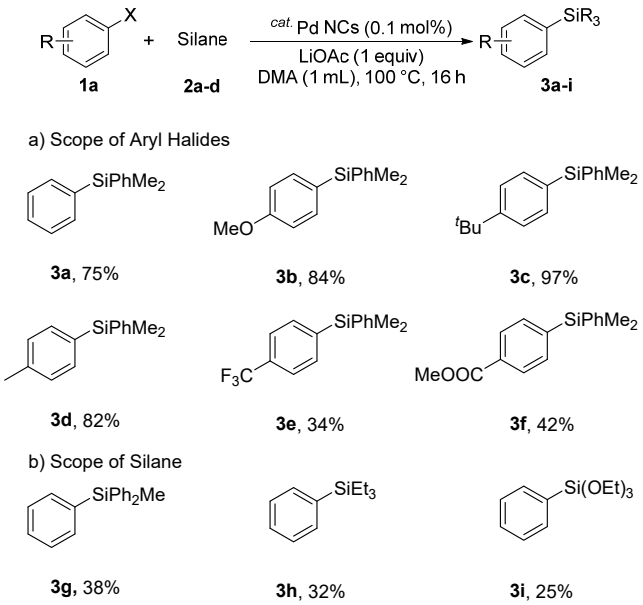


The author wanted to extend the coupling reaction to disilanes. Hexamethyldisilane is readily available as a Rochow direct process byproduct.[20] The reaction of iodobenzene with hexamethyldisilane at 120 °C afforded **5a** in 52% yield (Table 3, entry 1). Various bases were examined. NaOAc showed the best performance (entries 2–5). The same solvent effect was observed for DMF and DMAc (entry 6). The presence of a base was necessary for the reaction (entry 7).

Table 3. Optimisation of the arylsilylation condition with hexamethyldisilane[a]

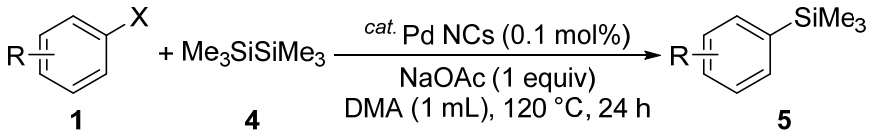


| Entry | Solvent | Base | Yield (%)[b] |
|---|---|---|---|
| 1 | DMAc | LiOAc | 70 |
| 2 | DMAc | NaOAc | 85 (70) |
| 3 | DMAc | KF | 73 |
| 4 | DMAc | $Na_2CO_3$ | 78 |
| 5 | DMAc | KOtBu | 27 |
| 6 | DMF | NaOAc | 69 |
| 7 | DMAc | - | 32 |

[a]Reaction conditions: **1a** (1.0 mmol), **4** (3.0 mmol), Pd NCs (0.1 mol %), and base (1.0 mmol) in solvent (1.0 mL) at 120 °C for 24 h. [b]The yields were determined by GC analysis. The isolated yield is shown in parenthesis.

Table 4 Coupling Reaction of Aryl Halides **1a** with hexamethyldisilane[a]

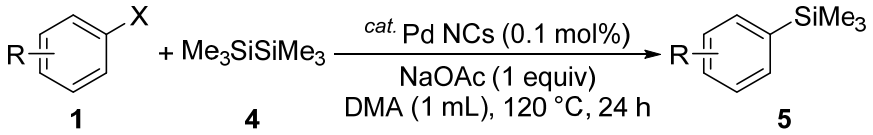


| Entry | X | R | Product | Yield[b] (%) |
|---|---|---|---|---|
| 1 | I | H | **5a** | 71 |
| 2 | | *p*-Me | **5b** | 65 |
| 3 | | *p*-OMe | **5c** | 73 |
| 4 | | p-$^t$Bu | **5d** | 86 |
| 5 | | *p*-COMe | **5e** | 66 |
| 6 | | *p*-COOMe | **5f** | 59 |
| 7 | | *p*-$CF_3$ | **5g** | 48 |
| 8 | Br | H | **5a** | 5[c] |
| 9 | Cl | H | **5a** | Trace[c] |

[a]Reaction conditions: **1a** (1.0 mmol), **2a** (3.0 mmol), Pd NCs (0.1 mol %), and base (1.0 mmol) in DMAc (1.0 mL) at 120 °C for 24 h. [b]Isolated yield. [c]GC Yield.

Iodobenzene derivatives bearing electron-donating groups, such as *p*-methyl, *p*-methoxy, and *p*-*tert*-butyl groups, gave the corresponding products in good yields (Table 4, entries 2–4). Electron-withdrawing groups were less effective (entries 5–7). However, the reaction of bromo/chlorobenzene under these conditions was sluggish.

Based on the experimental results and those reported in the literature, a plausible reaction mechanism are shown in Figure 9. [21] Iodobenzene or hydrosilane oxidatively adds to the Pd NCs. The desired coupling product is obtained by the σ-bond metathesis reaction.

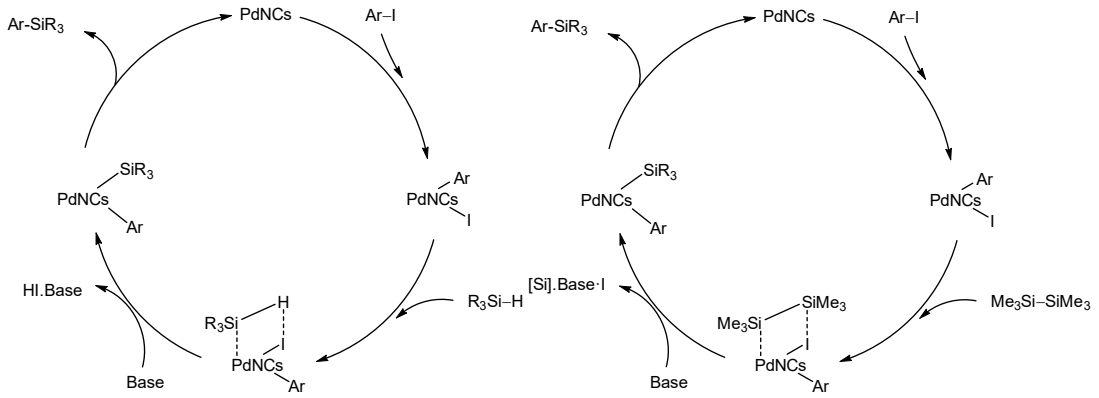


Figure S7 a plausible reaction mechanism of Pd NCs catalyzed coupling reactions of aryl halides with hydrosilanes(left)[1]/disilanes(right)

The author investigated possible reuse of the catalyst.[22] After the reaction, the author performed annular dark field scanning transmission electron microscopy (ADF-STEM) and inductively coupled plasma-atomic emission spectroscopy (ICP-AES) analysis. The particle size remained the same (Figure 10). Based on a previous study, the results suggest that the Pd NCs possess recyclability in the coupling reaction.

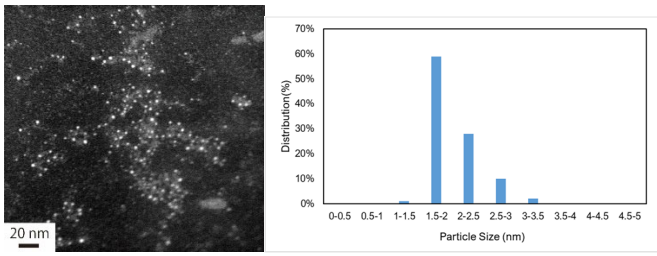


Figure 10. (a) ADF-STEM image (scale bar = 20 nm) and (b) particle size distribution of the Pd NCs after the reaction.

The author tested the recyclability of the Pd NCs. After performing the reaction with the disilane system (Table 4, entry 1), the hexane layer was extracted using 8 mL of hexane five times. The hexane layer (containing the starting materials and products) was removed. The DMAc was evaporated from the residual DMAc layer containing Pd NCs and the residue was reused as the catalyst for the reaction under the same conditions (Table 3, entry 1). The Pd NCs gave good yields five times. the author also tested the coupling reaction of aryl halide with hydrosilane (reaction conditions as in Table 1, entry 2). In the hydrosilane coupling reaction, the extraction solvent was modified. Product **3a** and the starting materials were extracted using a mixed solvent (hexane:ethyl acetate = 95:5). The Pd NCs catalyst tolerated multiple cycles.

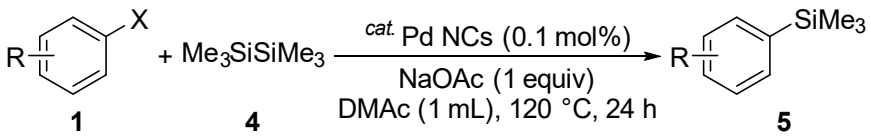


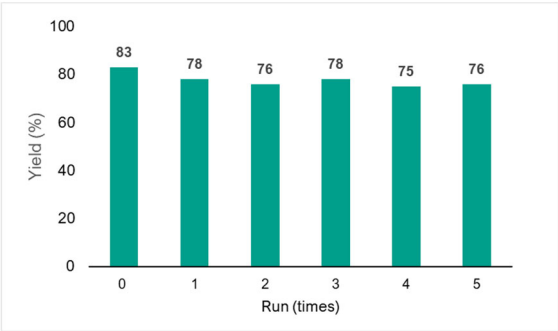


Figure 11. Multiple catalyst recycling for coupling of iodobenzene with disilane (conditions as in Table 4, entry 1)**.**

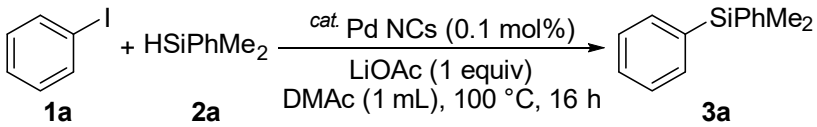


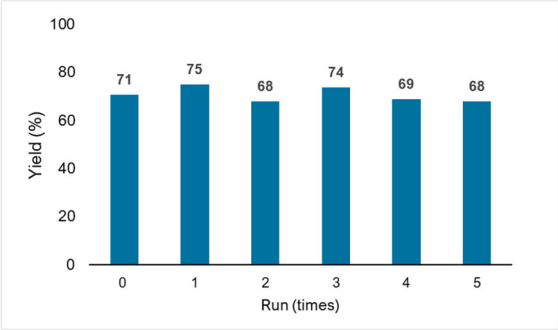


Figure 12. Multiple catalyst recycling for coupling of iodobenzene with hydrosilane (conditions as in Table 1, entry 2).

## Conclusion

The author has developed Pd NCs catalytic system for silylation of aryl halides with hydrosilanes/disilanes. The Pd NCs catalyst can be separated and reused at least five times without notable loss of the catalytic activity. DMAs displacement enables easy access to the active sites of the Pd NCs.

## Experimental

### General

GC analysis was performed with a flame ionisation detector using a 0.22 mm × 25 m capillary column (BP-5). The $^{1}H$ and $^{13}C$ NMR spectra were recorded at 400 and 100 MHz, respectively. The $^{1}H$ and $^{13}C$ NMR chemical shifts are reported in ppm with respect to the residual chloroform ($^{1}H$ 7.26 ppm, $^{13}C$ 77 ppm). The products were characterised by $^{1}H$ NMR, $^{13}C$ NMR, and GC–MS. The TEM and STEM images were obtained with a JEM-ARM200F(JEOL) instrument at an accelerating voltage of 200 kV. ICP-AES was performed with a ICPS-8100 spectrometer (Shimadzu). XPS analysis was performed with a PHI5000 VersaProbe (ULVAC-PHI) with Al Kα radiation. The measured spectra were calibrated by the C 1s electron peak (284.5 eV). TG analysis was performed with a Thremo Plus EVO device (Rigaku, Japan) at a heating rate of 10 °C $min^{-1}$ under $N_2$ flow.

All of the synthesised compounds (**3a**,[23a] **3b**,[23a] **3c**,[23a] **3d**,[23b] **3e**,[23a] **3f**,[23b] **3g**,[23e] **3h**,[23c] **3i**,[23d] **5a,**[24a] **5b**,[24c] **5c**,[24c] **5d**, **5e**,[24b] **5f,**[24d] and **5g** [24b]) are known compounds and have been previously reported.

All of the starting materials were commercially available and used without further purification. The DMF-protected Pd NCs were prepared according to a previously reported method.[15a]

(a) Preparation of the DMF-stabilised Pd NCs

DMF (50 mL) was added to a 300 mL three-necked round bottom flask. The solution was preheated to 140 °C (±2 °C) and stirred at 1500 rpm for 5 min. $PdCl_2$ solution (0.1 M, 500 μL) was then added to the hot DMF solution, which was allowed to react for 10 h under stirring (1500 rpm) at 140 °C (±2 °C). The resulting clear yellow solution was used as the 1 mM Pd NCs solution in DMF. After vacuum evaporation of the solvent, the residue was dissolved in selected solvents for the measurements and coupling reaction.

(A) Reaction of aryl halides with hydrosilanes

A mixture of iodobenzene (**1a**, 204 mg, 1 mmol), dimetheylphenylsilane (**2a**, 409 mg, 3 mmol), LiOAc (67 mg, 1 mmol), Pd NCs in DMAc (1 mL, 1 mM) as a catalyst, and solvent was stirred at 100 °C for 16 h in an Ar atmosphere. The product and substrate conversions and yields were estimated by GC from the peak areas based on an internal standard (*n*-decane). **3a** was obtained in 80% yield. **3a** was isolated by column chromatography [silica gel (230–400 mesh), *n*-hexane as eluent] in 75% yield (159 mg).

Characterization of the compounds

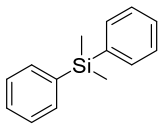


**3a** dimethyldiphenylsilane, colorless liquid, $^{1}H$-NMR (400 MHz $CDCl_3$) δ: 7.57-7.54 (m, 4H), 7.39-7.38 (m, 6H), 0.59 (s, 6H); $^{13}C$-NMR (100 MHz; $CDCl_3$) δ: 138.22 (C) 134.22 (CH), 129.11 (CH), 127.82 (CH), -2.42 ($CH_3$); GC-MS (EI) m/z (relative intensity) 212(23) $[M]^+$, 197(100), 198 (19), 105(9).

**3b** dimethyl(phenyl)(p-tolyl)silane, colorless liquid, $^{1}$H-NMR (400 MHz $CDCl_3$) δ: 7.57-7.55 (m, 2H), 7.48-7.46 (m, 2H), 7.39-7.38 (m, 3H), 7.23-7.21 (m,. 2H), 2.39 (s, 3H), 0.58 (s, 6H);$^{13}$C-NMR (100 MHz $CDCl_3$) δ: 138.96 (C), 138.50 (C), 134.53 (C), 134.23 (CH), 134.15 (CH), 129.00 (CH), 128.65 (CH), 127.76 (CH), 21.45 ($CH_3$), -2.32 ($CH_3$);GC-MS (EI) m/z (relative intensity) 226(18) $[M]^+$, 211(100), 212 (21), 105(7)

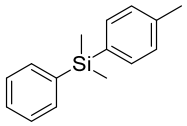


**3c** (4-ethoxyphenyl)dimethyl(phenyl)silane, colorless liquid, $^{1}$H-NMR (400 MHz $CDCl_3$) δ: 7.53-7.44 (m, 7H), 6.97-6.95 (m, 2H), 3.85 (s, 3H), 0.58 (s, 6H); $^{13}$C-NMR (100 MHz $CDCl_3$) δ: 160.48 (C), 138.66 (C), 135.62 (CH), 134.11 (CH), 128.97 (CH), 127.75 (CH), 113.58 (CH), 54.97 ($CH_3$), -2.32 ($CH_3$); GC-MS (EI) *m/z* (relative intensity) 242 (20) $[M]^+$, 227 (100), 135 (4).

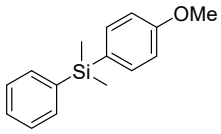


**3d** (4-(tert-butyl)phenyl)dimethyl(phenyl)silane, colorless liquid, $^{1}$H-NMR (400 MHz $CDCl_3$) δ: 7.21-7.01 (m, 9H), 0.98 (s, 9H), 0.21 (s, 6H);$^{13}$C-NMR (100 MHz $CDCl_3$) δ: 151.98 (C), 138.46 (C), 134.59 (C), 134.15 (CH), 134.04 (CH), 128.99 (CH), 127.75 (CH), 124.77 (CH), 34.62 (C), 31.22 ($CH_3$), -2.34 ($CH_3$); GC-MS (EI) *m/z* (relative intensity) 268 (16) $[M]^+$ 253 (100) 237 (6) 105 (10).

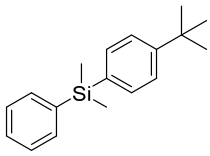


**3e** dimethyl(phenyl)(4-(trifluoromethyl)phenyl)silane, $^{1}$H-NMR (400 MHz $CDCl_3$) δ: 7.64-7.61 (m, 4H), 7.53-7.52 (m, 2H), 7.41-7.38 (m, 3H), 0.60 (s, 6H); $^{13}$C-NMR (100 MHz $CDCl_3$) δ: 143.36 (q, $^{4}J_{C\text{-}F}$ = 1.0 Hz, CH), 137.03 (CH), 134.41 (CH), 134.10 (CH), 130.99 (q, $^{2}J_{C\text{-}F}$= 32.2 Hz, CH,), 129.45 (CH), 127.97 (CH), 124.29 (q, $^{3}J_{C\text{-}F}$ = 3.7 Hz, CH), 124.19 (q, $^{1}J_{C\text{-}F}$ = 273.0 Hz, C,), -2.63 ($CH_3$); GC-MS (EI) *m/z* (relative intensity) 280(4) $[M]^+$, 265(100), 184(15).

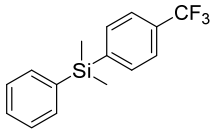


**3f** methyl 4-(dimethyl(phenyl)silyl)benzoate, colorless liquid,$^{1}$H-NMR (400 MHz $CDCl_3$) δ: 8.00 (dd, 2H, *J* = 8.3, 0.7 Hz), 7.60 (dd, 2H, *J* = 8.3, 0.7 Hz), 7.51-7.49 (m, 2H), 7.38-7.37 (m, 3H), 3.92 (s, 3H), 0.58 (d, 6H); $^{13}$C-NMR (100 MHz; $CDCl_3$) δ: 167.22 (C), 144.63 (C), 137.28 (C), 134.13 (CH), 134.11 (CH), 130.49 (C), 129.34 (CH), 128.51 (CH), 127.91 (CH), 52.12 ($CH_3$), -2.61 ($CH_3$); GC-MS (EI) *m/z* (relative intensity) 270(7) $[M]^+$, 256 (20), 255(100), 239(2)

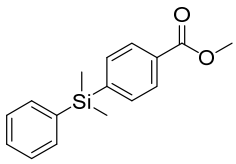


**3g** methyltriphenylsilane, colorless liquid, $^{1}$H-NMR (400 MHz $CDCl_3$) δ: 7.56-7.36 (m, 15H), 0.87 (s, 3H); $^{13}$C-NMR (100 MHz $CDCl_3$) δ: 136.06 (C), 135.25 (CH), 129.37 (CH), 127.83 (CH), -3.40 ($CH_3$); GC-MS (EI) *m/z* (relative intensity) 274 (5) $[M]^+$, 259 (100), 180 (12).

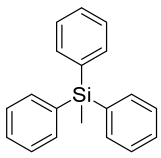

**3h** triethyl(phenyl)silane, colorless liquid,$^{1}$H NMR (400 MHz $CDCl_3$): δ 7.50–7.35 (m, 2H), 7.34–7.25 (m, 3H), 0.96 (t, 9H , *J* =8.0 Hz), 0.79 (q, 6H, *J* =7.2 Hz);$^{13}$C-NMR (100 MHz $CDCl_3$): δ 137.8 (C), 134.5 (CH), 129.0 (CH), 127.9 (CH), 7.7 ($CH_3$), 3.6 ($CH_2$); GC-MS (EI) *m/z* (relative intensity) 192(6) $[M]^+$, 163(59), 135(100), 107(77)

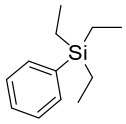


**3i** triethoxy(phenyl)silane, colorless liquid, $^{1}$H NMR (400 MHz $CDCl_3$): δ 7.68 (d, *J* = 6.4 Hz, 2H), 7.34 (m, 3H), 3.87 (q, *J* =7.2, 6H), 1.25 (t, 9H, *J* =6.8 Hz);$^{13}$C-NMR (100 MHz $CDCl_3$): δ 134.8 (C), 130.9 (CH), 130.4 (CH), ..127.9 (CH), 58.7 ($CH_2$), 18.2 ($CH_3$);GC-MS (EI) *m/z* (relative intensity) 240(23) $[M]^+$, 195(42), 145(100), 135(36).

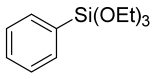


**5a** (Trimethylsilyl)benzene, $^{1}$H NMR (400 MHz $CDCl_3$) 7.66-7.46 (m, 2H), 7.40-7.33 (m, 3H), 0.27 (s, 9H); $^{13}$C-NMR (100 MHz; $CDCl_3$) δ: 140.47 (C), 133.28 (CH), 128.75 (CH), 127.71 (CH), -1.16 ($CH_3$).; GC-MS (EI) *m/z* (relative intensity) 150 (18) $[M]^+$, 136 (12), 135(100).

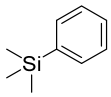


**5b** trimethyl(p-tolyl)silane: colorless liquid, $^{1}$H- NMR (400 MHz $CDCl_3$): δ 7.45 (d, 2H *J* = 8.0 Hz), 7.20 (d, 2H, *J* = 7.6 Hz), 2.37 (s, 3H), 0.27 (s, 9H); $^{13}$C-NMR (100 MHz $CDCl_3$): δ 138.6 (C), 136.8 (C), 133.3 (CH), 128.6 (CH), 21.5 (CH3), -1.1 ($CH_3$); GC-MS (EI) *m/z* (relative intensity) 164(13) $[M]^+$, 149(100), 121(9).

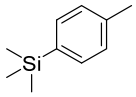


**5c** 4-methoxyphenyl)trimethylsilane: colorless liquid, $^{1}$H-NMR (400 MHz $CDCl_3$): δ 7.20 (d, 2H, *J* = 8.8 Hz), 6.67 (d, 2H, *J* = 8.4 Hz), 3.56 (s, 3H), 0.00 (s, 9H) ;$^{13}$C-NMR (100 MHz $CDCl_3$): δ 162.2 (C), 135.7 (CH), 132.2 (C), 114.4 (CH), 55.9 ($CH_3$), 0.00 ($CH_3$);GC-MS (EI) *m/z* (relative intensity) 180(16) $[M]^+$, 165(100), 135(9).

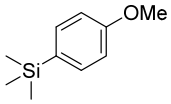


**5d** (4-(tert-butyl)phenyl)trimethylsilane: white solid, m.p 77.5-78, $^{1}$H-NMR (400 MHz $CDCl_3$): δ 7.49 (d, 2H, *J* = 8.4 Hz), 7.41 (d, 2H, *J* = 8.0 Hz), 1.34 (s, 9H), 0.27 (s, 9H);$^{13}$C-NMR (100 MHz $CDCl_3$): δ 151.7 (C), 136.9 (C), 133.2 (CH), 124.7 (CH), 34.6 (C), 31.2 ($CH_3$), -1.06($CH_3$); GC-MS (EI) *m/z* (relative intensity) 206(12) $[M]^+$, 191(100), 176(7).

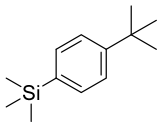


**5e** 1-(4-(trimethylsilyl)phenyl)ethan-1-one:colorless liquid, $^{1}$H-NMR (400 MHz $CDCl_3$) δ: 7.92-7.91 (m, 2H), 7.63-7.61 (m, 2H), 2.60 (s, 3H), 0.29 (s, 9H);$^{13}$C-NMR (100 MHz $CDCl_3$) δ: 198.33 (C), 147.21 (C), 137.17 (C), 133.48 (CH), 127.19 (CH), 26.58 ($CH_3$), -1.38 ($SiMe_3$); GC-MS (EI) m/z (relative intensity) 192 (14) $[M]^+$, 177(100), 162 (1), 119 (7).

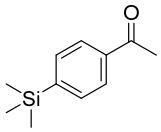

**5f** methyl 4-(trimethylsilyl)benzoate: colorless liquid, $^{1}$H-NMR (400 MHz $CDCl_3$) δ: 7.99 (d, 2H, *J* = 8.3 Hz), 7.59 (d, 2H, *J* = 8.2 Hz), 3.92 (s, 3H), 0.29 (s, 9H); $^{13}$C-NMR (100 MHz $CDCl_3$) δ: 167.28 (C), 146.84 (C), 133.27 (CH, s), 130.19 (C), 128.44 (CH), 52.09 ($CH_3$), -1.34 ($CH_3$); GC-MS (EI) *m/z* (relative intensity) 208 (5) $[M]^+$, 193 (100), 133 (14).

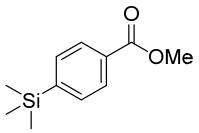


**5g** trimethyl(4-(trifluoromethyl)phenyl)silane: $^{1}$H-NMR (400 MHz $CDCl_3$) : δ 7.64 (d, 2H, *J* = 7.6 Hz), 7.59 (d, 2H, *J* = 8.0 Hz), 0.30 (s, 9H); $^{13}$C-NMR (100 MHz $CDCl_3$): δ 145.6 (C), 133.8 (CH), 130.8 (q, *J*= 31.6 Hz, C), 124.3 (q, *J*= 270.2 Hz, C), 124.2 (q, *J*= 3.9 Hz CH), -1.41($CH_3$) GC-MS (EI) *m/z* (relative intensity) 218(6) $[M]^+$, 203(100), 189(0.60).

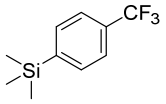

## Reference


(1) a) J. Wang, C. Ma, Y. Wu, R. A. Lamb, L. H. Pinto, W. F. Degrado, *J. Am. Chem. Soc.* **2011**, *133*, 13844-13487; b) A. K. Franz, S. O. Wilson, *J. Med. Chem.* **2013**, *56*, 388-405.

(2) a) M. Shimizu, K. Mochida, T. Hiyama, *Angew. Chem. Int. Ed.* **2008**, *47*, 9760-9764; b) X. M. Liu, C. He, J. Huang, J. Xu, *Chem. Mater.* **2005**, *17*, 434-441; c) G. W. Kim, D. R. Yang, Y. C. Kim, H. I. Yang, J. G. Fan, C. H. Lee, K. Y. Chai, J. H. Kwon, *Dyes Pigm.* **2017**, *136*, 8-16; d) H. Inubushi, Y. Hattori, Y. Yamanoi, H. Nishihara, *J. Org. Chem.* **2014**, *79*, 2974-2979; e) N. You, C. G. An, J. J. Kim, Y. P. Soo, *J. Org. Chem.* **2007**, *72*, 6241-6246.

(3) a) P. Somfai, B. Seashore-Ludlow, *Organosilicon Reagents: Vinyl-, Alkynyl-, and, Arylsilanes*, Elsevier Ltd., **2014**; b) T. Komiyama, Y. Minami, T. Hiyama, *ACS Catal.* **2017**, *7*, 631-651; c) A. S. Manoso, P. DeShong, *J. Org. Chem.* **2001**, *66*, 7449-7455.

(4) a) S. Luliński, J. Serwatowski, *J. Org. Chem.* **2003**, *68*, 9384-9388; b) A. S. Manoso, C. Ahn, A. Soheili, C. J. Handy, R. Correia, W. M. Seganish , P. DeShong, *J. Org. Chem.* **2004**, *69*, 8305-8314.

(5) Z. Xu, W. S. Huang, J. Zhang, L. W. Xu, *Synthesis* **2015**, 47, 3645-3668.

(6) a) H. Guo, X. Chen, C. Zhao, W. He, *Chem. Commun.* **2015**, *51*, 17410-17412; b) Y. Yamanoi, *J. Org. Chem.* **2005**, *70*, 9607-9609; c) N. Iranpoor, H. Firouzabadi, R. Azadi, *J. Organomet. Chem.* **2010**, *695*, 887.-890; (d) M. Murata, K. Suzuki, S. Watanabe, Y. Masuda, *J. Org. Chem.* **1997**, *62*, 8569-8571.

(7) a) M. Murata, M. Ishikura, M. Nagata, S. Watanabe, Y. Masuda, *Org. Lett.* **2002**, *4*, 1843-1845; b) Y. Yamanoi, H. Nishihara, *Tetrahedron Lett.* **2006**, *47*, 7157–7161; c) Y. Yamanoi, H. Nishihara, *J. Org. Chem.* **2008**, *73*, 6671-6678; d) M. Murata, H. Yamasaki, K. Uogishi, S. Watanabe, Y. Masuda, *Synthesis* **2007**, 2007, 2944-2946.

(8) (a) J. Y. Corey, *Chem. Rev.*, **2011**, *111*, 863-1071; (b) R. Boukherroub, C. Chatgilialoglu , G. Manuel, *Organometallics*, **1996**, *15*, 1508-1510.

(9) a) T. Iwasawa, T. Komano, A. Tajima, M. Tokunaga, Y. Obora, T. Fujihara, Y. Tsuji, *Organometallics* **2006**, *25*, 4665-4469; b) E. Shirakawa, T. Kurahashi, H. Yoshida, T. Hiyama, *Chem. Commun.* **2000**, 1895-1896; c) E. McNeill, T. E. Barder, S. L. Buchwald, *Org. Lett.* **2007**, 9, 3785-3788.

(10) a) Y. Lu, W. Chen, *Chem. Soc. Rev.* **2012**, *41*, 3594-3623; b) L. Zhang, E. Wang, *Nano Today* **2014**, *9*, 132-157; c) A. Mathew, T. Pradeep, *Part. Part. Syst. Charact.* **2014**, *31*, 1017-1053.

(11) a) S. Campisi, M. Schiavoni, C. Chan-Thaw, A. Villa, *Catalysts* **2016**, *6*, 185; b) Y. Dai, Y. Wang, B. Liu , Y. Yang, *Small*, **2015**, *11*, 268-289; c) T. Nagata, Y. Adachi , Y. Obora, *Synlett* **2018**, *29*, 2655-2659; d) Y. Adachi, H. Kawasaki, T. Nagata , Y. Obora, *Chem. Lett.* **2016**, *45*, 1457-1459.

(12) a) A. Bej, K. Ghosh, A. Sarkar, D. W. Knight, *RSC Adv.* **2016**, *6*, 11446-11453; b) D. Roy, Y. Uozumi, *Adv. Synth. Catal.* **2018**, *360*, 602-625; c) C. Deraedt , D. Astruc, *Acc. Chem. Res.* **2014**, *47*, 494-503.

(13) a) W. Huang, Q. Hua, T. Cao, *Catal. Lett.* **2014**, *144*, 1355-1369; b) Z. Niu, Y. Li, *Chem. Mater.* **2014**, *26*, 72-83.

(14) a) H. Kawasaki, *Nanotechnol. Rev.* **2013**, *2*, 5-25; b) I. Pastorizo-Santos, L. M. Liz-Marzán, *Adv. Funct. Mater.* **2009**, *19*, 679-688; c) H. Oka, K. Kitai, T. Suzuki, Y. Obora, *RSC Adv.* **2017**, *7*, 22869-22874; d) K. Oikawa, S. Itoh, H. Yano, H. Kawasaki, Y. Obora, *Chem. Commun.* **2017**, *53*, 1080-1083; e) Y. Isomura, T. Narushima, H. Kawasaki, T. Yonezawa, Y. Obora, *Chem. Commun.* **2012**, *48*, 3784-3786; f) H. Yamamoto, H. Yano, H. Kouchi, Y. Obora, R. Arakawa, H. Kawasaki, *Nanoscale* **2012**, *4*, 4148-4154.

(15) a) M. Hyotanishi, Y. Isomura, H. Yamamoto, H. Kawasaki, Y. Obora, *Chem. Commun.* **2011**, *47*, 5750-5752; b) H. Yano, Y. Nakajima, Y. Obora, *J. Organomet. Chem.* **2013**, *745–746*, 258-261; c) K. Onishi, K. Oikawa, H. Yano, T. Suzuki, Y. Obora, *RSC Adv.* **2018**, *8*, 11324-11329.

(16) R. Azuma, S. Nakamichi, J. Kimura, H. Yano, H. Kawasaki, T. Suzuki, R. Kondo, Y. Kanda, K. I. Shimizu, K. Kato, Y. Obora, *ChemCatChem* **2018**, *10*, 2378-2382.

(17) J. Jang, S. Byun, B. M. Kim, S. Lee, *Chem. Commun.* **2018**, *54*, 3492-3495.

(18) a) M. G. Mason, *Phys. Rev. B* **1983**, *27*, 748-762; b) G. K. Wertheim, S. B. DiCenzo, D. N. E. Buchanan, *Phys. Rev. B* **1986**, *33*, 5384-5390.

(19) a) M. Chiba, M. N. Thanh, Y. Hasegawa, Y. Obora, H. Kawasaki, T. Yonezawa, *J. Mater. Chem. C* **2015**, *3*, 514-520; b) M. Ren, Y. Jin, W. Chen, W. Huang, *J. Phys. Chem. C*, **2015**, *119*, 27588-27593.

(20) a) E. G. Rochow, *J. Am. Chem. Soc.* **1945**, *67*, 963-965; b) W. J. Ward, A. Ritzer, K. M. Carroll, J. W. Flock, *J. Catal.* **1986**, *100*, 240-249.

(21) J. Cao, Y.-M. Cui, Z. Xu, J. Zhang, L.-W. Xu, Z.-J. Zheng, J.-Z. Xu, *Chem. Asian J.* **2017**, *12*, 1749-1757.

(22) a) Á. Molnár, *Chem. Rev.* **2011**, *111*, 2251-2320; b) Á. Molnár, A. Papp, *Coord. Chem. Rev.* **2017**, *349*, 1-65.

(23) a) M. Uchiyama, Y. Kobayashi, T. Furuyama, S. Nakamura, Y. Kajihara, T. Miyoshi, T. Sakamoto, Y. Kondo, K. Morokuma, *J. Am. Chem. Soc.* **2008**, *130*, 472-480; b) H. Guo, X. Chen, C. Zhao, W. He, *Chem. Commun.* **2015**, *51*, 17410–17412; c) N. Iranpoor, H. Firouzabadi, R. Azadi, *J. Organomet. Chem.* **2010**, *695*, 887-890; d) M. Murata, H. Yamasaki, T. Ueta, M. Nagata, M. Ishikura, S. Watanabe, Y. Masuda, *Tetrahedron* **2007**, *63*, 4087-4094; e) N. Tsukada, J. F. Hartwig, *J. Am. Chem. Soc.* **2005**, *127*, 5022-5023.

(24) a) H. Inubushi, H. Kondo, A. Lesbani, M. Miyachi, Y. Yamanoi, H. Nishihara, *Chem. Commun.* **2013**, *49*, 134-136; b) M. Tobisu, Y. Kita, Y. Ano, N. Chatani, *J. Am. Chem. Soc.* **2008**, *130*, 15982-15989; c) A. P. Lothian, C. A. Ramsden, M. M. Shaw, R. G. Smith, *Tetrahedron* **2011**, *67*, 2788-2793; d) M. Tobisu, Y. Kita, N. Chatani, *J. Am. Chem. Soc.* **2006**, *128*, 8152-8153.

**Chapter 4.** *N,N*-Dimethylformamide-protected $Fe_2O_3$ combined with Pt nanoparticles : Characterization and catalysis in alkene hydrosilylation

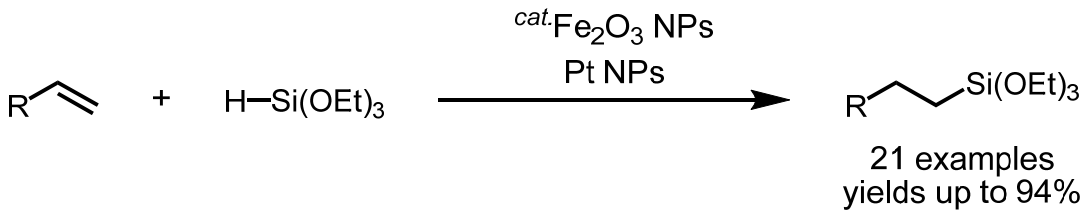

## Introduction

Alkene hydrosilylation plays the most important role in the production of organosilicon compounds.[1] The high-performance organosilicon products of hydrosilylation are widely used in consumer products such as silicon rubbers, lubricants, and adhesives.[2] Silane coupling agents, which combine organic resins and inorganic materials, can serve as a performance enhancer for semiconductor sealants and as a penetrating sealer(Figure 1) .[3]

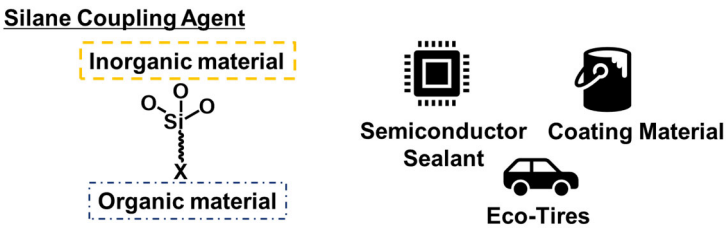


Figure 1. Schematic illustration of the silane coupling agents and usage example

For over more than half a century, the hydrosilylation reaction has mainly relied on a platinum complex (e.g. Speier's,[4] Karsted,[5] and Markó's[6] catalysts) because of the high catalytic activity and turnover number (Scheme 1). However, it is difficult to remove and recover the Pt from the products and to suppress the side reactions. The Pt residues, which are known to form Pt colloids, cause the production of by-products and degrade the overall product performance.[7]

Therefore, to overcome these drawbacks, earth-abundant transition metal catalysts, which are inexpensive, have been developed for the catalytic hydrosilylation of alkenes.[8] The hydrosilylation of alkenes with alkoxysilanes, which is important for the production of industrially relevant silane coupling agent, is a more challenging transformation. Base metal complexes that bear a well-defined ligand have been explored. Remarkable bench-stable Fe,[9a] Co,[10] and Ni[11] catalysts have been developed by Nagashima and Chirik. In addition, one-pod transformation of alkanes to linear alkylsilanes has been developed using Ir and Fe pincer complex. [9b] However, the availability of suitable ligands has been overlooked. Therefore, the development of practical ligands is still a challenge.

**Scheme 1.** Precious/base metal complex catalysts for hydrosilylation.

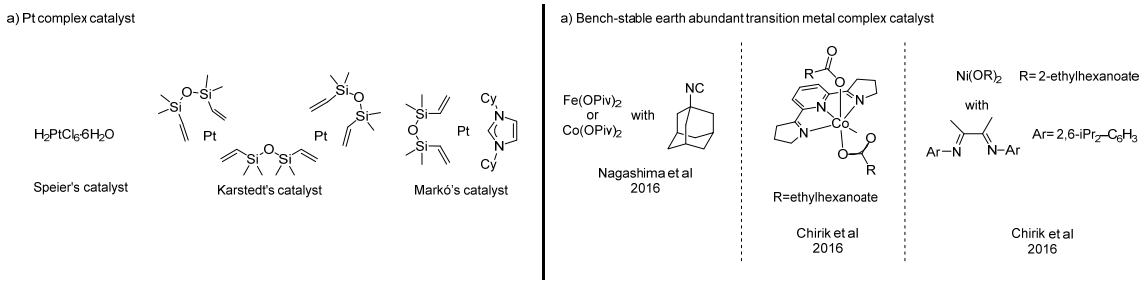


The catalytic application of metal nanoparticles [12] and single-atom-catalysts (SAC) [13] not only results in a reduction in material cost but also offers an alternative solution for hydrosilylation. Such heterogeneous catalysts are more recyclable than a homogeneous catalyst. Many heterogeneous hydrosilylation catalysts, such as supported precious/base metal NPs and SAC, have been investivated. [14, 15] In addition, the single-pod integration $CeO_2$-supported Ru and Rh based SAC achieved selective hydrosilylation process via tandem alkene isomerization-hydrosilylation even terminal and internal alkene mixture.[15e]

Previously, our group introduced unsupported metal nanoparticles (M NPs). The M NPs were synthesized by reduction of a metal precursor in the presence of *N,N*-dimethylformamide (DMF). DMF serves as a stabilizer, reductant, and solvent for the synthesis of M NPs. [16] Previously, our group reported DMF-protected $Fe_2O_3$ NPs for the hydrosilylation of alkenes with primary and secondary silanes.[17] Notably, a reaction with tertiary hydrosilanes, which are commercially important scaffolds, would be most beneficial. However, DMF-protected-$Fe_2O_3$ NPs-catalyzed hydrosilylation is not effective for a reaction with tertiary hydrosilanes. To solve this problem, the author focused on a combination of catalysts for directing practical hydrosilylation. [18]

Herein, the combination of DMF-protected $Fe_2O_3$ NPs and Pt NPs for the hydrosilylation of alkenes with alkoxysilanes. The characterization of the combination $Fe_2O_3$/Pt NPs suggests that they will exhibit a highly efficient catalytic activity under mild conditions.

## Results and discussions

Initially, the author selected 1-dodecene (**1a;** 0.5 mmol) and triethoxysilane (**2a;** 3 mmol) as model substrates with which to perform the hydrosilylation (Table 1). Notably, no silylated product was obtained and the starting alkene was recovered with the use of either the $Fe_2O_3$ NPs or the Pt NPs (entries 1 and 2). A mixture of $Fe_2O_3$ NPs and Pt NPs ($Fe_2O_3$/Pt NPs) resulted in an excellent yield of the hydrosilylation product (entry 3). In particular, when the $Fe_2O_3$ NPs catalyst was used, a substantial amount of tetraethoxysilane was produced. On the other hand, when Pt NPs was used, the disproportionation reaction was significantly suppressed. Although homogeneous Pt complexes are known to be highly active catalysts in the hydrosilylation of alkenes, the DMF-protected Pt NPs were not active in the hydrosilylation of C−C multiple bonds. Our group previously reported that the DMF-protected $Fe_2O_3$ NPs have been successfully employed as active catalysts in the hydrosilylation of alkenes with primary and secondary hydrosilanes that implied Si−H activation.[17] the hydrosilylation could be performed even under an $O_2$ atmosphere (entry 5). However, the alkenes **1a** were recovered, and **2a** was converted to give byproducts. Thus air atmosphere is the best for the reaction. ()

**Table 1** Hydrosilylation of 1-dodecene with triethoxysilane.[a]

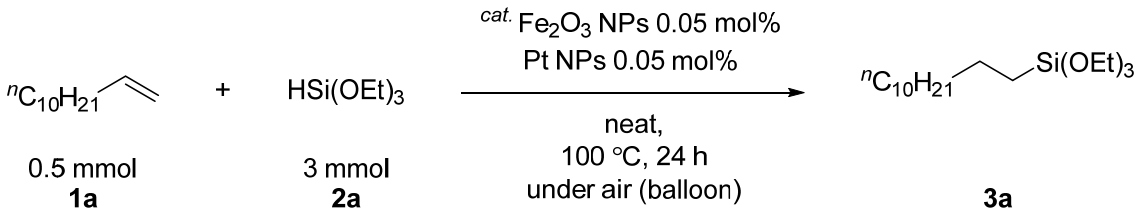


| Entry | **Catalyst** | **Conv.(%)** | | **T** (°C) | Atmosphere (balloon) | Yield of **3a**[a] | Yield of **TEOS**[b] |
|---|---|---|---|---|---|---|---|
| | | **1a** | **2a** | | | | |
| 1 | $Fe_2O_3$ NPs | 20 | 41 | 100 | Air | n.d. | 18 |
| 2 | Pt NPs | 10 | 15 | 100 | Air | n.d. | 3 |
| 3 | $Fe_2O_3$ /Pt NPs | >99 | 64 | 100 | Air | >99 | 20 |
| 4 | $Fe_2O_3$ /Pt NPs | 4 | 15 | 100 | Ar | n.d. | 2 |
| 5 | $Fe_2O_3$ / Pt NPs | 80 | 99 | 100 | $O_2$ | 59 | 37 |

a) b) GC yield n.d. = not detected by GC. c)TEOS yield based on **2a**.

a) Reaction conditions: 1-dodecene **1a** (0.5 mmol), hydrosilane **2a** (3 mmol), $Fe_2O_3$ NPs (0.05 mol%), Pt NPs (0.05 mol%) 100 °C, 24 h. b) GC yield, the number in parentheses shows the yield of isolated product. c) Not detected by GC.

The screening of other trisubstituted hydrosilanes, such as $HSiMe(OEt)_2$ and $HSiMe_2Ph$, was shown to give the desired products in good to excellent yields (Scheme 2, **3b–3f**). To synthesize industrially important silane coupling agents, the functional group tolerance is known to play an important role in silicon chemistry. [2, 19] Oxygen based functional alkenes (-epoxy, -esters, ketones) were tolerated and gave the corresponding products (**3g–3m**) in good to moderate yields. Sulfur-containing alkenes gave the silylated products (**3n** and **3o**) in a yield of 9%. **3p** had a remote chloride and could be produced by hydrosilylation. **3q,** an isocyanurate ring-bearing product, which is used as a toner external additive, was also obtained in a good yield. The reaction of primary and secondary silanes gave desired products **3s**, **3t**, and **3u** in good yields, respectively. Unfortunately, the desired product was not obtained from allyl chloride styrene derivatives and octadecylsilane. The reaction with octadecylsilane was sluggish under these conditions.

**Scheme 2.** DMF-protected $Fe_2O_3$/Pt NPs catalyzed hydrosilylation of various functional alkenes with hydrosilanes.[a]

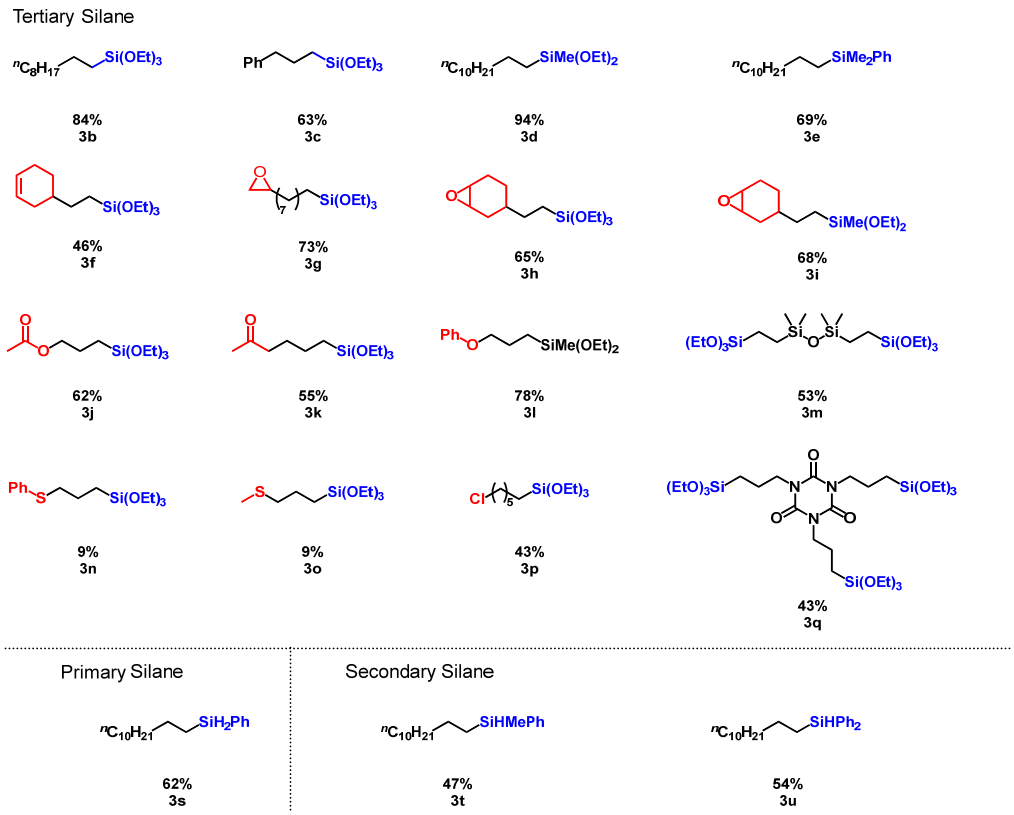


[a]Reaction conditions: same as entry 1 in Table 1, yield of isolated product. [b] $Fe_2O_3$ NPs : Pt NPs = 4 : 1 (0.1 mol%), Reaction time 48 h. [c] $Fe_2O_3$ NPs (0.25 mol%) and Pt NPs (0.25 mol%) were used. Reaction temperature (90 °C).[d]Reaction time 72 h.

To further demonstrate the synthetic utility of the combination of DMF-protected $Fe_2O_3$ and Pt NPs catalyst, the author performed the hydrosilylation on the 1-g, 10-g, and 1-kg scales (Scheme 3). First, the reaction of **1a** (5 mmol) and **2b** (30 mmol) afforded the silylated adduct in a yield of 84% (entry 1). In the 10-g scale transformation, the excess amount of the hydrosilane based on the alkene could be reduced from 6 equivalents to 1.2 equivalents. The use of **1a** (50 mmol) and **2a** (100 mmol) in the presence of $Fe_2O_3$ NPs (0.005 mol%) and Pt NPs (0.005 mol%) afforded **3a** in an excellent yield (86%, entry 2). The author continued to optimize the amount of hydrosilane. Product **3a** was obtained in 85% yield with the reaction of **1a** (50 mmol) and **2a** (60 mmol) in the presence of $Fe_2O_3$ NPs (0.005 mol%) and Pt NPs (0.005 mol%) (entry 3). The scale-up reaction of **1o** (50 mmol) and **2b** (60 mmol) also gave the desired product **3r** in good yield (entry 4). In addition, the reaction was successfully performed with hydrosilane as the limiting substrate. The reaction of **1o** (60 mmol) and **2b** (50 mmol) in the presence of $Fe_2O_3$ NPs (0.005 mol%) and Pt NPs (0.005 mol%) produced **3r** in a yield of 91% (entry 5). Finally, the hydrosilylation was scaled to 1 kilogram in the presence of $Fe_2O_3$ NPs (0.005 mol%) and Pt NPs (0.005 mol%), **1o** (6.55 mol) and **2b** (6.29 mol). Product **3r** was obtained in an excellent yield (91%, 1.412 kg, entry 6). The large-scale experiment disclosed byproducts that were difficult to observe on the small scale (disiloxane **4** and siloxane **5**). For details, see supporting information Figure 2-8.

**Scheme 3.** Large-scale hydrosilylation.

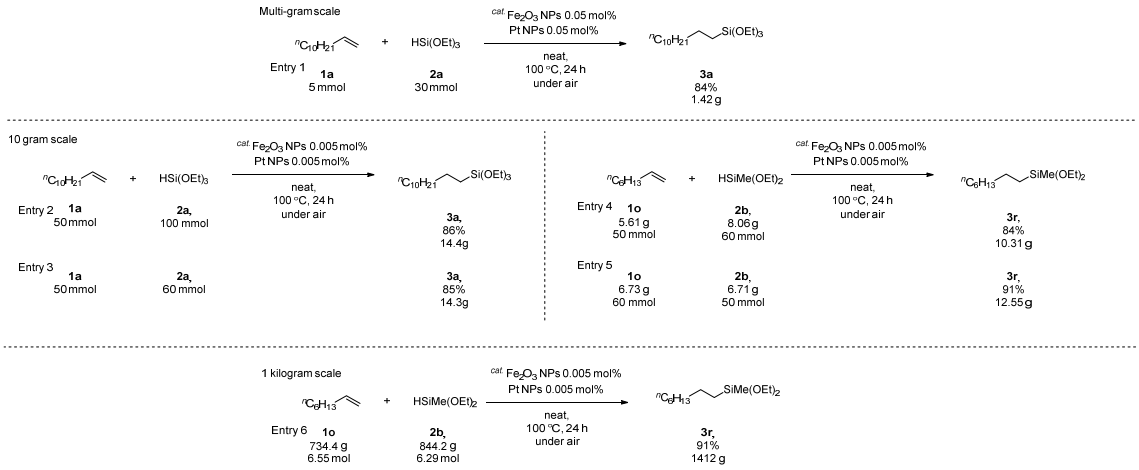

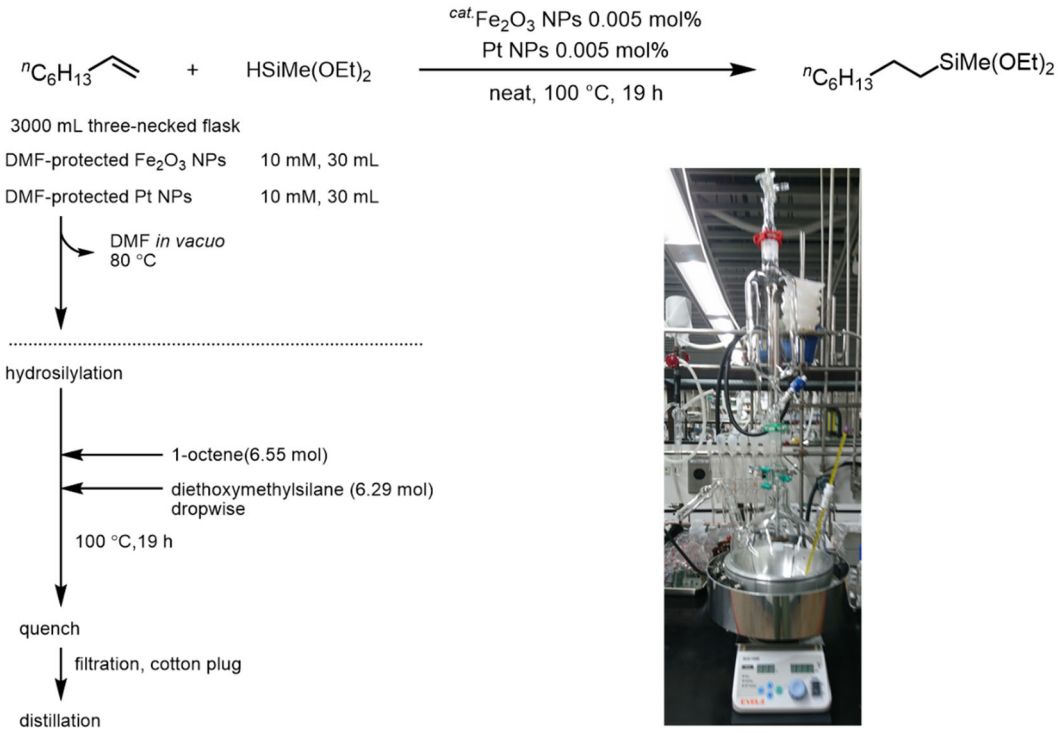


**Figure 2.** Reaction setup

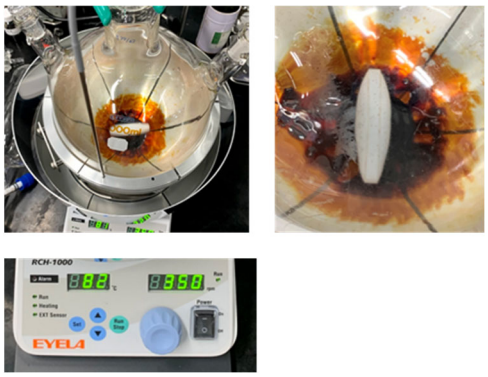

**Figure 3.** DMF removal under reduced pressure (80 °C).

**Figure 4**. After addition of diethoxymethylsilane.

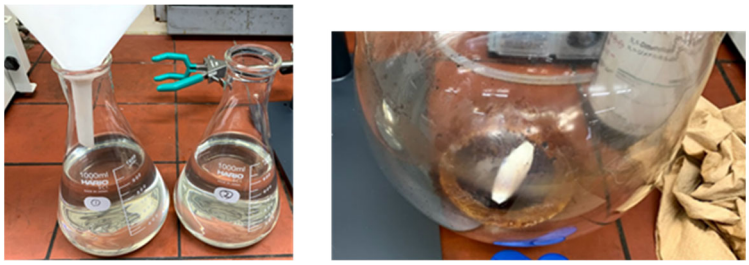

**Figure 5**. reaction mixture after filtration and catalyst sludge.

**Figure 6**. Distillation set up.

**Figure 7**. **3r** after distillation.

By-product identification

As reported previous hydrosilylation reactions, byproducts such as 2-octene (isomerization of olefins), methyltriethoxysilane (redistribution of hydrosilane) were confirmed (GC-MS). The large-scale experiment (1 kg) disclosed byproducts that were difficult to observe on the small scale (0.5 mmol). Distillation residue (a yellow oil) was passed t neutralized tb rough a plug of to remove catalyst sludge. was to remove metal nanoparticles, recycling Preparative HPLC was performed with a LaboACE LC-5060 (Japan Analytical Industry Co., Ltd.) instrument equipped with JAIGEL-1HR+ JAIGEL-2HR columns and RI-700 LA detector, using $CDCl_3$ as eluent. Main byproduct **4(siloxane)** and **5(siloxane)** was analyzed by $^{1}H$ NMR, $^{13}C$ NMR, HRMS, FT-IR.

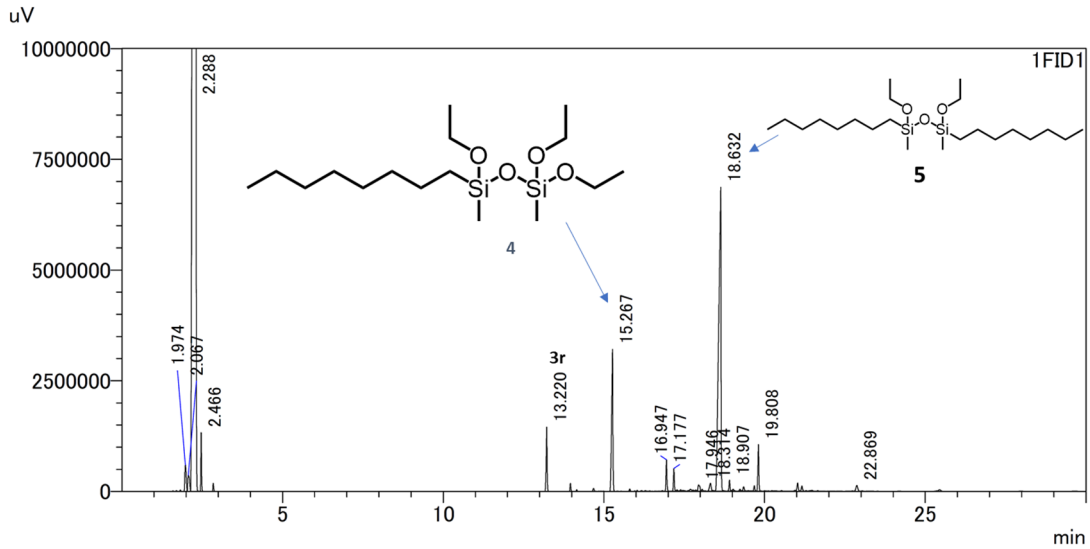


**Figure 8.** Distillation residue.

Recycling experiments were carried out to demonstrate the recyclability of the DMF-protected $Fe_2O_3$/Pt NPs catalyst system. After the reaction, the DMF protected $Fe_2O_3$/Pt NPs were recovered by extraction (hexane/DMF). The catalysts remained in the DMF layer, and the products and starting materials moved to the hexane layer. The author checked the recovery rate of both Fe and Pt by using inductively coupled plasma atomic emission spectroscopy (ICP-AES). After extraction, the DMF layer contained the Fe NPs and Pt NPs (recovery rates Fe, >99%, Pt, 96%). After DMF evaporation, the catalysts were reused for the subsequent hydrosilylation. As shown in Figure 9, the DMF-protected $Fe_2O_3$ NPs and Pt NPs retained their catalytic activity at least five times. To assess catalyst stability at intermediate conversion levels, recycling experiments for 2 h were conducted. The yields were maintained at 67-60% in the 1st to 3rd run and slightly decreased in the 4th and 5th run (53% and 48%) (Figure 9b).

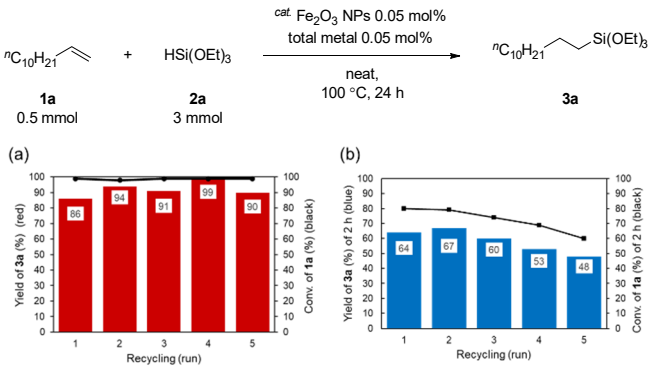


**Figure 9.** Recycling experiment of $Fe_2O_3$ and Pt NPs in the hydrosilylation of **1a** with **2a**: (a) 24 h reaction and (b) 2 h reaction.

2.2 Characterizations of $Fe_2O_3$ NPs and Pt NPs

The transmission electron microscopy (TEM) image (Figure 10) clearly showed that the average particle sizes of the $Fe_2O_3$ and Pt NPs were determined to be 3–4 nm and 2–3 nm, respectively. Powder XRD measurement was performed to understand the catalyst (Figure 11). Characteristic XRD pattern was not observed because of the ultra small size.[20]

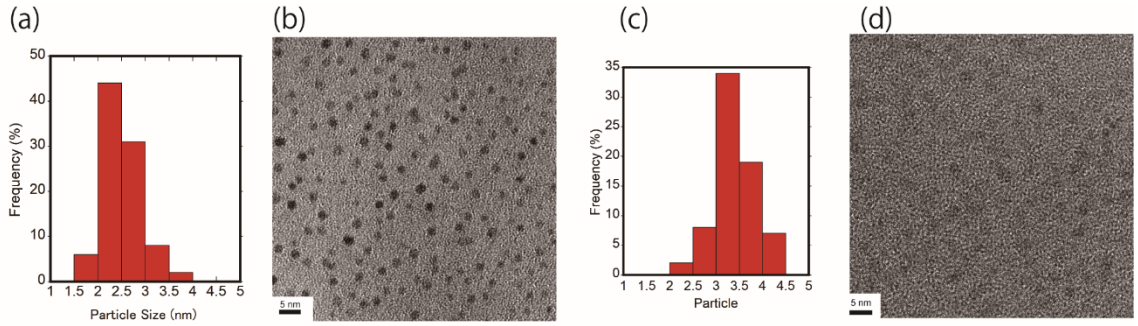


**Figure 10.** (a) (c) Size distribution of the nanoparticles and (b) (d) BF-TEM image of (a) (b) Pt NPs and (c) (d) $Fe_2O_3$ NPs.

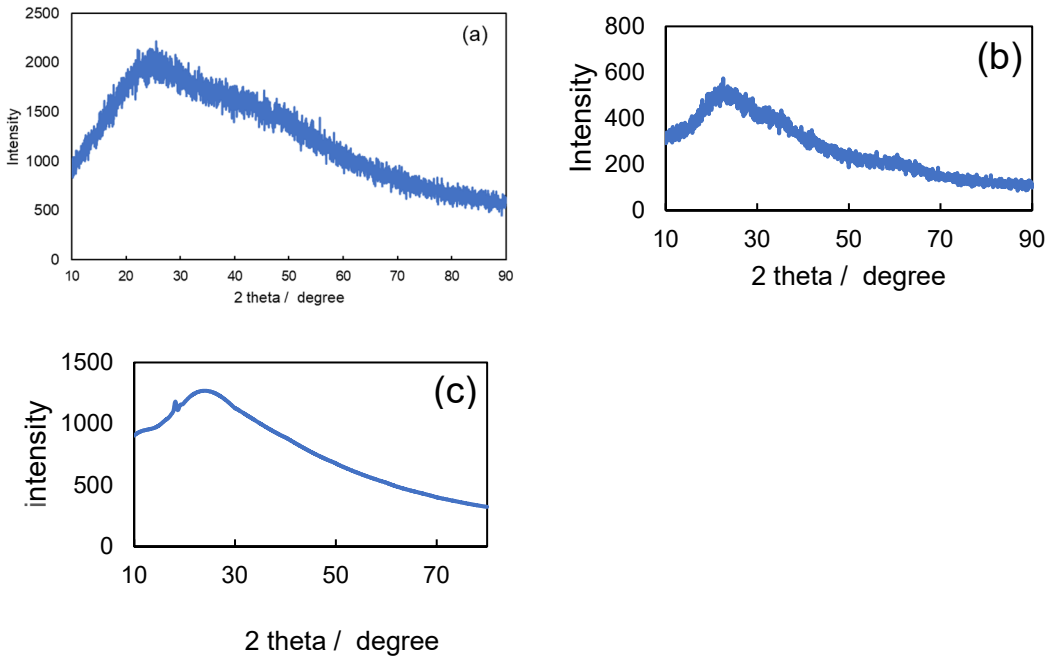


**Figure 11.** XRD charts (a) Pt NPs (b) $Fe_2O_3$ NPs (c)after reaction $Fe_2O_3$/Pt NPs.

Figure 12a shows the Fe K-edge normalized X-ray absorption near-edge region structure (XANES) spectra of $Fe_2O_3$ NPs, $Fe_2O_3$/Pt NPs, and the reference samples (Fe foil and $Fe_2O_3$). As reported in our previous work,[17] the oxidation state of Fe species in the DMF-protected $Fe_2O_3$ NPs is similar to that in a-$Fe_2O_3$. The oxidation state of the $Fe_2O_3$/Pt NPs was identical to that in the $Fe_2O_3$ NPs. The Fe K-edge XANES results

showed that the Pt NPs did not affect the $Fe_2O_3$ NPs. Additionally, Figure 12b shows the Pt $L_{III}$-edge XANES spectra of the DMF-protected Pt NPs, $Fe_2O_3$/Pt NPs, and the reference samples (Pt foil and $PtO_2$). The white line intensities of the Pt NPs and $Fe_2O_3$/Pt NPs were located between those of the Pt foil and $PtO_2$ (Figure 12b). No significant difference was found between the Pt NPs and $Fe_2O_3$/Pt NPs. Therefore, there was no interaction between the $Fe_2O_3$ NPs and Pt NPs before the reaction.

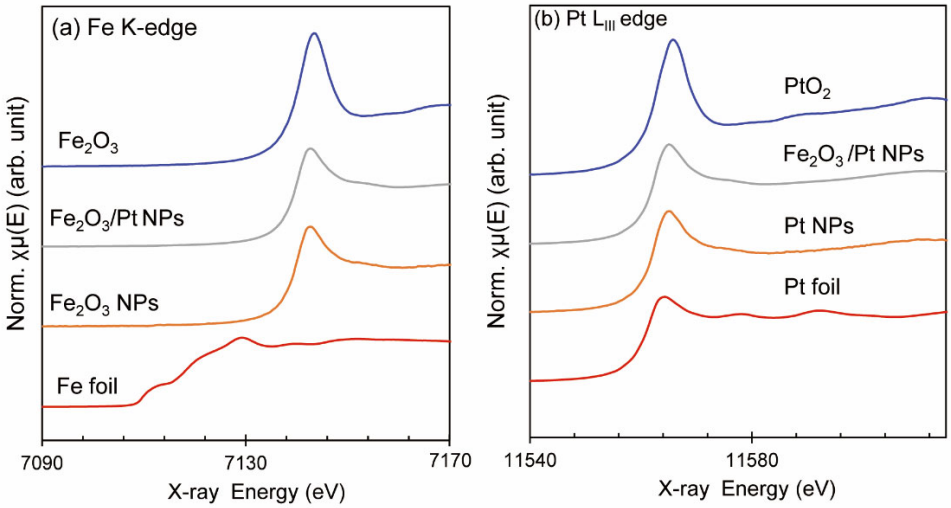


**Figure 12.** (a) Fe K-edge XANES spectra of DMF-protected $Fe_2O_3$ NPs, mixture of $Fe_2O_3$-Pt NPs, and the reference samples (Fe foil, $Fe_2O_3$). (b) Pt $L_{III}$-edge XANES spectra of DMF-protected Pt NPs, mixture of $Fe_2O_3$ NPs-Pt NPs, and the reference samples (Pt foil and $PtO_2$).

To examine the active species, the author investigated the time-course for the reaction.(Figure 13) This reaction system had an induction period of approximately 10 hours. The induction period for the reaction system with $Fe_2O_3$ Pt NPs recovered after the first catalyst recycling test was also investigated and was around only 1 hour. The active catalyst species assisted by hydrosilane/oxygen may be generated during the reaction course.

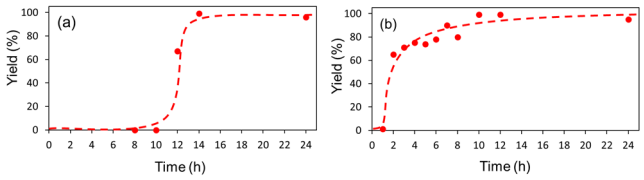


**Figure 13**. Reaction profiles for hydrosilylation using (a) pristine $Fe_2O_3$/Pt $NP_S$ and (b) recovered $Fe_2O_3$ Pt NPs.

In addition, the reactions were carried out under these conditions by changing the ratio of $Fe_2O_3$ NPs and Pt NPs, and no significant difference was observed in the yields of **3a** (Table 2).

**Table 2**

Effect of the $Fe_2O_3$ NPs/ Pt NPs ratio in the hydrosilylation of 1-dodecene (**1a**) with triethoxysilane (**2a**)[a]

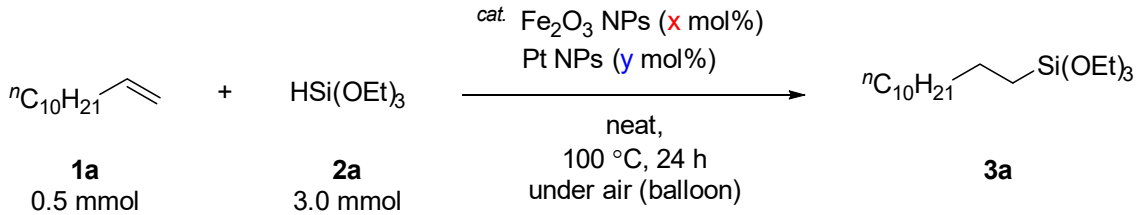


| Entry | $Fe_2O_3$ NPs (x mol%) | Pt NPs (y mol%) | Yield of **3a** |
|---|---|---|---|
| 1 | 0.05 | 0.005 | 68 |
| 2 | 0.05 | 0.0125 | 72 |
| 3 | 0.05 | 0.025 | 78 |
| 4 | 0.025 | 0.05 | 83 |
| 5 | 0.0125 | 0.05 | 75 |
| 6 | 0.005 | 0.05 | 81 |

a)GC yield

However, the use of small amount of Pt NPs (0.025 mol%) under these conditions resulted in a retardation in the formation of **3a** during the course of reaction. (Figure 14).

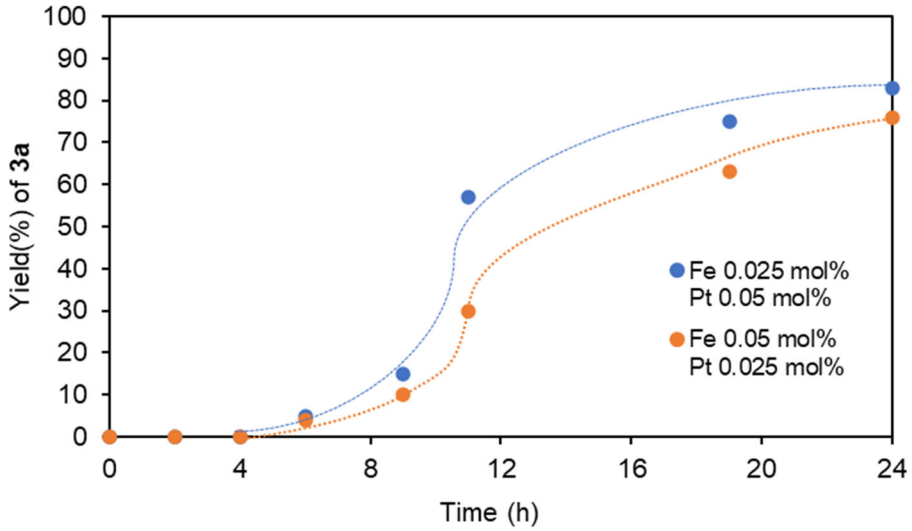


**Figure 14.** Time-dependence curve for the formation of **3a** under the conditions as shown in entry 3, Table 2 (orange plot) and entry 4, Table 2 (blue plot).

After the reaction, the $Fe_2O_3$/Pt NPs catalyst was collected and observed with a scanning electron microscope (Figure 15). Material with a size of several hundred nanometers to the micron-order was observed. Elemental mapping showed that this material was mainly derived from silicon. In addition, it was clear that these substances were also composed of Fe and Pt. This result implied that Fe and Pt interacted with each other inside or on the surface of the silicon substances such as siloxane derived from hydrosilane/oxygen. High resolution HR-TEM, STEM image of after reaction (Figure 16) suggested that the size of Pt NPs was retained before and after the reaction. However, Fe EDS signal intensity was low.

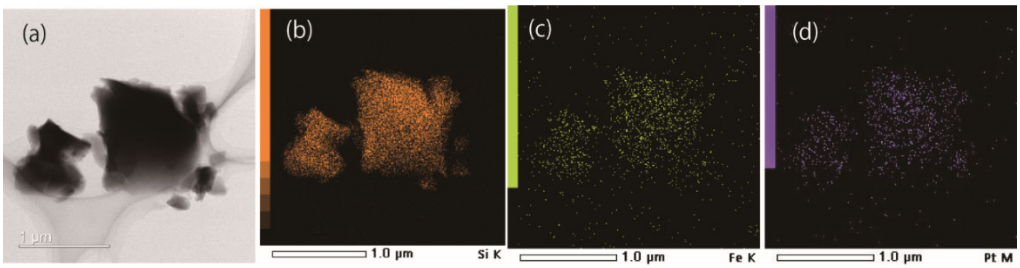


**Figure 15.** STEM image $Fe_2O_3$/Pt NPs after recycling (a) and elemental mapping, (b) Si, (b) Fe, and (c) Pt.

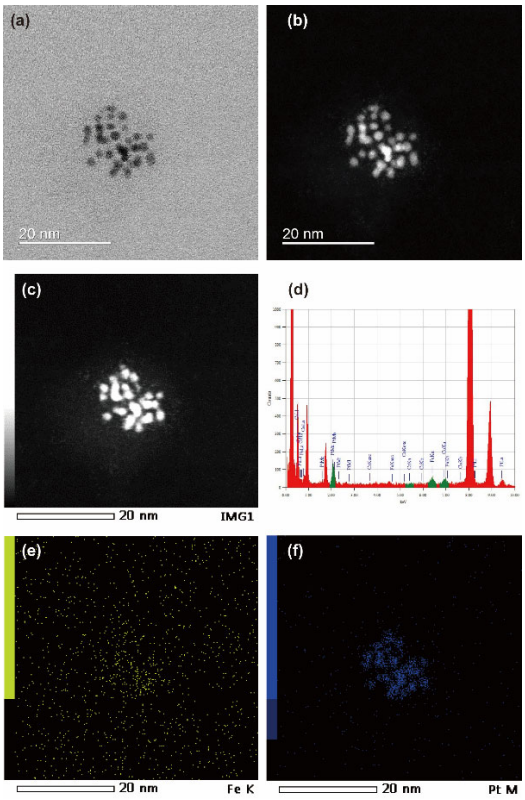


**Figure 16.** Image of (a) BF-TEM (b) DF-TEM (c) HAADF-STEM. (d) EDS analysis result. elemental mapping (e)Fe and (f)Pt

Using recovered $Fe_2O_3$/Pt NPs catalyst, hydrosilylation were performed under various conditions to understand changes to the catalyst upon recycling (Table 3).

Table 3. Recovered $Fe_2O_3$ /Pt NPs catalyzed hydrosilylation of 1-dodecene (**1a**) with triethoxysilane (**2a**)[a]

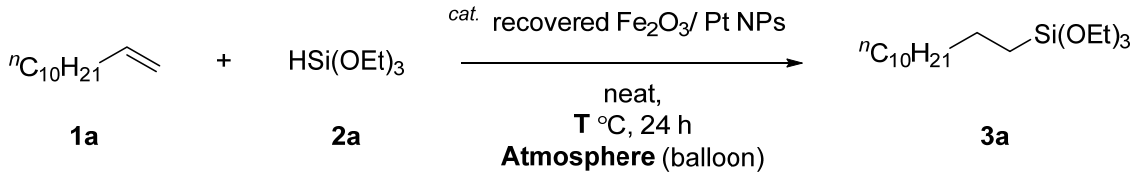


| Entry | **1a** (mmol) | **2a** (mmol) | **T** (°C) | Atmosphere (balloon) | Yield of **3a** |
|---|---|---|---|---|---|
| 1 | 0.5 | 3 | 100 | Ar | 86 |
| 2 | 0.5 | 3 | 100 | Air | >99 |
| 3 | 0.5 | 0.6 | 100 | Ar | 83 |
| 4 | 0.5 | 3 | 80 | Ar | 95 |
| 5 | 0.5 | 3 | 60 | Ar | 15 |

a)GC yield

The DMF molecules coordinate on the metal nanoparticles, which would inhibit the aggregation during the reaction.[16,17] Then silicon-containing compounds such as siloxanes generated by $O_2$ weakly coordinated on the surface of the Fe/Pt catalyst. The active catalyst species may be generated by partial liberation of the DMF molecules surrounded on the metal nanoparticles, and weak coordination of siloxanes to the open site would stabilize the active species during the course of the catalytic reaction.[7b,c] Therefore, the recovered $Fe_2O_3$/Pt NPs catalysts gave the desired products in high yields even under an inert gas atmosphere without the need for an excess amount of hydrosilane. In addition, the recovered $Fe_2O_3$/ Pt NPs catalysts afforded desired products 85% at 80 °C.

To check the electronic state of the $Fe_2O_3$ NPs and Pt NPs catalysts, XPS analysis was conducted. Figure 17 shows the XPS profiles of Pt 4f for the (a) Pt NPs before reaction, and (b) Pt NPs after reaction. All measurements showed two peaks at 72.6 eV (Pt $4f_{7/2}$) and 75.9 eV (Pt $4f_{5/2}$). Pt NPs indicating $Pt^{2+}$ species.[16c] Pt 4f did not shift in the presence of the $Fe_2O_3$ NPs. The results were consistent with the XANES analysis of the Pt $L_{III}$ edge. After reaction, although the use of Pt NPs on their own did not show any catalytic activity, both the Pt NPs only and the $Fe_2O_3$/Pt NPs did not affect the oxidation state.

The author also analyzed the XPS Fe $2p_{3/2}$ region for the $Fe_2O_3$ NPs and $Fe_2O_3$/Pt NPs (Figure 18). For the $Fe_2O_3$ NPs, broad peaks appeared, which were assigned to $Fe^{2+}$ peak, $Fe^{3+}$ (quartet) peaks and surface peak.[21b,c] Before the reaction, the $Fe_2O_3$ NPs and $Fe_2O_3$ /Pt NPs, $Fe^{2+}$ peak intensities were increased than that of bulk $\alpha$-$Fe_2O_3$. As a comparison, the author also performed XPS measurements before and after the reaction using the $Fe_2O_3$ NPs as a catalyst, where the reaction did not proceed. After reaction, the surface peak was increased for the $Fe_2O_3$ /Pt NPs compared with the $Fe_2O_3$ NPs. With the decrease in coordination, $Fe^{3+}$ ions located in $Fe_2O_3$ NPs surface would surrounded by a lower electron density.[21b]

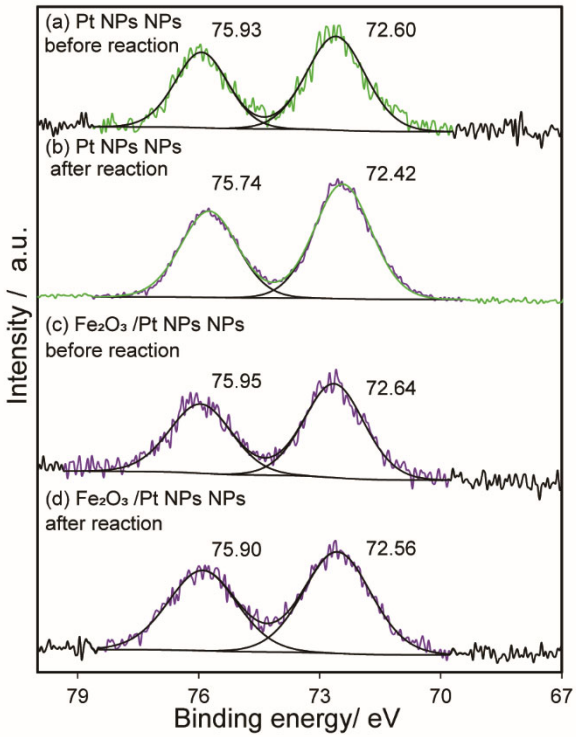


**Figure 17.** XPS profiles of the Pt 4f region for (a) Pt NPs before reaction, (b) Pt NPs after reaction, (c) $Fe_2O_3$/Pt NPs before reaction, and (d) $Fe_2O_3$/Pt NPs after reaction.

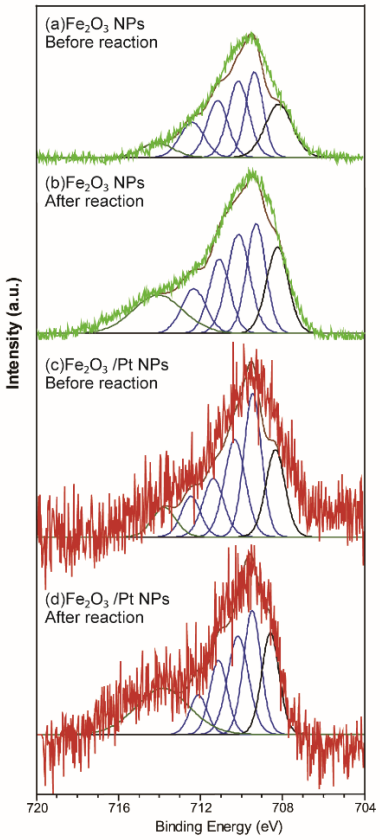


**Figure 18.** The Fe $2p_{3/2}$ region background-subtracted spectra $Fe^{2+}$ (black) $Fe^{3+}$(quartet, blue), and surface peak (green) from (a) $Fe_2O_3$ NPs before reaction, (b) $Fe_2O_3$ NPs after reaction, (c) $Fe_2O_3$/Pt NPs before reaction, and (d) $Fe_2O_3$/Pt NPs after reaction.

## Conclusion

The author developed a combination of DMF-protected $Fe_2O_3$ and Pt NPs that can catalyze anti-Markovnikov selective hydrosilylation of alkenes with hydrosilanes. The combination catalyst of DMF-protected $Fe_2O_3$ and Pt NPs can be applied to a variety of functional alkenes, as well as to large-scale experiments up to the kilogram scale. The DMF-protected $Fe_2O_3$/Pt NPs could be recycled at least five times. The in situ activated $Fe_2O_3$/Pt NPs catalyst exhibits a short induction time and high catalytic activity.

## Experimental

General

GC analysis was performed with a GC-2025 (Shimadzu) a flame ionization detector (FID) using a 0.22 mm × 25 m capillary column (BP-5 SGE). NMR spectra were recorded on a JNM-ECZ400S (JEOL). $^{1}$H, and $^{13}$C, NMR spectra were measured at 400 and 100 MHz, respectively. Compound **3r** $^{1}$H(600 MHz),$^{13}$C(150 MHz) spectra were recorded using a AVANCE III HD 600 spectrometer (Bruker) with a 5 mm CPBBO BB-1H/19F/D Z-GRD. $^{1}$H NMR chemical shifts were referenced to tetramethylsilane signal (0 ppm) or the residual solvent resonance as an internal standard. $^{13}$C NMR chemical shifts were referenced to residual solvent peaks (77 ppm). The high-resolution EI and ESI mass spectra were obtained on a JEOL JMS-T100GCv and a Thermo Scientific Exactive.

Metal nanoparticle catalyst preparation.

(A) DMF-protected $Fe_2O_3$ NPs were prepared by a modified method.[17] To a 20-mL vial bottle, $Fe(OAc)_2$ (Aldrich, >99.99%) was weighed and dissolved in DMF (10 mL) so that the Fe concentration was 0.1 mol/L. To a 300-mL three-necked round bottom flask, DMF (50 mL) was added and the solution was preheated to 140 °C (±2 °C), and stirred at 1500 rpm for 5 min. Then, the 0.1 mol/L $Fe(OAc)_2$ DMF solution (500 μL) was added to a hot DMF solution, which was heated for 10 h at 140 °C.

(B) DMF-protected Pt NPs were prepared by a modified method.[16c] To a 20-mL vial bottle, $H_2PtCl_6{\cdot}6H_2O$ (Aldrich, >99.99%) was weighed and dissolved in DMF (10 mL) so that the Fe concentration was 0.1 mol/L. To a 300-mL three-necked round bottom flask, DMF (50 mL) was added and the solution was preheated to 140 °C (±2 °C), and stirred at 1500 rpm for 5 min. Then, the 0.1 mol/L $H_2PtCl_6{\cdot}6H_2O$ DMF solution (500 μL) was added to a hot DMF solution, which was heated for 10 h at 140 °C.

Catalytic hydrosilylation reactions

An as-prepared 1 mM Pt NPs solution in DMF (0.25 mL) and 1 mM $Fe_2O_3$ NPs solution in DMF (0.25 mL) were added to a reaction vessel (30 mL) and the DMF was evaporated. Then, alkene **1a** (70 mg, 0.5 mmol), and hydrosilane **2a** (325 mg, 3.0 mmol) were added and the mixture was stirred at 100 °C for 24 h under air. The conversions and yields of products were estimated from the peak areas based on an internal standard using GC, and the product **3a** was quantitatively obtained. The product **3a** was isolated by column chromatography (230–400 mesh silica gel, neutralized, n-hexane) and in a yield of 81% (135 mg)

Catalyst characterization.

Transmission electron microscopy (TEM) and annular dark field scanning transmission electron microscopy (ADF-STEM) observations were carried out using a JEM-ARM200F microscope (JEOL), equipped with an energy dispersive X-ray (EDX) analyzer using a copper micro grid, at an accelerating voltage of 200 kV. X-ray absorption spectroscopy (XAS) measurements of the catalysts were conducted at the BL01B1 beamline of SPring-8 Japan Synchrotron Radiation Research Institute. A Si(311) double crystal was used as a monochromator. The spectra were recorded at the Pt $L_{III}$- and Fe K- edges in the transmission mode at room temperature. The obtained XAS data were analyzed using Athena software version 0.9.26 included in the Demeter package.[23] X-ray diffraction (XRD) measurement were performed Miniflex 600-C(Rigaku) Cu Kα 40 kV, 15 mA, D/teX Ultra2 detector using a non-reflective silicon sample plate. X-ray photoelectron spectroscopy (XPS) analysis for the metal NPs was performed by using a PHI5000 VersaProbe III (Al Kα radiation 1487 eV) spectrometer (ULVAC-PHI). Each measured spectrum background was subtracted shirley-type background. The binding energies were calibrated with C 1s.

Characterization of the compounds

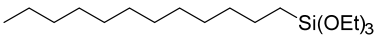


**3a**[14d] dodecyltriethoxysilane, 81%, 135 mg, a colorless oil, $^1$H-NMR (400MHz $CDCl_3$) δ: 3.82 (q, 6H, *J* = 7.1 Hz), 1.43-1.21 (m, 29H), 0.88 (t, 3H, *J* = 6.9 Hz), 0.65-0.61 (m, 2H); $^{13}$C-NMR (100MHz $CDCl_3$) δ: 58.30 ($CH_2$), 33.23 ($CH_2$), 31.95 ($CH_2$), 29.71 ($CH_2$), 29.68 ($CH_2$), 29.58 ($CH_2$), 29.38 ($CH_2$), 29.29 ($CH_2$), 22.77 ($CH_2$), 22.71 ($CH_2$), 18.32 ($CH_3$), 14.14 ($CH_3$), 10.38 ($CH_2$); GC-MS (EI) *m/z* (relative intensity) 332 (0.3)$[M]^+$, 165 (4), 164 (11), 163 (100), 119 (18).

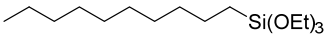


**3b**[15c] decyltriethoxysilane, 84%, 128 mg, a colorless oil, $^1$H-NMR (400MHz $CDCl_3$) δ: 3.82 (q, 6H, *J* = 7.0 Hz), 1.41-1.21 (m, 25H), 0.88 (t, 3H, *J* = 6.9 Hz), 0.65-0.61 (m, 2H);$^{13}$C-NMR (100MHz $CDCl_3$) δ: 58.30 ($CH_2$), 33.23 ($CH_2$), 31.94 ($CH_2$), 29.66 ($CH_2$), 29.57 ($CH_2$), 29.36 ($CH_2$), 29.28 ($CH_2$), 22.77 ($CH_2$), 22.71 ($CH_2$), 18.32 ($CH_3$), 14.14 ($CH_3$), 10.38 ($CH_2$); GC-MS (EI) *m/z* (relative intensity) 304 (2)$[M]^+$, 258 (7), 163 (100), 135 (17), 119 (64).

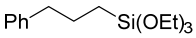


**3c**[14d] triethoixy(3-phenylpropyl)silane, 63%, 89mg, a colorless oil, $^1$H-NMR (400MHz $CDCl_3$) δ: 7.29-7.25 (m, 2H), 7.18-7.17 (m, 3H), 3.80 (q, 6H, *J* = 7.0 Hz), 2.64 (t, 2H, *J* = 7.7 Hz), 1.74 (t, 2H, *J* = 8.2 Hz), 1.22 (t, 9H, *J* = 6.8 Hz), 0.70-0.66 (m, 2H);$^{13}$C-NMR (100MHz $CDCl_3$) δ: 142.41 (C), 128.54 (CH), 128.22 (CH), 125.66 (CH), 58.34 ($CH_2$), 39.22 ($CH_2$), 24.83 ($CH_2$), 18.30 ($CH_3$), 10.15 ($CH_2$);GC-MS *m/z* (relative intensity) 282 (6) $[M]^+$ , 237 (5), 163 (100), 119 (23).

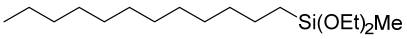


**3d**[15d] dodecyldiethoxymethylsilane, 94%, 142 mg, a colorless oil, $^{1}$H-NMR (400 MHz $CDCl_3$) δ: 3.76 (q, 4H, *J* = 7.0 Hz), 1.36-1.20 (m, 26H), 0.88 (t, 3H, *J* = 6.9 Hz), 0.62-0.60 (m, 2H), 0.11 (s, 3H); $^{13}$C-NMR (100 MHz $CDCl_3$) δ: 58.05 ($CH_2$), 33.35 ($CH_2$), 31.95 ($CH_2$), 29.71 ($CH_2$), 29.70 ($CH_2$), 29.67 ($CH_2$), 29.59 ($CH_2$), 29.38 ($CH_2$), 29.34 ($CH_2$), 22.86 ($CH_2$), 22.71 ($CH_2$), 18.42 ($CH_3$), 14.14 ($CH_3$), 13.82 ($CH_2$), -4.87 ($CH_3$); GC-MS (EI) *m/z* (relative intensity) 302 (0.1)$[M]^+$, 287 (8), 133 (100), 119 (8), 89 (9).

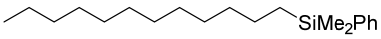


**3e**[22a] dodecyldimethylphenylsilane, 69%, 105 mg, a colorless oil, $^{1}$H-NMR (400 MHz $CDCl_3$) δ: 7.53-7.34 (5H, m), 1.25 (20H, s), 0.89 (3H, t, *J* = 6.8 Hz), 0.74 (2H, t, *J* = 7.9 Hz), 0.25 (6H, s); $^{13}$C-NMR (100 MHz $CDCl_3$) δ: 139.77 (C), 133.54 (CH), 128.69 (CH), 127.65 (CH), 33.62 ($CH_2$), 31.92 ($CH_2$), 29.69 ($CH_2$), 29.67 ($CH_2$), 29.64 ($CH_2$), 29.59 ($CH_2$), 29.36 ($CH_2$), 29.30 ($CH_2$), 23.84 ($CH_2$), 22.69 ($CH_2$), 15.67 ($CH_2$), 14.13 ($CH_3$), -3.03 ($CH_3$); GC-MS (EI) *m/z* (relative intensity) 289 (5)$[M - CH_3]^+$, 226 (8), 141 (8), 135 (100), 121 (24).

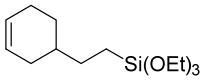


**3f** [10] 2-(3-cyclohexenylethyl)trimethoxysilane, 46%, 63 mg, a colorless oil,$^{1}$H-NMR (400MHz $CDCl_3$) δ: 5.65-5.65 (2H, m), 3.82 (6H, q, *J* = 7.0 Hz), 2.10-2.02 (3H, m), 1.79-1.74 (1H, m), 1.64-1.60 (1H, m), 1.50-1.41(1H,m) 1.41-1.35 (2H, m), 1.22 (10H, m), 0.66 (2H, m);$^{13}$C-NMR (100MHz $CDCl_3$) δ: 127.01 (CH), 126.59 (CH), 58.30 (CH), 36.23 (CH), 31.47 ($CH_2$), 29.35 ($CH_2$), 28.39 ($CH_2$), 25.30 ($CH_2$), 18.27 ($CH_3$), 7.44 ($CH_2$); GC-MS *m/z* (relative intensity) 272 (10) $[M]^+$ , 226 (100), 198 (40), 163 (90)

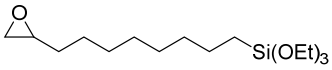


**3g**[10] triethoxy(8-(oxiran-2-yl)octyl)silane 73%, 116 mg a colorless oil, $^{1}$H-NMR (400 MHz $CDCl_3$) δ: 3.75 (6H, q, *J* = 7.0 Hz), 2.83 (1H, t, *J* = 4.2 Hz), 2.68 (1H, dd, *J* = 5.0, 4.0 Hz), 2.40 (1H, dd, *J* = 5.0, 2.7 Hz), 1.46-1.14 (23H, m), 0.56 (2H, t, *J* = 8.1 Hz); $^{13}$C-NMR (100 MHz $CDCl_3$) δ: 58.27 ($CH_2$), 52.41 (CH), 47.15 ($CH_2$), 33.13 ($CH_2$), 32.48 ($CH_2$), 29.43 ($CH_2$), 29.41 ($CH_2$), 29.13 ($CH_2$), 25.95 ($CH_2$), 22.72 ($CH_2$), 18.29 ($CH_3$), 10.33 ($CH_2$); GC-MS (EI) *m/z* (relative intensity) 273(0.1)$[M - OCH_2CH_3]^+$ 163 (100), 135 (25), 119 (36), 149 (14), 79 (14).

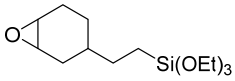


**3h**[10] 1,2-epoxy-4-(2-triethoxysilylethyl)cyclohexane 65%, 94mg, a colorless oil, mixture of isomers, $^{1}$H-NMR (400MHz $CDCl_3$) δ: 3.81 (6H, q, *J* = 7.0 Hz), 3.16-3.12 (2H, m), 2.21-1.96 (2H, m), 1.82-1.71 (1H, m), 1.40-1.08 (14H, m), 0.90-0.86 (1H, m), 0.60-0.57 (2H, m);$^{13}$C-NMR (100MHz $CDCl_3$) δ: 58.29 (CH), 53.17 (CH), 52.67 (CH), 51.93 (CH), 51.85 (CH), 35.15 (CH), 32.16 (CH), 31.37 ($CH_2$), 30.24 ($CH_2$), 29.52 ($CH_2$), 28.96 ($CH_2$), 26.57 ($CH_2$), 25.28 ($CH_2$), 23.86 ($CH_2$), 23.50 ($CH_2$), 18.24 ($CH_3$), 7.41 ($CH_2$), 7.27 ($CH_2$); GC-MS *m/z* (relative intensity) 259 (10) $[M\text{-}CH_3CH_2]^+$, 242(5), 226(6), 163(100), 135 (34), 119(41).

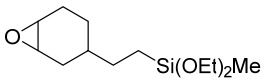


**3i**[15d] 2-(3,4-epoxycyclohexyl)ethylmethyl diethoxysilane, 65%, 88 mg, mixture of isomers, a colorless oil, $^{1}$H-NMR (400 MHz $CDCl_3$) δ: 3.75 (4H, q, *J* = 7.0 Hz), 3.16-3.13 (2H, m), 2.21-1.95 (3H, m), 1.43-1.04 (12H, m), 0.58-0.56 (2H, m), 0.10 (3H, s);$^{13}$C-NMR (100MHz $CDCl_3$) δ: 58.10 ($CH_2$), 53.26 (CH), 52.73 (CH), 52.00 (CH), 51.92 (CH), 35.36 (CH), 32.29 (CH), 31.49 ($CH_2$), 30.35 ($CH_2$), 29.69 ($CH_2$), 29.14 ($CH_2$, 26.70 ($CH_2$), 25.36 ($CH_2$), 23.98 ($CH_2$), 23.59 ($CH_2$), 18.41 ($CH_3$), 10.84 ($CH_2$), 10.74 ($CH_2$), -4.99 ($CH_3$); GC-MS *m/z* (relative intensity) 229 (0.4) $[M\text{-}CH_3CH_2]^+$ ,133(100), 105(30), 105(30).

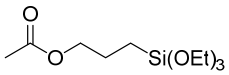


**3j**[10] 3-(triethoxysilyl)propyl acetate, 62%, 82 mg, a colorless oil, $^{1}$H-NMR (400 MHz $CDCl_3$) δ: 4.01 (2H, t, *J* = 6.9 Hz), 3.80 (6H, q, *J* = 7.0 Hz), 2.02 (3H, s), 1.75-1.67 (2H, m), 1.20 (9H, t, *J* = 7.0 Hz), 0.62 (2H, t, *J* = 8.4 Hz); $^{13}$C-NMR (100MHz $CDCl_3$) δ: 171.17 (C), 66.52 ($CH_2$), 58.41 ($CH_2$), 22.15 ($CH_2$), 20.99 ($CH_3$), 18.26 ($CH_3$), 6.49 ($CH_2$); GC-MS (EI) *m/z* (relative intensity) 249 (3) $[M - CH_3]^+$, 218 (17), 177 (100), 163 (95), 135 (51), 119 (49), 79 (32).

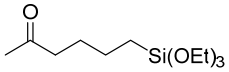


**3k**[10] 6-(triethoxysilyl)hexan-2-one, 55%, 72 mg, a colorless oil, $^{1}$H-NMR (400 MHz $CDCl_3$) δ: 3.74 (6H, q, *J* = 7.0 Hz), 2.36 (2H, t, *J* = 7.4 Hz), 2.06 (3H, s), 1.58-1.51 (2H, m), 1.39-1.31 (2H, m), 1.15 (9H, t, *J* = 7.0 Hz), 0.57 (2H, t, *J* = 8.3 Hz); $^{13}$C-NMR (100 MHz $CDCl_3$) δ: 209.40 (C), 58.48 ($CH_2$), 43.61 ($CH_2$), 30.00 ($CH_3$), 27.35 ($CH_2$), 22.63 ($CH_2$), 18.43 ($CH_3$), 10.43 ($CH_2$); GC-MS (EI) *m/z* (relative intensity) 216 (29)$[M - OCH_2CH_3]^+$, 163 (100), 135 (37), 119 (43), 79 (27).

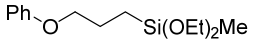

**3l**[15d] diethoxymethyl(3-phenoxypropyl)silane, 78%, 105 mg, a colorless oil, $^{1}$H-NMR (400 MHz $CDCl_3$) δ: 7.29-7.25 (2H, m), 6.90 (3H, tt, *J* = 8.5, 2.0 Hz), 3.93 (2H, t, *J* = 6.7 Hz), 3.77 (4H, q, *J* = 7.0 Hz), 1.89-1.82 (2H, m), 1.21 (6H, t, *J* = 7.0 Hz), 0.76-0.72 (2H, m), 0.15 (3H, s). $^{13}$C-NMR (100 MHz $CDCl_3$) δ: 158.99 (C), 129.37 (CH), 120.43 (CH), 114.44 (CH), 69.94 ($CH_2$), 58.13 ($CH_2$), 22.83 ($CH_2$), 18.38 ($CH_3$), 9.89 ($CH_2$), -4.92 ($CH_3$).; GC-MS (EI) *m/z* (relative intensity) 268(9)$[M]^+$ , 226(33), 175(26), 133 (100).

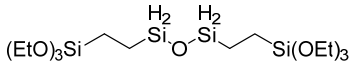

**3m**[10] 1,3-bis(triethoxysilylethyl)tetramethyldisiloxane, 53%, 136mg, a colorless oil, $^{1}$H-NMR (400 MHz $CDCl_3$) δ: 3.78 (q, 12H, *J* = 7.0 Hz), 1.19 (18H, t, *J* = 7.0 Hz), 0.50 (8H, s), 0.00 (12H, s); $^{13}$C-NMR (100MHz $CDCl_3$) δ: 58.35 ($CH_2$), 18.29 ($CH_3$), 9.16 ($CH_2$), 1.75 ($CH_2$), -0.45 ($CH_3$); GC-MS (EI) *m/z* (relative intensity) 351(0.2)$[M-Si(OEt)_3]^+$ , 323(44), 249(100), 205 (42).

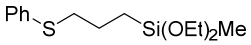

**3n**[22a] diethoxymethyl(3-(phenylthio)propyl)silane, 9%, 14mg, a colorless oil, $^{1}$H-NMR (400 MHz $CDCl_3$) δ: 7.33-7.13 (m, 5H), 3.73 (q, 4H, *J* = 7.0 Hz), 2.93 (t, 2H, *J* = 7.3 Hz), 1.75-1.67 (m, 2H), 1.18 (t, 6H, *J* = 7.0 Hz), 0.77-0.73 (m, 2H), 0.09 (s, 3H);$^{13}$C-NMR (100MHz $CDCl_3$) δ: 136.69 (C), 128.97 (CH), 128.78 (CH), 125.66 (CH), 58.10 ($CH_2$), 36.65 ($CH_2$), 22.81 ($CH_2$), 18.35 ($CH_3$), 13.32 ($CH_2$), -4.89 ($CH_3$). GC-MS (EI) *m/z* (relative intensity) 284(24)$[M]^+$ , 269(6), 239(8), 133 (100).

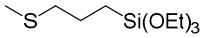

**3o**[20a] triethoxy(3-(methylthio)propyl)silane, 9%, 11mg, a colorless oil,$^{1}$H-NMR (400 MHz $CDCl_3$) δ: 3.82 (q, 6H, *J* = 7.0 Hz), 2.51 (t, 2H, *J* = 7.3 Hz), 2.08 (s, 3H), 1.75-1.67 (m, 2H), 1.22 (t, 9H, *J* = 7.0 Hz), 0.73 (t, 2H, *J* = 8.3 Hz); $^{13}$C-NMR (100 MHz $CDCl_3$) δ: 58.52 ($CH_2$), 37.38 ($CH_2$), 22.77 ($CH_2$), 18.44 ($CH_3$), 15.46 ($CH_3$), 8.90 ($CH_2$); GC-MS (EI) *m/z* (relative intensity) 252 (25)$[M]^+$, 191 (81), 163 (100), 147 (59) , 119 (72).

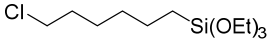

**3p**[22b] (6-chlorohexyl)triethoxysilane, 43%, 61 mg a colorless oil, $^{1}$H-NMR (400MHz $CDCl_3$) δ: 3.81 (q, 6H, *J* = 7.0 Hz), 3.52 (t, 2H, *J* = 6.7 Hz), 1.76 (quin, 2H, *J* = 6.7 Hz), 1.45-1.34 (m, 6H), 1.22 (t, 9H, *J* = 7.0 Hz), 0.63 (t, 2H, *J* = 8.1 Hz);$^{13}$C-NMR (100MHz $CDCl_3$) δ: 58.46 ($CH_2$), 45.33 ($CH_2$), 32.66 ($CH_2$), 32.47 ($CH_2$), 26.65 ($CH_2$), 22.79 ($CH_2$), 18.45 ($CH_3$), 10.45 ($CH_2$); GC-MS (EI) *m/z* (relative intensity) 177 (100), 163 (95), 135 (51), 119 (49), 79 (32) HRMS(EI):calculated for $[M]^+(C_{10}H_{22}ClO_2Si)$ *m/z* : 237.1078: found $[M]^+$ 237.1078; IR(neat, $cm^{-1}$) 2975, 2886,

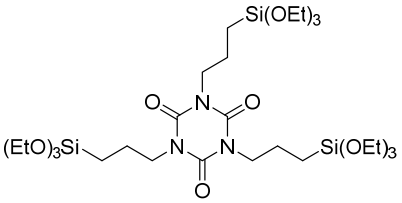

1456, 1390, 1104, 1080, 958, 794.

**3q**, tris(3-triethoxysilylpropyl) isocyanurate, 43%, 165 mg, a colorless oil, $^{1}$H-NMR (400 MHz $CDCl_3$) δ: 3.82-3.75 (m, 24H), 1.73-1.68 (m, 6H), 1.18 (t, 27H, *J* = 7.1 Hz), 0.60 (t, 6H, *J* = 8.5 Hz);$^{13}$C-NMR (100 MHz $CDCl_3$) δ: 148.84 (C), 58.39 ($CH_2$), 45.29 ($CH_2$), 21.28 ($CH_2$), 18.23 ($CH_3$), 7.58 ($CH_2$); FT-IR(neat); 2975, 2928, 2887, 1675 $cm^{-1}$ HRMS(ESI):calculated for $[M+Na]^+$($C_{30}H_{63}O_{12}N_3NaSi_3$) *m/z* : 764.3612: found $[M+Na]^+$ 764.3605.

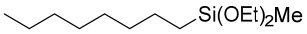


**3r** [10] methyloctyldiethoxysilane, 91%, a colorless oil, $^{1}$H-NMR (600 MHz $CDCl_3$) δ: 3.75 (q, 4H, *J* = 7.0 Hz), 1.35-1.20 (m, 18H), 0.87 (t, 3H, *J* = 7.0 Hz), 0.61 (t, 2H, *J* = 8.1 Hz), 0.10 (s, 3H); $^{13}$C-NMR (150 MHz $CDCl_3$) δ: 58.04 ($CH_2$), 33.34 ($CH_2$), 31.93 ($CH_2$), 29.29 ($CH_2$), 29.24 ($CH_2$), 22.86 ($CH_2$), 22.69 ($CH_2$), 18.42 ($CH_2$), 14.12 ($CH_3$), 13.82 ($CH_2$), -4.87 ($CH_3$); GC-MS (EI) *m/z* (relative intensity) 231(7)$[M-CH_3]^+$ , 133 (100), 119(9), 89 (12).

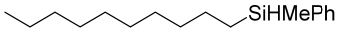


**3s** [22c] dodecylphenylsilane, 62%, a colorless oil, $^{1}$H-NMR (400MHz $CDCl_3$) δ: 7.58-7.56 (m, 2H), 7.39-7.36 (m, 3H), 4.28 (td, 2H, *J* = 3.6, 1.7 Hz), 1.49-1.20 (m, 22H), 0.96-0.87 (m, 5H); $^{13}$C-NMR (100MHz $CDCl_3$) δ: 135.19 (CH), 132.82 (C), 129.44 (CH), 127.93 (CH), 32.84 ($CH_2$), 31.92 ($CH_2$), 29.66 ($CH_2$), 29.53 ($CH_2$), 29.36 ($CH_2$), 29.26 ($CH_2$), 25.06 ($CH_2$), 22.69 ($CH_2$), 14.12 ($CH_3$), 10.00 ($CH_2$). GC-MS (EI) *m/z* (relative intensity) 198(13)$[M-C_6H_6]^+$ , 113(39), 99 (100), 85(22).

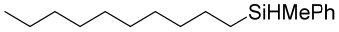


**3t** [17] decylmethylphenylsilane, 47%, a colorless oil, $^{1}$H-NMR (400 MHz $CDCl_3$) δ: 7.54-7.52 (m, 2H, m), 7.37-7.34 (m, 3H), 4.34 (td, 1H, *J* = 7.2, 3.7 Hz), 1.35-1.28 (m, 16H), 0.89-0.81 (m, 5H), 0.32 (d, 3H, *J* = 3.8 Hz); $^{13}$C-NMR (100MHz $CDCl_3$) δ: 136.80 (C), 134.29 (CH), 129.11 (CH), 127.80 (CH), 33.19 ($CH_2$), 31.91 ($CH_2$), 29.64 ($CH_2$), 29.56 ($CH_2$), 29.34 ($CH_2$), 29.29 ($CH_2$), 24.31 ($CH_2$), 22.69 ($CH_2$), 14.12 ($CH_3$), 13.35 ($CH_2$), -5.66 ($CH_3$);GC-MS (EI) *m/z* (relative intensity) 242(1)$[M-CH_3]^+$ ,184(14), 127(31), 121 (100), 113(85).

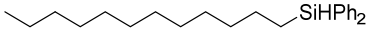


**3u** [22d] dodecyldiphenylsilane, 54%, a colorless oil, $^{1}$H-NMR (400 MHz $CDCl_3$) δ: 7.56 (dd, 4H, *J* = 7.3, 1.5 Hz), 7.40-7.34 (m, 6H), 4.85 (t, 1H, *J* = 3.7 Hz), 1.48-1.12 (m, 22H), 0.89 (t, 3H, *J* = 6.9 Hz); $^{13}$C-NMR (100 MHz $CDCl_3$) δ: 135.12 (CH), 134.71 (C), 129.44 (CH), 127.92 (CH), 33.17 ($CH_2$), 31.92 ($CH_2$), 29.65 ($CH_2$), 29.53 ($CH_2$), 29.35 ($CH_2$), 29.21 ($CH_2$), 24.38 ($CH_2$), 22.69 ($CH_2$), 14.12 ($CH_3$), 12.12 ($CH_2$). GC-MS (EI) *m/z* (relative intensity) 274(7) $[M-C_6H_6]^+$ , 196(20), 183 (100), 175(30), 105(23).

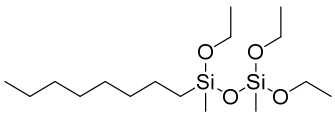


**4** 1,1,3-triethoxy-1,3-dimethyl-3-octyldisiloxane, a colorless oil, $^{1}$H-NMR (400MHz $CDCl_3$) δ: 3.78-

3.76 (m, 6H), 1.31-1.18 (m, 20H), 0.87 (t, 4H, $J$ = 6.9 Hz), 0.59 (t, 2H, m), 0.11-0.11 (m, 6H); $^{13}$C-NMR (100MHz $CDCl_3$) δ: 58.11 ($CH_2$), 58.01($CH_2$), 33.36 ($CH_2$), 32.00 ($CH_2$), 29.38 ($CH_2$), 29.31 ($CH_2$), 22.89 ($CH_2$), 22.75 ($CH_2$), 18.46 ($CH_3$), 18.31($CH_3$), 15.60 ($CH_2$), 14.18 ($CH_3$), -2.73 ($CH_3$), -5.41($CH_3$); FT-IR(neat); 2964, 2923, 2856, 1457, 1387, 1267, 1079 cm$^{-1}$; GC-MS *m/z* (relative intensity) 335 (5) [M -$CH_3$]$^+$, 305(10), 237(100), 93(35); HRMS(EI):calculated for [M−$CH_3$]$^+$($C_{15}H_{35}O_4Si_2$) *m/z* : 335.2074: found [M−$CH_3$]$^+$ 335.2067.

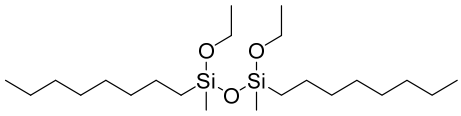

**5** 1,3-diethoxy-1,3-dimethyl-1,3-dioctyldisiloxane, a colorless oil, $^1$H-NMR (400MHz $CDCl_3$) δ: 3.74 (q, 4H, $J$ = 7.0 Hz), 1.37-1.19 (m, 30H), 0.88 (t, 6H, $J$ = 6.9 Hz), 0.56 (t, 4H, $J$ = 7.9 Hz), 0.08 (s, 6H); $^{13}$C-NMR (100MHz $CDCl_3$) δ: 57.82 ($CH_2$), 33.32 ($CH_2$), 31.93 ($CH_2$), 29.32 ($CH_2$), 29.25 ($CH_2$), 22.92 ($CH_2$), 22.68 ($CH_2$), 18.42 ($CH_3$), 15.69 ($CH_2$), 14.11 ($CH_3$), -2.62 ($CH_3$); FT-IR(neat); 2956, 2923, 2854, 1390, 1113, 1053, 1048 cm$^{-1}$; GC-MS *m/z* (relative intensity) 403 (2) [M −$CH_3$]$^+$, 305(100), 261(15), 193(5), 135 (34), 119(41); HRMS(EI):calculated for [M−$CH_3$]$^+$($C_{21}H_{47}O_3Si_2$) *m/z* : 418.3064: found [M−$CH_3$]$^+$ 418.3057.

## Reference


(1) (a) Y. Nakajima, S. Shimada, *RSC Adv.* **2015**, *5*, 20603-20616; b) B. Marciniec, Hydrosilylation: A Comprehensive Review on Recent Advances; Springer: Berlin, 2009; c) L. D. de Almeida, H. Wang, K. Junge, X. Cui, M. Beller, *Angew. Chem. Int. Ed.* **2020**, *60*, 550-565.

(2) D. Troegel, J. Stohrer, *Coord. Chem. Rev.* **2011**, *255*, 1440-1459.

(3) a) M. K. Harun, S. B. Lyon, J. Marsh, *Prog. Org. Coat.* **2003**, *46*, 21-27; b) M. R. Hayward, J. H. Johnston, T. Dougherty, K. De Silva, *Compos. Interfaces* **2018**, *26*, 263-273; c) I. Jerman, M. Mihelčič; D. Verhovšek, J. Kovač, B. Orel, *Sol. Energy Mater. Sol. Cells* **2011**, *95*, 423-431; d) B. L. Leigh, E. Cheng, L. Xu, C. Andresen, M. R. Hansen, C. A. Guymon, *Biomacromolecules* **2017**, *18*, 2389-2401; e) M. Öhman, D. Persson, *Surf. Interface Anal.* **2012**, *44*, 133-143; f) Sterman, S.; Marsden, J. G., Silane Coupling Agents. *Ind. Eng. Chem.* **1966**, *58*, 33-37.

(4) J. L. Speier, J. A. Webster, G. H. Barnes, *J. Am. Chem. Soc.* **1957**, *79*, 974-979

(5) a) B. D. Karstedt, U.S. Patent 3715334A, 1973; b) T. K. Meister, K. Riener, P. Gigler, J. Stohrer, W. A. Herrmann, F. E. Kühn, *ACS Catal.* **2016**, *6*, 1274–1284.

(6) I. E. Marko, S. Sterin, O. Buisine, G. Mignani, P. Branlard, B. Tinant, J. P. Declercq, *Science* **2002**, *298*, 204-206.

(7) a) P. Steffanut, J. A. Osborn, A. DeCian, J. Fisher, *Chem. Eur. J.* **1998**, *4*, 2008-2017; b) L. N. Lewis, *J. Am. Chem. Soc.* **1990**, *112*, 5998-6004; c) L. N. Lewis, N. Lewis, *J. Am. Chem. Soc.* **2002**, *108*, 7228-7231; d) T. J. Geldbach, D. Zhao, N. C. Castillo, G. Laurenczy, B. Weyershausen, P. J. Dyson, *J. Am. Chem. Soc.* **2006**, *128*, 9773-9780.

(8) a) X. Du, Z. Huang, *ACS Catal.* **2017**, *7*, 1227-1243; b) J. V. Obligacion, P. J. Chirik, *Nat. Rev. Chem.* **2018**, *2*, 15-34.

(9) a) D. Noda, A. Tahara, Y. Sunada, H. Nagashima, *J. Am. Chem. Soc.* **2016**, *138*, 2480 -2483. b) X. Jia, Z. Huang, *Nat. Chem.* **2016**, *8*, 157-161.

(10) C. H. Schuster, T. Diao, I. Pappas, P. J. Chirik, *ACS Catal.* **2016**, *6*, 2632-2636.

(11) I. Pappas, S. Treacy, P. J. Chirik, *ACS Catal.* **2016**, *6*, 4105-4109.

(12) a) L. Liu, A. Corma, *Chem. Rev.* **2018**, *118*, 4981-5079; b) J. M. Asensio, D. Bouzouita, P. van Leeuwen, B. Chaudret, *Chem. Rev.* **2020**, *120*, 1042-1084.

(13) a) J. Liu, *ACS Catal.* **2016**, *7*, 34-59; b) X. F. Yang, A. Wang, B. Qiao, J. Li, J. Liu, T. Zhang, *Acc. Chem. Res.* **2013**, *46*, 1740-1748. c)

(14) a) T. Galeandro-Diamant,; R.Sayah,; M. L. Zanota,; S. Marrot,; , L. Veyre; C. Thieuleux,; V. Meille, *Chem. Commun.* **2017**, *53*, 2962-2965; b) T. Galeandro-Diamant, I. Suleimanov, L. Veyre, M. Bousquié, V. Meille, C. Thieuleux, *Catal. Sci. Technol.* **2019**, *9*, 1555-1558; c) H. Miura, K. Endo, R. Ogawa, T. Shishido, *ACS Catal.* **2017**, *7*, 1543-1553; d) V. Pandarus, R. Ciriminna, G. Gingras, F. Béland, S. Kaliaguine, M. Pagliaro, *Green Chem.* **2019**, *21*, 129-140; e) J. Wen, Y. Chen, S. Ji, J. Zhang, D. Wang, Y. Li, *Nano Res.* **2019**, *12*, 2584-2588; f) J.-w. Zhang, G.-p. Lu, C. Cai, *Green Chem.* **2017**,

*19*, 2535-2540; g) T. Mitsudome, S. Fujita, M. Sheng, J. Yamasaki, K. Kobayashi, T. Yoshida, Z. Maeno, T. Mizugaki, K. Jitsukawa, K. Kaneda, *Green Chem.* **2019**, *21*, 4566-4570.

(15) a) L. Chen, I. S. Ali, G. E. Sterbinsky, J. T. L. Gamler, S. E. Skrabalak, S. L. Tait *ChemCatChem* **2019**, *11*, 2843-2854; b) Y. Chen, S. Ji, W. Sun, W. Chen, J. Dong, J. Wen, J. Zhang, Z. Li, L. Zheng, C. Chen, Q. Peng, D. Wang, Y. Li *J. Am. Chem. Soc.* **2018**, *140*, 7407-7410; c) Y. Zhu, T. Cao, C. Cao, J. Luo, W. Chen, L. Zheng, J. Dong, J. Zhang, Y. Han, Z. Li, C. Chen, Q. Peng, D. Wang, Y. Li, *ACS Catal.* **2018**, *8*, 10004-10011; d) X. Cui, K. Junge, X. Dai, C. Kreyenschulte, M. M. Pohl, S. Wohlrab, F. Shi, A. Bruckner, M. Beller, *ACS Cent. Sci.* **2017**, *3*, 580-585; e) B. B. Sarma, J. Kim, J. Amsler, G. Agostini, C. Weidenthaler, N. Pfander, R. Arenal, P. Concepcion, P. Plessow, F. Studt, G. Prieto, *Angew. Chem. Int. Ed.* **2020**, *59*, 5806–5815.

(16) a) H. Kawasaki, *Nanotechnol. Rev.* **2013**, *2*, 5-25; b) T. Nagata, Y. Obora *ACS Omega* **2020**, *5*, 98-103; c) H. Kawasaki, H. Yamamoto, H. Fujimori, R. Arakawa, M. Inada, Y. Iwasaki, *Chem. Commum.* **2010**, *46*, 3759-3761.

(17) R. Azuma, S. Nakamichi, J. Kimura, H. Yano, H. Kawasaki, T. Suzuki, R. Kondo, Y. Kanda, K.-i. Shimizu, K. Kato, Y. Obora, *ChemCatChem* **2018**, *10*, 2378-2382.

(18) a) K. D. Gilroy, A. Ruditskiy, H. C. Peng, D. Qin, Y. Xia, *Chem. Rev.* **2016**, *116*, 10414-10472; b) M. Sankar, N. Dimitratos, P. J. Miedziak, P. P. Wells, C. J. Kiely, G. J. Hutchings, *Chem. Soc. Rev.* **2012**, *41*, 8099-8139.

(19) Y. Naganawa, K. Inomata, K. Sato, Y. Nakajima, *Tetrahedron Lett.* **2020**, *61,* 151513.

(20) C. F. Holder, R. E. Schaak, *ACS Nano* **2019**, *13*, 7359–7365.

(21) a) L. K. Ono, B. Yuan, H. Heinrich, B. R. Cuenya, *J. Phys. Chem. C* **2010**, *114*, 22119–22133; b) A. P. Grosvenor, B. A. Kobe, M. C. Biesinger, N. S. McIntyre, *Surf. Interface Anal.* **2004**, *36*, 1564–1574; c) M. C. Biesinger, B. P. Payne, A. P. Grosvenor, L. W. M. Lau, A. R. Gerson, R. S. C. Smart, *Appl. Surf. Sci.* **2011**, *257*, 2717–2730.

(22) a) V. Srinivas, Y. Nakajima, K. Sato, S. Shimada, *Org. Lett.* **2018**, *20*, 12-15; b) P. Zak, M. Bolt, M. Kubicki, C. Pietraszuk, *Dalton Trans.* **2018***, 47,* 1903-1910; c) X. Wu, G. Ding, W. Lu, L. Yang, J. Wang, Y. Zhang, X. Xie, Z. Zhang *Org. Lett.* **2021**, *23*, 1434-1439; d) Z. Yu, Z. Dai, J. Li, Y. Yan, J. Peng, *New J. Chem.* **2021**, *45*, 10383-10387.

(23) B. Ravel, M. Newville, *J. Synchrotron Radiat.* **2005**, *12*, 537−541.

**Chapter 5.** Dimethylformamide-stabilized Ru nanoparticles catalyzed Guerbet reactions.

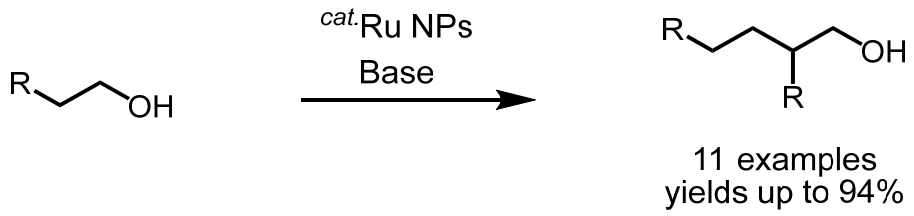

## Introduction

Catalytic hydrogen autotransfer has attracted considerable interest as a green and atom-economical alkylation process.[1] Owing to the importance of sustainability, minimizing the production of undesired byproduct is highly desired. In particular, Guerbet reaction, which pioneered in the 1890s by Marcel Guerbet,[2] gave Guerbet alcohols, which can be obtained by dehydrative condensation of aliphatic alcohols are widely found in surfactants, lubricants, personal care products.[3] Heterogeneous catalysts were evolved for this transformation.[4] Owing to the harsh conditions and low selectivity motivates researchers to develop a highly efficient process for the Guerbet reaction.[5]

It is also noteworthy that developments in this area by applying homogeneous catalysts including Ir,[6] Ru,[7] Mn.[8] However, the cost and ease of handling in synthesizing highly active ligands are underestimated.

Transition metal nanoparticles (M NPs) are highly active at low catalyst loadings owing to their large surface areas compared with those of the corresponding bulk metals.[8] Our group has focused a simple method for the synthesis of DMF-stabilized M-NPs and their use in catalytic reactions. In this methodology, DMF is used as a reductant, protectant, and solvent. Among the various M NPs,[9] Ir-NPs show high catalytic activity for β-benzylation of a linear alcohol and β-dimethylation of secondary alcohols with methanol via the hydrogen autotransfer system.[10] Herein, The author report synthesis of DMF-protected Ru NPs, their structural characterization, and their use as a catalyst in the Guerbet reaction (Homo β-alkylation) with primary alcohols.

## Results and discussions

The DMF-protected Ru NPs were synthesized according to the following procedure. $RuCl_3 \cdot H_2O$ was dissolved hydrochloric acid solution. DMF (50 mL) was added to a 300 mL three-necked round bottom flask, and the solution preheated to 140 ˚C (± 2 ˚C) and stirred 1300 to 1500 rpm for 5 min. Then the 0.1 M $RuCl_3 \cdot nH_2O$ solution was added to the hot DMF solution, which allowed to react for 10 h on stirring (1500 rpm) at 140 ˚C (± 2 ˚ C). The brown solution to afford Ru NPs. Annular dark-field scanning transmission microscopy (ADF-STEM) image shows the formation of Ru NPs of a mean diameter of 3.2 nm (Figure 1).

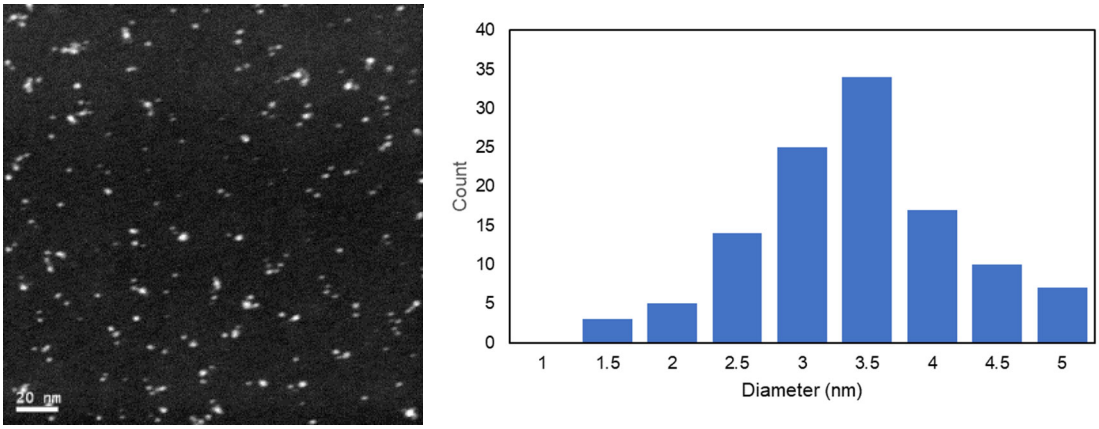


Figure 1. (a) ADF-STEM image, size distribution histogram of DMF-protected Ru NPs.

The author investigated the Guerbet reaction of 1-dodecanol(**1a**) as a model substrate under various conditions (Table 1). The reaction of 1-dodecanol (**1a**) (1 mmol) was performed in the presence of Ru NPs (0.05 mol%) and potassium tert-butoxide (KOtBu) (1 mmol) as a base (1 mL) at 150 °C for 24 h to give the main β-alkylated product(**2a**) in a moderate yield of 93% and 98% selectivity (entry 1). Second, the effect of base were tested, A strong base such as KOH gave whereas a weak inorganic base (e.g. $Cs_2CO_3$ and $K_2CO_3$) were ineffective (entries 2-4). Other Ru complex gave the desired products in moderate yield (entries 5-7). The use of metal nanoparticles precursor ($RuCl_3$ $H_2O$) as catalyst result in low yield (entry 8). The reaction did not proceed without Ru NPs (entry 9) and base (entry 10), which shows that a catalyst and base are necessary for alkylation.

Table 1 Guerbet reaction of 1-dodecanol with Ru NPs and other catalysts.[a]

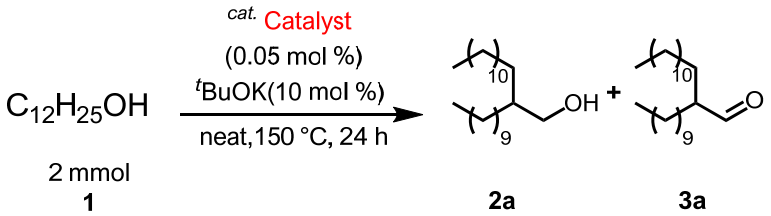


| Entry | Catalysts | Base | Conv. (%) | Yield (%) 2a : | 3a | Entry | Catalysts | base | Conv. (%) | Yield (%) 2a : | 3a |
|---|---|---|---|---|---|---|---|---|---|---|---|
| 1 | Ru NPs | tBuOK | 95 | 93[98] (83) | <1 | 7 | $Ru_3(CO)_{12}$ | K$^t$OBu | 47 | 28 | 13 |
| 2 | Ru NPs | KOH | 85 | 83 | <1 | 8 | $RuCl_3$ $nH_2O$ | K$^t$OBu | 40 | 33 | 1 |
| 3 | Ru NPs | $Cs_2CO_3$ | 12 | 2 | <1 | 9 | None | K$^t$OBu | 12 | n.d. | <1 |
| 4 | Ru NPs | $K_2CO_3$ | 8 | trace | <1 | 10 | Ru NPs | none | 10 | n.d. | <1 |
| 5 | [Ru(*p*-cymene)$Cl_2$]$_2$ | KO$^t$Bu | 35 | 30 | 4 | | | | | | |
| 6 | $(PPh_3)_3RuCl_2$, | KO$^t$Bu | 60 | 55 | 3 | | | | | | |

a Reaction conditions: **1a** (2 mmol) was reacted in the presence of catalyst (0.05 mol %) and (10 mol %) at 150 °C for 24h.the yields derived from GC analysis.

On the basis of the results, we next examined the reaction of various primary alcohols under the optimized conditions (Table 2). The isolation of products using primary alcohols was successful (**2b**–**i**). Moreover, branched primary alcohols and 3-Cyclohexyl-1-propanol were allowed to give the corresponding β-branched products in moderate and high yields (**2j**–**k**).

Table 2. The Ru NPs catalyzed Guerbet reaction of various primary alcohols.

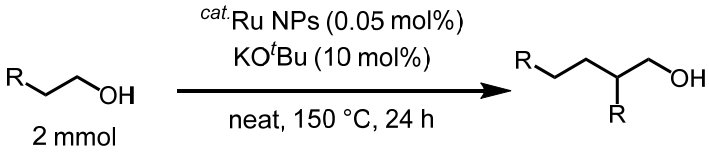


| Entry | Starting Alcohol | Isolated yield (%) | Entry | Starting Alcohol | Isolated yield (%) |
|---|---|---|---|---|---|
| 1 | 1-Hexadecanol (**2b**) | 72 | 6 | 1-hexanol (**2g**) | 60 |
| 2 | 1-Tetradecanol (**2c**) | 76 | 7 | 1-Pentanol (**2h**) | 46 |
| 3 | 1-Decanol (**2d**) | 75 | 8 | 1-Butanol (**2i**) | 39 |
| 4 | 1-Nonanol(**2e**) | 69 | 9 | 3,7-Dimethyl-1-octanol(**2j**) | 39 |
| 5 | 1-Octanol (**2f**) | 74 | 10 | 3-Cyclohexyl-1-propanol(**2k**) | 64 |

The recyclability of the DMF protected Ru NPs in this reaction was also investigated (Figure 2). After performing the reaction with 1-octanol, the substrates and the desired product **2g** were removed by vacuum distillation at 130 °C for 1 h under 0.3 mmHg. The base was removed by reprecipitation. In the first and second cycles, product was obtained in 73% and 67% yields, respectively. Thus, the Ru NPs can be reused. the size of the nanoparticles slightly increased during the course of the reaction resulted in a decrease of yield of products.

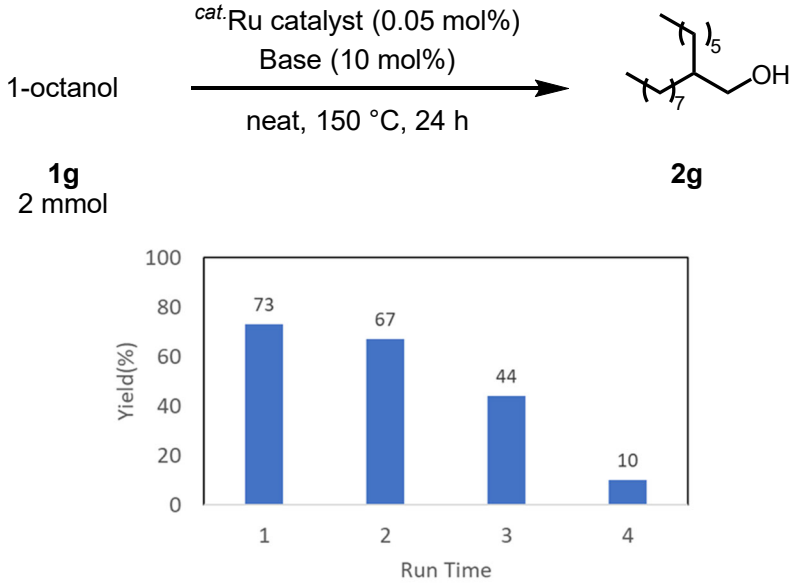


Figure 2. Recycling of a Ru NPs catalyst following the Guerbet reaction

Catalyst characterization

To elucidate the reasons for the high catalytic activity of Ru NPs, the author characterized using electron microscopy, FT-IR, TG-TOF-MS, XAFS, XPS.

First, we analyzed reaction mixture using annular dark-field (ADF) scanning transmission electron microscopy (STEM). After reaction, Ru NPs mean diameter were slightly increased 4.4 nm (Figure 3).

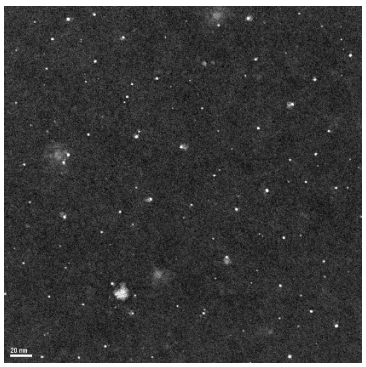

Figure 3. ADF-STEM image of DMF-protected Ru NPs after reaction

FT-IR measurements were performed. Figure 3 show the Ru NPs spectrum after removing the solvent DMF. The author found that the C=O and C-N vibration modes of DMF in DMF-protected Ru NPs were different to those in DMF solvent. The IR absorption attributed to metal carbonyl not in DMF was observed around 1950 $cm^{-1}$. It is suggested that CO generated from DMF interacts strongly with metals (Figure 4).[11]

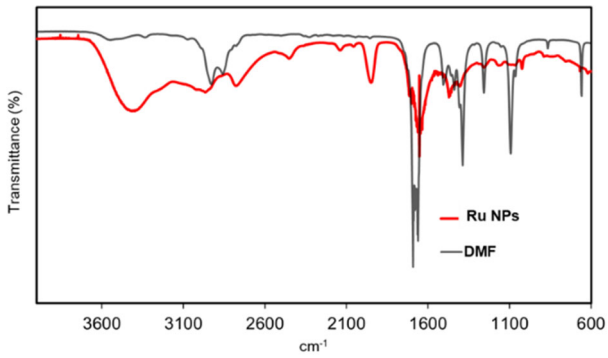


Figure 4. FT-IR spectra of (gray) DMF solvent and (red) DMF-protected Ru NPs

The thermal stability of Ru NPs was examined by Thermo Gravimetry (TG) at a heating rate of 10 °C/min in a $N_2$ atmosphere (Figure 5). TG results indicate that the DMF-protected Ru NPs are stable up to reaction temperature (~150 °C).

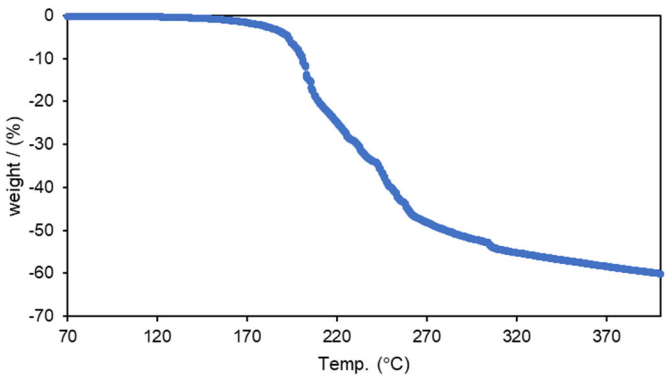


Figure 5. TG profile of DMF-protected Ru NPs

The TG-EI-HR-TOFMS measurement of the Ru NPs was performed, and the mass spectrum $H_2O$, DMF, CO, $CO_2$, dimethylamine was observed (Figure 6). These compounds were derived from DMF and M NPs.[12] Three ions (DMF, $CO_2$ and CO) were used to analyze the thermal behavior of the Ru NPs. the extracted ion chromatograms (EIC) of the above three ions are shown in Figure 6. The CO, coordinating on Ru NPs, was detected at around 280 °C and over 400 °C.

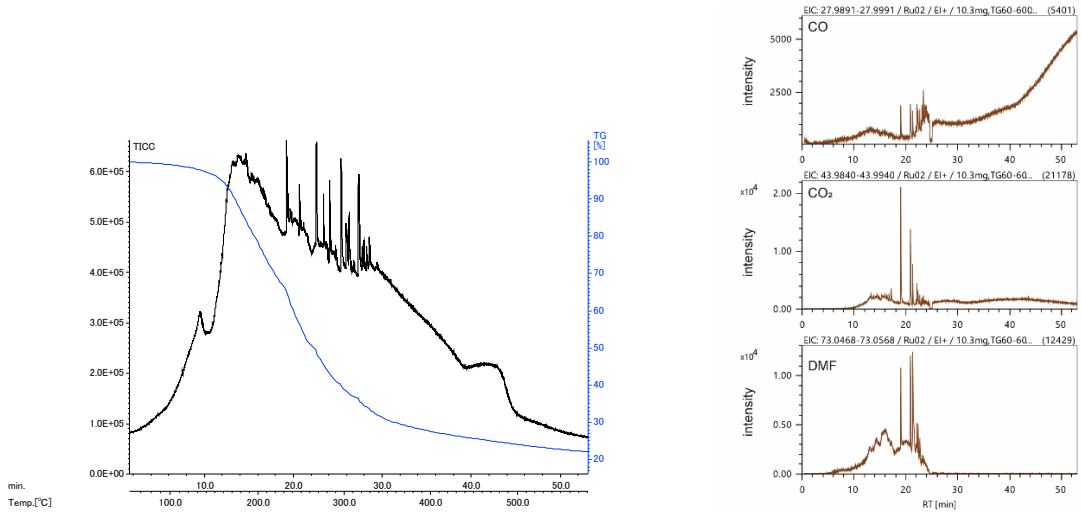


Figure 6. TG curve(blue) and Total ion chromatogram(black) of DMF-protected Ru NPs in He atmosphere and Extracted Ion Chromatogram of CO, $CO_2$, and DMF.

The XANES for Ru K-edge position of Ru NPs is situated between Ru foil and $RuO_2$ (Figure 7), suggesting that the oxidation state of Ru in the sample is δ+ ($0 < \delta < 4$). The Ru state maintained even after reaction.

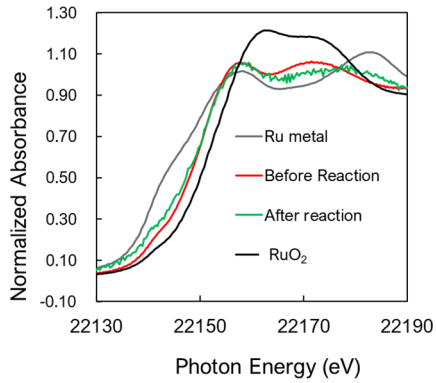


Figure 7. Ru K-edge XANES spectra of Ru powder, $RuO_2$, Ru NPs, after reaction of Ru NPs

Figure 8 shows the X-ray photoelectron spectroscopy (XPS) results for the DMF-protected Ru NPs. Ru signals ascribed to Ru $3p_{3/2}$ and Ru $3p_{1/2}$ are detected at 461.5 eV and 483 eV, respectively, in the Ru 3p region (Figure 8).[12] The Ru species in the DMF-protected Ru NPs were close to those of metallic Ru.

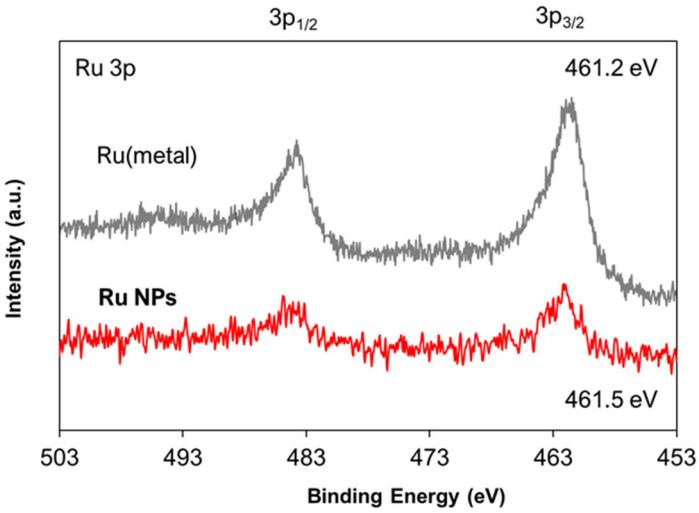


Figure 8. Ru 3p XPS spectra of Ru powder(gray) and DMF-protected Ru NPs(red).

Based on our experiments, a plausible catalytic mechanism is proposed for the β-alkylation of primary alcohols. As depicted figure 9, primary alcohol was oxidized to give aldehyde. The initially formed aldehyde is condensed to give the unsaturated aldehyde. Thereafter, the α,β-unsaturated aldehyde would undergo a hydrogenation reaction in the presence of Ru NPs to generate the desired product **2a**. Figure 10 shows time-dependent production of desired products and intermediates. Aldehydes produced during the reaction were immediately consumed. The Ru NPs catalyst were minimized byproducts formation due to their dehydrogenation/hydrogenation properties

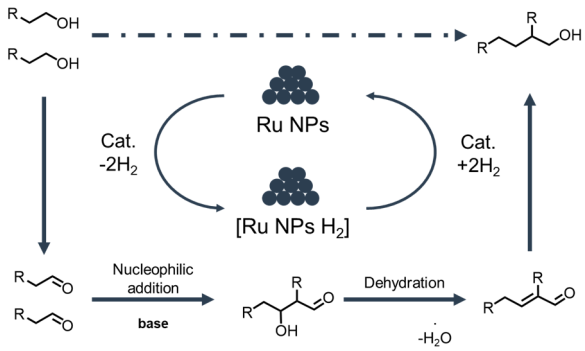


Figure 9. plausible reaction mechanism of Guerbet reaction of primary alcohols.

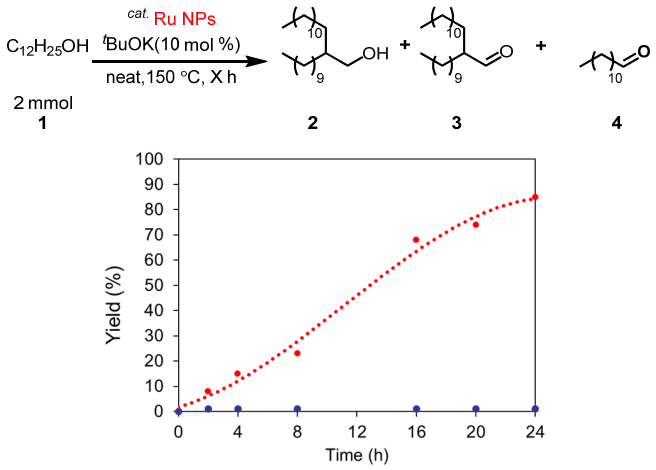


Figure 9. Time dependent production of 2(red), 3 and 4(blue).

## Conclusion

DMF-protected Ru NPs catalyst for Guerbet reactions. In conclusion, β-alkylation of primary alcohols to branched alcohols under mild reaction conditions was achieved using a DMF-protected Ru NPs catalyst. The Ru NPs catalyst promoted Guerbet reaction under external ligand- and solvent- free conditions. Various primary alcohols were converted into the corresponding branch alcohols in high yields. This catalytic system has the significant advantages of mild operating conditions, simple catalyst preparation procedures, high catalyst reusability, and a broad substrate scope, thus enabling green sustainable Guerbet reactions.

## Experimental

### General procedure

### Preparation of DMF-protected Ru nanoparticles

To a 20 mL vial bottle, $RuCl_3$ $nH_2O$ (Tanaka kikinzoku) was weight and dissolved so that The Ru concentration 0.1 mol/L. To a 300 mL three-necked round bottom flask, DMF (50 mL) was added and the solutions. DMF was pre-heated at 140 C After heating the reaction mixture to room temperature,

### Guerbet reaction of 1-dodecanol

To a reaction vessel (10 mL), Ru-NPs (0.001 mmol) DMF was evaporated under reduced pressure (80 °C, 40 hPa), then, 1-dodecanol **1a** (372.68 mg, 2 mmol), and potassium tert-butoxide (21 mg, 0.02 mmol) were added, and the mixture was stirred at 150 °C for 24 h. the reaction mixture was cooled to room temperature, and the product was isolated by silica gel column chromatography (*n*hexane : EtOAc = 9:1). The product **2a** was obtained 83% yield as a colorless oil.

### Catalyst characterization

Ru K-edge X-ray absorption fine structure (XAFS) spectra were collected at the BL14B2 of SPring-8 at the Japan Synchrotron Radiation Research Institute (JASRI) (proposal 2018B1126). A Si(311) double-crystal monochromator was used for the measurements. The XAFS spectrum was recorded at room temperature

### Compound Characterization

**2a**, 2-decyltetradecanol, $^1$H-NMR (400MHz $CDCl_3$) δ: 3.54 (2H, d, $J$ = 5.5 Hz), 1.27-1.25 (42H, m), 0.88 (6H, t, $J$ = 6.9 Hz) $^{13}$C-NMR (100 MHz $CDCl_3$) δ: 65.75 ($CH_2$), 40.52 (CH), 31.92 ($CH_2$), 30.92 ($CH_2$), 30.06 ($CH_2$), 29.67 ($CH_2$), 29.65 ($CH_2$), 29.63 ($CH_2$), 29.35 ($CH_2$), 29.34 (CH2), 26.88 ($CH_2$), 22.68 ($CH_2$), 14.11 ($CH_3$); GC-MS (EI) m/z (relative intensity) 336 (4) $[M-H_2O]^+$ , 308(2), 111(49), 97(73), 71(80), 57 (100), 43(67).

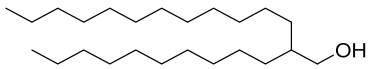


**2b**, tetradecyloctadecanol, $^1$H-NMR (400 MHz $CDCl_3$) δ: 3.47 (d, 2H, $J$ = 5.4 Hz), 1.38-1.19 (m, 58H), 0.81 (t, 6H, $J$ = 6.4 Hz); $^{13}$C-NMR (100 MHz $CDCl_3$) δ: 65.75 ($CH_2$), 40.53 (CH), 31.93 (CH), 30.93 ($CH_2$), 30.07 ($CH_2$), 29.70 ($CH_2$), 29.66 ($CH_2$), 29.37 ($CH_2$), 26.89 ($CH_2$), 22.69 ($CH_2$), 14.11 ($CH_3$); GC-MS(EI) m/z (relative intensity) 448 (3) $[M- H_2O]^+$ 252 (4) 71 (80) 57 (100)

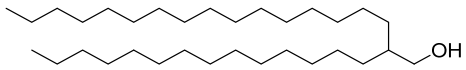

**2c**, 2-dodecylhexadecanol, $^{1}$H-NMR (400MHz $CDCl_3$) δ: 3.51 (2H, d, $J$ = 5.5 Hz), 1.43-1.24 (50H, br m), 0.86 (6H, t, $J$ = 6.9 Hz); $^{13}$C-NMR (100 MHz $CDCl_3$) δ: 65.74 ($CH_2$), 40.53 (CH), 31.93 ($CH_2$), 30.93 ($CH_2$), 30.07 ($CH_2$), 29.69 ($CH_2$), 29.66 ($CH_2$), 29.36 ($CH_2$), 26.89 ($CH_2$), 22.69 ($CH_2$), 14.11 ($CH_3$); GC-MS(EI) m/z (relative intensity) 392 (3) $[M- H_2O]^+$ 97 (66) 57 (100)

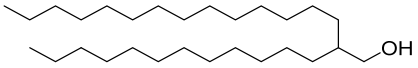


**2d**, 2-octyldodecanol, colorless oil, $^{1}$H-NMR (400 MHz $CDCl_3$) δ: 3.53 (2H, d, $J$ = 5.4 Hz), 1.45 (1H, br s), 1.29 (33H, br s), 0.88 (6H, t, $J$ = 6.9 Hz);$^{13}$C-NMR (100 MHz $CDCl_3$) δ: 65.71 ($CH_2$), 40.53 (CH), 31.95 ($CH_2$), 30.93 ($CH_2$), 30.11 ($CH_2$), 29.72 ($CH_2$), 29.69 ($CH_2$), 29.66 ($CH_2$), 29.39 ($CH_2$), 26.91 ($CH_2$), 22.72 ($CH_2$), 14.14 ($CH_3$); GC-MS (EI) m/z (relative intensity) 280 (3) $[M-H_2O]^+$, 252 (2) 85 (49), 97 (59), 111 (43) 71 (72), 57 (100), 43(63).

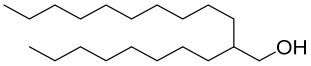


**2e**, 2-heptylundecanol, colorless oil, $^{1}$H-NMR (400 MHz $CDCl_3$) δ: 3.54 (2H, d, $J$ = 5.4 Hz), 1.27 (30H, br), 0.88 (6H, t, $J$ = 6.7 Hz); $^{13}$C-NMR (100 Hz $CDCl_3$) δ: 65.76 ($CH_2$), 40.56 (CH), 31.93 ($CH_2$), 30.95 ($CH_2$), 30.10 ($CH_2$), 30.07 ($CH_2$), 29.68 ($CH_2$), 29.66 ($CH_2$), 29.37 ($CH_2$), 29.35 ($CH_2$), 26.92 ($CH_2$), 22.71 ($CH_2$), 14.13 ($CH_3$); GC-MS (EI) m/z (relative intensity) 252 (2) $[M-H_2O]^+$, 111 (31) 85 (47), 71 (64), 57 (100), 43(63).

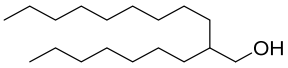


**2f** 2-hexyldecanol, colorless oil, $^{1}$H-NMR (400MHz $CDCl_3$) δ: 3.54 (2H, d, $J$ = 5.4 Hz), 1.42-1.31 (26H, m), 0.88 (6H, t, $J$ = 6.6 Hz); $^{13}$C-NMR (100 MHz $CDCl_3$) δ: 40.55 ($CH_2$), 31.92 (CH), 31.90 ($CH_2$), 30.95 ($CH_2$), 30.09 ($CH_2$), 29.76 ($CH_2$), 29.63 ($CH_2$), 29.36 ($CH_2$), 26.91 ($CH_2$), 26.88 ($CH_2$), 22.70 ($CH_2$), 14.12 ($CH_3$); GC-MS (EI) m/z (relative intensity) 224 (3) $[M-H_2O]^+$, 85 (43), 97 (38), 111 (34) 71 (72), 57 (100), 43(63).

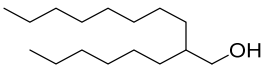


**2g**, 2-butyloctanol, colorless oil, $^{1}$H-NMR (400 MHz $CDCl_3$) δ: 3.54 (2H, d, $J$ = 5.4 Hz), 1.27 (18H, br), 0.88 (6H, t, $J$ = 6.7 Hz); $^{13}$C-NMR (100 MHz $CDCl_3$) δ: 65.70 ($CH_2$), 40.50 (CH), 31.85 ($CH_2$), 30.93 ($CH_2$), 30.61 ($CH_2$), 29.72 ($CH_2$), 29.10 ($CH_2$), 26.84 ($CH_2$), 23.08 ($CH_2$), 22.65 ($CH_2$), 14.06 ($CH_3$); GC-MS (EI) m/z (relative intensity) 168 (3) $[M-H_2O]^+$, 140(4), 111(23), 71 (49), 57 (100), 43(67).

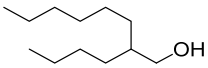

**2h** 2-propylheptanol, colorless oil, $^{1}$H-NMR (400 MHz $CDCl_3$) δ: 3.54 (2H, d, $J$ = 5.5 Hz), 1.49-1.26 (14H, m), 0.92-0.87 (6H, m); $^{13}$C-NMR (100 MHz $CDCl_3$) δ: 65.68 ($CH_2$), 40.26 (CH), 33.22 ($CH_2$), 32.26 ($CH_2$), 30.85 ($CH_2$), 26.52 ($CH_2$), 22.64 ($CH_2$), 19.99 ($CH_2$), 14.45 ($CH_3$), 14.07 ($CH_3$); GC-MS (EI) m/z (relative intensity) 140 (3) $[M-H_2O]^+$, 71 (67) 57 (67) 43(100).

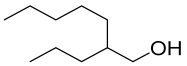


**2i** 2-ethylhexanol, colorless oil, $^{1}$H-NMR (400 MHz $CDCl_3$) δ: 3.55 (2H, d, $J$ = 5.1 Hz), 1.46-1.28 (10H, m), 0.92-0.88 (6H, m); $^{13}$C-NMR (100 MHz $CDCl_3$) δ: 65.28 ($CH_2$), 41.93 (CH), 30.09 ($CH_2$), 29.09 ($CH_2$), 23.30 ($CH_2$), 23.07 ($CH_2$), 14.08 ($CH_3$), 11.07 ($CH_3$); GC-MS (EI) m/z (relative intensity) 112 (2) $[M-H_2O]^+$, 85 (41), 70 (23), 70(23), 57(100), 43 (91).

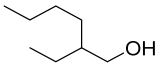


**2j** 2,4-dicyclohexylbutanol, colorless oil, $^{1}$H-NMR (400 MHz $CDCl_3$) δ: 3.52-3.44 (2H, m), 1.67-1.50 (12H, m), 1.31-1.02 (5H, m), 0.87- 0.80 (4H, m); $^{13}$C-NMR (100 MHz $CDCl_3$) δ: 65.91 ($CH_2$), 39.08 ($CH_2$), 37.88 ($CH_2$), 37.63 (CH), 37.27 (CH), 34.99 (CH), 33.78 ($CH_2$), 33.71 ($CH_2$), 33.44 ($CH_2$), 33.41 ($CH_2$), 31.62 ($CH_2$), 26.72 ($CH_2$), 26.67 ($CH_2$), 26.41 ($CH_2$), 26.36 ($CH_2$), 23.94 ($CH_2$); FT-IR(neat) 3307, 2853, 2919, 1447, 1020 $cm^{-1}$; GC-MS (EI) *m/z* (relative intensity) 248 (9) $[M-H_2O]^+$, 96 (100), 83 (62), 55 (85); HRMS(EI) *m/z* $[M-H_2O]^+$ calcd for $C_{18}H_{32}$, 248.2504; found, 248.2503.

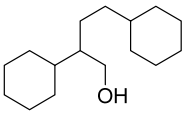


**2k** 2-(1,5-Dimethylhexyl)-5,9-dimethyl-1-decanol, colorless oil,$^{1}$H-NMR (400 MHz $CDCl_3$) δ: 3.64-3.51 (2H, m), 1.56-1.49 (2H, m), 1.38-1.08 (20H, m), 0.86-0.84 (18H, m); A mixture of 4 diastereomers, $^{13}$C-NMR (100 MHz $CDCl_3$) δ: 64.25 ($CH_2$), 64.17 ($CH_2$), 63.69 ($CH_2$), 63.62 ($CH_2$), 45.82 (CH), 45.75 (CH), 45.72 (CH), 45.59 (CH), 39.33 ($CH_2$), 39.30 ($CH_2$), 39.28 ($CH_2$), 39.27 ($CH_2$), 37.33 ($CH_2$), 37.23 ($CH_2$), 37.22 ($CH_2$), 37.03 ($CH_2$), 35.58 ($CH_2$), 35.52 ($CH_2$), 35.26 ($CH_2$), 35.15 ($CH_2$), 34.50 ($CH_2$), 34.39 ($CH_2$), 34.36 ($CH_2$), 34.21 ($CH_2$), 33.28 (CH), 33.20 (CH), 33.19 (CH), 33.14 (CH), 33.11 (CH), 32.74 (CH), 32.71 (CH), 27.97 (CH), 27.96 (CH), 27.94 (CH), 25.91 (CH), 25.90 ($CH_2$), 25.49 ($CH_2$), 25.46 ($CH_2$), 24.80 ($CH_2$), 24.78 ($CH_2$), 24.75 ($CH_2$), 24.20 ($CH_2$), 24.18 ($CH_2$), 22.72 ($CH_3$), 22.71 ($CH_3$), 22.69 ($CH_3$), 22.60 ($CH_3$), 22.59 ($CH_3$), 19.78 ($CH_3$), 19.71 ($CH_3$), 19.69 ($CH_3$), 19.59 ($CH_3$), 16.21 ($CH_3$), 16.00 ($CH_3$), 15.61 ($CH_3$), 15.49 ($CH_3$); FT-IR(neat) 3278, 2957, 2952, 2867, 1459, 1367, 1045 $cm^{-1}$; GC-MS (EI) *m/z* (relative intensity) 280 (2) $[M-H_2O]^+$ 71 (80) 57 (100) 43(60); HRMS(EI) *m/z* $[M-H_2O]^+$ calcd for $C_{20}H_{40}$, 280.3130; found, 280.3128.

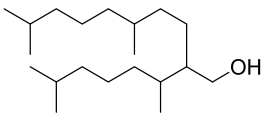

## Reference


(1) a) A. Corma, J. Navas, M. J. Sabater, *Chem. Rev.* **2018**, *118*, 1410-1459; b) Y. Obora, *ACS Catal.* **2014**, *4*, 3972–3981; c) K.-i. Shimizu, *Catal. Sci. Technol.* **2015**, *5*, 1412-1427; d) F. Huang, Z. Liu, Z. Yu, *Angew. Chem. Int. Ed* **2016**, *55*, 862; d) H. Li, A. Riisager, S. Saravanamurugan, A. Pandey, R. S. Sangwan, S. Yang, R. Luque *ACS Catal.* **2018** *8*, 148-187.

(2) a) a) M. Guerbet, *C. R. Hebd. Séances Acad. Sci.* **1899**, *128*, 511–513; b) A. J. O'Lenick, *J. Surfactants Deterg.* **2001**, *4*, 311–315

(3) a) R. Varadaraj, J. Bock, P. Valint, S. Zushma, N. Brons, *J. Phys. Chem.* **1991**, *95*, 1679–1681; b) E.-O. Alami, K. Holmberg, *Adv. Colloid Interface Sci.* **2003**, *100-102*, 13–46.

(4) a) D. Liu, X. Chen, G. Xu, J. Guan, Q. Cao, B. Dong, Y. Qi, C. Li, X. Mu, *Sci. Rep.* **2016**, *6*, 21365; b) J. T. Kozlowski, R. J. Davis, *ACS Catal.* **2013**, *3*, 1588–1600; c) K. A. Goulas, S. Sreekumar, Y. Song, P. Kharidehal, G. Gunbas, P. J. Dietrich, G. R. Johnson, Y. C. Wang, A. M. Grippo, L. C. Grabow, A. A. Gokhale, F. D. Toste, *J. Am. Chem. Soc.* **2016**, *138*, 6805–6812; d) S. Hanspal, Z. D. Young, H. Shou, R. J. Davis, *ACS Catal.* **2015**, *5*, 1737–1746; e) V. N. Panchenko, E. A. Paukshtis, D. Yu Murzin, I. L. Simakova *Ind. Eng. Chem. Res.* **2017,** *56*, 13310-13321.

(5) a) D. Gabriëls, W. Y. Hernández, B. Sels, P. Van Der Voort, A. Verberckmoes, *Catal. Sci. Technol.* **2015**, *5*, 3876-3902; b) H. Aitchison, R. L. Wingad, D. F. Wass, *ACS Catal.* **2016**, *6*, 7125-7132.

(6) Ir a) T. Matsu-ura, S. Sakaguchi, Y. Obora, Y. Ishii, *J. Org. Chem.* **2006**, *71*, 8306–8308; b) K. Koda, T. Matsu-ura, Y. Obora, Y. Ishii, *Chem. Lett.* **2009**, *38*, 838–839.

(7) Ru a) Y. Xie, Y. Ben-David, L. J. W. Shimon, D. Milstein, *J. Am. Chem. Soc.* **2016**, *138*, 9077–9080; b) S. Manojveer, S. Salahi, O. F. Wendt, M. T. Johnson, *J. Org. Chem.* **2018**, *83*, 10864–10870.

(8) Mn a) S. Fu, Z. Shao, Y. Wang, Q. Liu, *J. Am. Chem. Soc.* **2017**, *139*, 11941-11948; b)

(9) T. Nagata, Y. Obora, *ACS Omega* **2020**, *5*, 98–103.

(10) a) K. Oikawa, S. Itoh, H. Yano, H. Kawasaki, Y. Obora, *Chem. Commun.* **2017**, *53*, 1080–1083; b) M. Kobayashi, H. Yamaguchi, T. Suzuki, Y. Obora, *Org. Biomol. Chem.* **2021**, *19*, 1950–1954.

(11) A.-C. Boucher, V. Le Rhun, F. Hahn, N. Alonso-Vante, *J. Electroanal. Chem.* **2003**, *554-555*, 379–384.

(12) T. S. Rodrigues, M. Zhao, T.-H. Yang, K. D. Gilroy, A. G. M. da Silva, P. H. C. Camargo, Y. Xia, *Chem. - Eur. J.* **2018**, *24*, 16944–16963.

(13) D. J. Morgan, *Surf. Interface Anal.* **2015**, *47*, 1072–1079.

# Chapter 6. General Conclusion

In this thesis, metal nanoparticles have been utilized as highly active organic transformations catalyst. Thiolate-protected Au nanocluster $Au_{25}(SC_2H_4)_{18}$ and *N,N*-dimethylformamide (DMF)-protected metal nanoparticles catalyst in various organic transformation have been demonstrated. Representative examples are given of external-stabilizer/protectant-free metal NPs syntheses by reduction with DMF. These applications have enabled a versatile organic transformation such as hydroamination, C-Si cross-coupling reactions, hydrosilylation, and β-alkylation with primary alcohols to be achieved. These reactions proceed under low catalyst loadings and ligandless conditions.

In chapter 2, the author described Thiolate protected Au nanoclusters-catalyzed intermolecular hydroamination of terminal alkynes. The reactions smoothly proceeded by employing aromatic terminal alkynes and anilines in the presence of $Au_{25}(SC_2H_4Ph)_{18}$ catalyst under oxygen atmosphere without any solvents. Several alkynes and anilines were subjected to the reaction and the corresponding imines were obtained in moderate-to-high yields. The catalyst was recovered by precipitation with hexane and reused to give ketimines.

In chapter 3, DMF-stabilized Pd nanoclusters catalyzed coupling reactions of aryl halides with hydrosilanes/disilanes reports the use of Pd NPs stabilized with DMF for the coupling reactions of aryl halides with hydrosilanes/disilanes. There are some interesting results showing ligand exchange from DMF to DMAc and also the reduction of surface Pd by the action of X-rays in XPS measurements. Moreover, the catalyst could be reused without significant loss of activity.

In chapter 4, the mixture of $Fe_2O_3$ NPs and Pt NPs catalyst that were active in the hydrosilylation of alkenes. While DMF-stabilized $Fe_2O_3$ or Pt NPs independently did not proceed the reaction, the one-pot integration of both catalysts achieves good to excellent yields to terminal anti-Markovnikov products. The author performed analysis of functional group tolerance and recyclability of this catalyst system. Moreover, the reaction is scaled up to the kg level while retaining the high selectivity and yield of lower scale tests.

In chapter 5, β-alkylation of primary alcohols has been accomplished using DMF-protected Ru NPs. The catalytic protocol requires no additives and solvent. The Ru NPs catalyst shows high catalytic activity and can be recycled three times.

# List of Publications

The present Thesis is composed of the following papers

(1) ”Thiolate-Protected $Au_{25}(SC_2H_4Ph)_{18}$ Nanoclusters as a Catalyst for Intermolecular Hydroamination of Terminal Alkynes” Tatsuki Nagata, Yurina Adachi, Yasushi Obora, *Synlett*, **2018**, 29, 2655-2659

(2) ”Dimethylformamide-stabilised palladium nanoclusters catalysed coupling reactions of aryl halides with hydrosilanes/disilanes” Tatsuki Nagata, Takeru Inoue, Xianjin Lin, Shinya Ishimoto, Seiya Nakamichi, Hideo Oka, Ryota Kondo, Takeyuki Suzuki, Yasushi Obora, *RSC Adv.* **2019**, *9*, 17425-17431.

(3) *“N,N*-Dimethylformamide-Protected Single-Sized Metal Nanoparticles and Their Use as Catalysts for Organic Transformations” Tatsuki, Nagata, Yasushi. Obora, *ACS Omega* **2020**, *5*, 98–103.

(4) “Transition-Metal-Mediated/Catalyzed Synthesis of Pyridines, Pyrimidines, and /Triazines by [2+ 2+ 2] Cycloaddition Reactions” Tatsuki, Nagata, Yasushi. Obora, *Asian J. Org. Chem.* **2020**, *9*, 1532–1547.

(5) *“N,N*-Dimethylformamide-protected $Fe_2O_3$ combined with Pt nanoparticles : Characterization and catalysis in alkene hydrosilylation” Tatsuki Nagata, Tatsuya Tanaka, Xianjin Lin, Ryota Kondo, Takeyuki Suzuki, Yasuharu Kanda, Takashi Toyao, Ken-ichi Shimizu, Yasushi Obora, *Chemcatchem*, **2021**, in press DOI:10.1002/cctc.202101672.

II Following publications are not included in this thesis.

(6) “Thiolate-protected Gold Nanoclusters $Au_{25}$(phenylethanethiol)$_{18}$: An Efficient Catalyst for the Synthesis of Propargylamines from Aldehydes, Amines, and Alkynes” Yurina Adachi, Hideya Kawasaki, Tatsuki Nagata, Yasushi Obora, *Chem. Lett.* **2016**, *45*, 1457-1459**.**

(7) “Synthesis and Characterization of *N,N*-Dimethylformamide-Protected Palladium Nanoparticles and Their Use in the Suzuki–Miyaura Cross-Coupling Reaction” Jyunya Ishida, Masato Nakatsuji, Tatsuki Nagata, Hideya Kawasaki, Takeyuki Suzuki, Yasushi Obora, *ACS Omega*, **2020**, 5, 95-98-9604.

(8) “Effect of Water in Fabricating Copper Nanoparticles onto Reduced Graphene Oxide Nanosheets: Application in Catalytic Ullmann-Coupling Reactions” Pattira Suktanarak, Tatsuya Tanaka, Tatsuki Nagata, Ryota Kondo, Takeyuki Suzuki, Thawatchai Tuntulani, Pannee Leeladee, Yasushi Obora, *Bull. Chem. Soc. Jpn.* **2020**, *93*, 1164-1170.

## Acknowledgements

This thesis presents the studies that the author carried out at the Faculty of Chemistry, Materials, Bioengineering, Kansai University, during the years from 2016 to 2021 under the supervision of Professor Yasushi Obora. The author would like to express his deepest appreciation to Professor Hideya Kawasaki, Fumio Sanda for his continuous guidance, valuable suggestions, and encouragement throughout the present thesis. The author is also grateful to Professor Takeyuki Suzuki and Professor Ryota Kondo for their helpful suggestions, Yousuke Murakami and Takeshi Ishibashi at SANKEN (Osaka University), for TEM observation, Nao Eguchi for ICP-AES measurement, Prof. Hiroyuki Uchiyama for measurement of XPS, Professor Ken-ichi Shimizu, Assistant professor Takashi Toyao, Dr. Zen Maeno, and member of Shimizu laboratory for XAFS beamtime, measurement and helpful discussions.

Sincere thanks are due to all colleagues in the Obora Laboratory for their discussion.

Finally, the authors would like to give his greatest thanks to his family, especially his parents for their constant assistance and kind-hearted encouragement.

Tatsuki Nagata